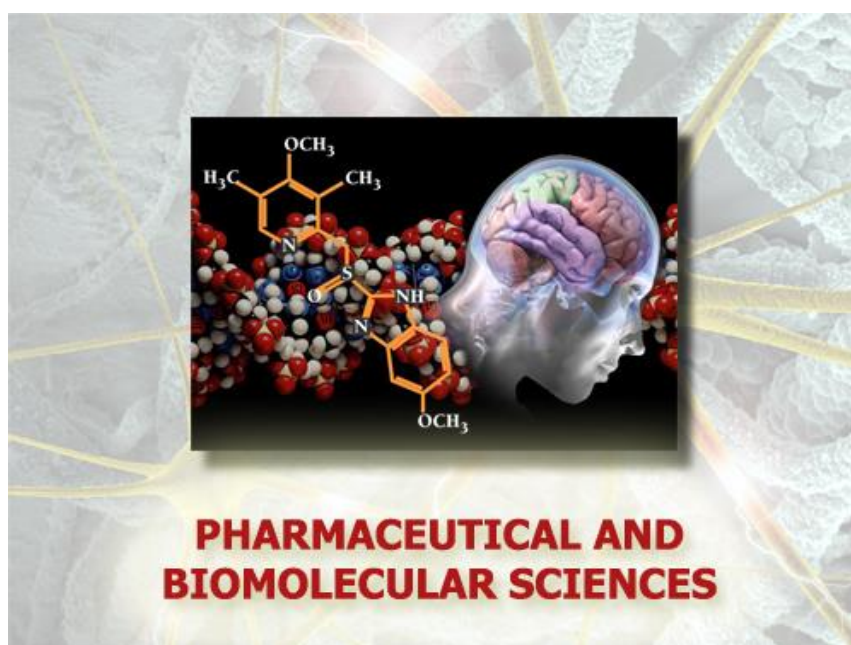


Università degli Studi di Torino



Scuola di Dottorato in
Scienze della Natura e Tecnologie Innovative

**Dottorato in
Scienze Farmaceutiche e Biomolecolari
(XXXIV ciclo)**



**Enabling technologies and innovative
materials for green chemistry and process
intensification**

Candidato: Fabio Bucciol

Tutor: Prof. Giancarlo Cravotto

Università degli Studi di Torino



**Dottorato in
Scienze Farmaceutiche e Biomolecolari**

**Tesi svolta presso il
Dipartimento di Scienza e Tecnologia del Farmaco**

CICLO: XXXIV

TITOLO DELLA TESI: Enabling technologies and innovative materials for green chemistry and process intensification

TESI PRESENTATA DA: Fabio Buccioli

TUTOR: Prof. Giancarlo Cravotto

COORDINATORE DEL DOTTORATO: Prof.ssa Roberta Cavalli

ANNI ACCADEMICI: 2018/2021

SETTORE SCIENTIFICO-DISCIPLINARE DI AFFERENZA: CHIM/06

“Science is the acceptance of what works and the rejection of what does not. That needs more courage than we might think.”

Jacob Bronowski

“What I love about science is that as you learn, you don’t really get answers. You just get better questions.”

John Green

Index

1.0 General Introduction	1
1.1 Green Chemistry	1
1.1.1 Atom economy and green metrics	2
1.1.2 Green Solvents	5
1.1.3 Renewable feedstocks	6
1.1.4 Heterogeneous catalysis	8
1.2 Process intensification	8
1.2.1 PI and scalability of a reaction	9
1.2.2 Enabling technologies for PI	10
1.2.3 Flow chemistry	15
2.0 Synthesis of new heterogeneous materials	20
2.1 Synthesis and application of cyclodextrin-based insoluble polymers	20
2.1.1 Introduction and state of the art	20
2.1.2 Preparation and purification	22
2.1.3 Characterization	23
2.1.4 Adsorption of dyes as model compounds	26
2.1.5 Adsorption of pharmaceuticals and bioactive compounds	31
2.1.6 Conclusion	36
2.2 US-assisted preparation of Au and Ag nanoparticles over pectin	37
2.2.1 Introduction and state of the art	37
2.2.2 Deposition and characterization of the metal nanoparticles	38
2.2.3 Doping with tetracycline derivatives	43
2.2.4 Antimicrobial tests and results	44
2.2.5 Conclusion	46
2.3 US-assisted preparation of metallic heterogeneous catalysts	47
2.3.1 Introduction	47
2.3.2 Preparation of Rh-based catalysts	48
2.3.3 Preparation of Co-based catalysts	48
2.3.4 Deposition of Rh and Au nanoparticles over cyclodextrin-based polymer	49
2.3.5 Model reactions over the β CDPIS-based catalysts	50
2.3.6 Conclusion	52
3.0 Enabling technologies for synthesis and PI	56
3.1 Squalene and FAME recovery from ODD and hydrogenation to squalane	56
3.1.1 Introduction and state of the art	56
3.1.2 Conversion of FFA to FAME	57
3.1.3 Squalene and FAME isolation	59
3.1.4 Squalene hydrogenation to squalane	61
3.1.5 Conclusion	62
3.2.0 MW-assisted reductive amination of aldehydes and ketones	63
3.2.1 Introduction and state of the art	63
3.2.2 Reductive amination of benzaldehyde	64
3.2.3 Reductive amination of different aldehydes	67
3.2.4 Reductive amination of ketones	68
3.2.5 Conclusion	75
3.3.0 MW-assisted hydroformylation of olefines	76
3.3.1 Introduction and state of the art	76
3.3.2 Hydroformylation experiments	76

3.3.3	<i>One-pot hydroformylation and reductive amination of olefines</i>	80
3.3.4	<i>Conclusion</i>	82
3.4.0	One-pot MW-assisted synthesis of isosorbide from glucose	83
3.4.1	<i>Introduction and state of the art</i>	83
3.4.2	<i>Glucose hydrogenation to sorbitol</i>	85
3.4.3	<i>Sorbitol dehydration</i>	86
3.4.4	<i>One-pot reaction</i>	87
3.4.5	<i>Conclusion</i>	89
4.0	Scaled processes	92
4.1	<i>MW-assisted hydrogenation of LA to GVL in a flow reactor</i>	92
4.1.1	<i>Conclusion</i>	95
4.2.0	Caffeine and chlorogenic acid isolation from green coffee extract	96
4.2.1	<i>Caffeine isolation via CD complexation</i>	97
4.2.2	<i>Ion-exchange resin treatment of crude caffeine</i>	99
4.2.3	<i>Chlorogenic acids recovery</i>	102
4.2.4	<i>Conclusion</i>	104
5.0	General conclusion	106
6.0	Materials and methods	108
6.1	<i>Synthesis and characterization of cyclodextrin insoluble polymers</i>	108
6.2	<i>Synthesis and characterization of doped pectin</i>	108
6.3	<i>Synthesis of Rh and Co-based catalysts</i>	109
6.4	<i>MW-assisted syntheses and relative analysis</i>	109
6.5	<i>Caffeine and chlorogenic acids isolation</i>	109
7.0	Acknowledgements	110

List of used acronyms

1,1-DPE	1,1-diphenylethylene	LA	Levulinic Acid
1,2-PDO	1,2-propandiol	L-AA	L-Ascorbic Acid
1,3-PDO	1,3-propandiol	MB	Methylene Blue
AE	Atom Economy	MeOH	Methanol
ATR	Attenuated Total Reflection	MOF	Metal Organic Framework
BA	Benzaldehyde	MS	Mass Spectrometry
BET	Brunauer-Emmett-Teller	MV	Methyl Violet
BSE	Back-Scattered Electrons	MW	Microwave
BSTFA	N,O-Bis(trimethylsilyl)trifluoroacetamide	nPrOH	<i>N</i> -Propanol
CD	Cyclodextrin	ODD	Oil Deodorizer Distillate
CDPIS	Cyclodextrin Insoluble Polymer	OXY	Oxytetracycline
ChIA	Chlorogenic Acids	PEG	Polyethylene glycol Polyethylene
CV	Column Volume	PET	Terephthalate
DAD	Diode Array Detector	PI	Process Intensification Polyisobutene
DLS	Dynamic Light Scattering	PIT	Terephthalate <i>Para</i> -toluene sulfonic acid
DMF	Dimethylformamide	PTSA	Randomly Methylated Cyclodextrin
DMSO	Dimethyl sulfoxide	RAMEB	Raspberry Ketone
DOXY	Doxycycline	RK	Supercritical CO ₂
DR	Diffuse Reflectance	scCO₂	
EDC	1-Ethyl-3-(3-dimethylaminopropyl)carbodiimide	UV	Ultraviolet
EF	Environmental Factor	Vis	Visible
EMY	Effective Mass Yield		
EPA	Environment Protection Agency		
EtOAc	Ethyl Acetate		
EtOH	Ethanol		
FA	Formic Acid		
FAME	Fatty Acid Methyl Ester		
FESEM	Field Emission Scanning Electron Microscopy		
FFA	Free Fatty Acid		
FID	Flame Ionization Detector		
GC	Gas Chromatography		
GVL	Gamma-Valerolactone		
HHT	High Graphitization Degree		
HMF	Hydroxymethylfurfural		
HPLC	High Performance Liquid Chromatography		
HSM	Hydroxy succinimide		
<i>i</i>PrOH	<i>iso</i> -propanol		
IR	Infrared		

1.0 General introduction

The search for greener and more efficient chemical processes and synthesis has been the driving force behind scientific research in late years. The urge for a shift in paradigm increases as society tries to overlap economic and technological growth with the scarcity of natural resources we face. As the public opinion concerns with environmental preservation, public institutions demand greener protocols from chemical and pharmaceutical companies both with strict regulations and funds to boost the transition. However, this transition cannot happen if not from the roots of the system that is basic and applied research. Therefore, there is an argument for process intensification and green chemistry to be together.

In this thesis research work on the synthesis of new materials for heterogeneous catalysis and adsorption processes, and studies on green chemical syntheses and conversion are presented. The focus has been on the application of green chemistry principles on known but useful chemical reaction, coupled with the application of enabling technologies for process intensification, to start filling the gap between base research and real-life application. First, the guiding principles of this work are presented and discussed as a general introduction. A good start is presenting green chemistry and process intensification, the pillars on which the thesis is built and expanded.

1.1 Green Chemistry

Everyone has an instinctive understanding of what “green” means and therefore what green chemistry might be about; as scientist, however, we need a solid definition to properly apply it in our works. According to EPA (United States Environmental Protection Agency) green chemistry is “*the design of chemical products and processes that reduce or eliminate the use or generation of hazardous substances*”. So, our first goal in designing green processes should be avoiding toxic solvents or cancerous reagents in favour of less hazardous alternatives: a synthesis that substitutes chloroform with a non-toxic and bio-compatible solvent such as ethanol or even water is easy to consider green, however the preservation of selectivity and yield may not be so easy to translate. Indeed, waste reduction should also be considered in this design: if the same synthesis consumes large volumes of water that later needs to be removed by heating, only to produce small amounts of product with low yields, is it really green?

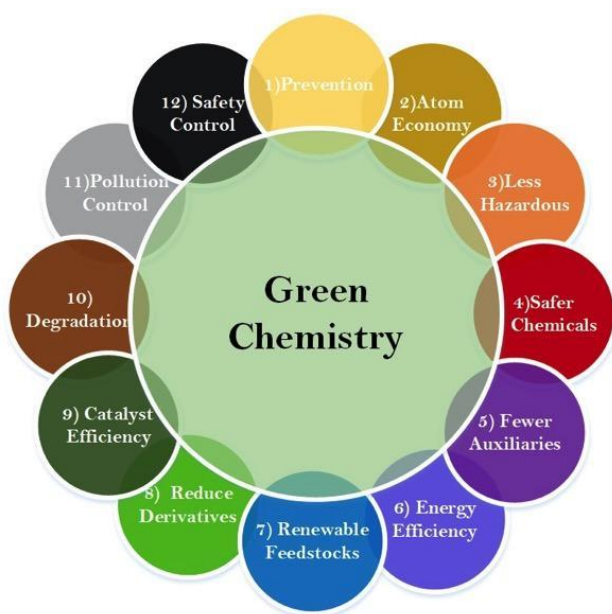


Figure 1: green chemistry principles (from Sylvatex).

Green chemistry is indeed a complex puzzle and perhaps it is better defined with its twelve principles (**Fig. 1**), introduced by Anastas and Warner in 1991 and then expanded in later works^{1,2}. Some of these will be discussed in further details as they have been extensively employed in this thesis. After its formal introduction, green chemistry was rapidly established in scientific institutions, for example with the institutions of renown awards such as the US Presidential Green Chemistry Challenge Awards (1996), the creation of the Green Chemistry Institute (1997) and the growing success of the journal *Green Chemistry* edited by the Royal Society of Chemistry (1999). In the same years different green metrics were introduced to quantify the

efficiency of chemical reaction and measure, in a sense, their sustainability.

Nowadays many research works focus on the application of green chemistry principles and in its role in leaving the oil-based chemistry in favour of renewable feedstocks tending towards what is called “biorefinery approach”. Now that we have established the bind and principles of green chemistry, ad in-depth discussion on the most important aspects for this thesis can be tackled.

1.1.1 Atom economy and green metrics

Atom economy (AE) was the first green metric to be introduced, but its simplicity and effectiveness makes it one of the most used even nowadays³⁻⁶: this concept was firstly introduced by Trost in 1991⁷ and tries to convey the efficiency of the synthesis of complex products without wasting atoms from the reagents⁸. In practical terms, it is the simple calculation of how many atoms from the reagents remain in the structure of the product. It reflects the efficiency of a synthesis and, if maximized, is directly linked to waste reduction; however, it should be noted that it does not account for the yield of the reaction but only analyses the performed reaction in its simplest and ideal form.

$$AE = \frac{MW \text{ product}}{\sum MW \text{ reagents}}$$

AE varies from different reactions but can also differ for the same reaction if run with different reagents. If we take for example the synthesis of benzylamine, many different approaches are possible. One might be starting from benzyl bromide, form the benzyl azide and then run a Staudinger reaction to get benzylamine: in this case AE is only 0.20 (**Fig.2**).

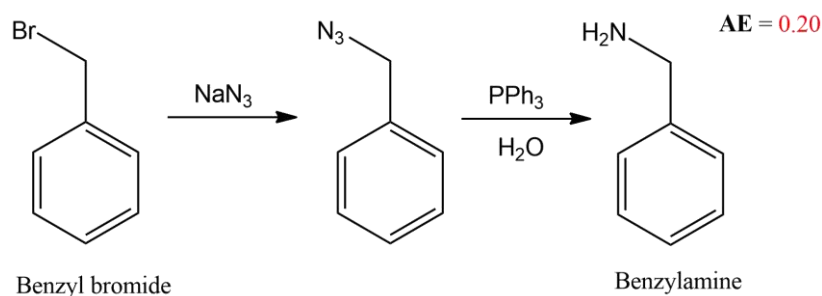


Figure 2: synthesis of benzylamine from benzyl bromide and its AE.

If we change the synthesis completely and run a reductive amination on benzaldehyde AE increases to 0.85 using H_2 as a reductant. This same synthesis can vary, however, if we decide to use NaBH_4 instead for the reduction step, lowering the AE to 0.66 (**Fig. 3**).

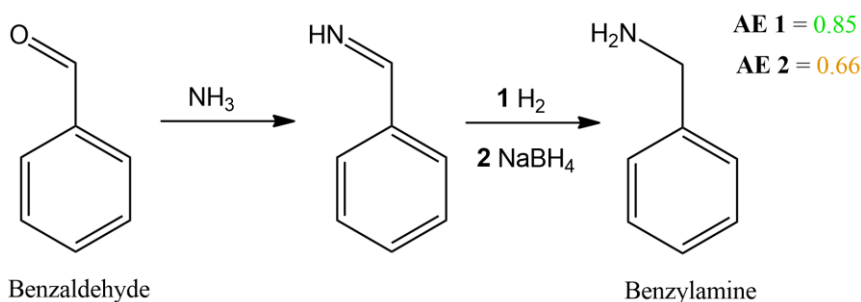


Figure 3: synthesis of benzylamine from benzaldehyde and possible AE.

The power of AE is its readily application; it is easy to calculate and understand and gives immediate feedback on the feasibility of a reaction. This is the root of its success and widespread, however this metric comes with limitations too: as previously mentioned, AE does not account for the yield, which may be influenced by equilibriums or side-reactions, nor the use of excess of reagent or volume or solvent⁹. All these parameters play a significant role on the success and scalability of a synthesis and, if they can be overcome in laboratory, can be much more problematic in pilot or plant scale.

Perhaps a more comprehensive metric is the environmental factor (EF), introduced in 1992¹⁰ to overcome the limitations of AE and is the ration between the mass of the wastes and the mass of the product. This offers a wide flexibility of application: from the basic stoichiometry to the real reaction accounting for solvent and excess of reagent or even include pre-treatments and workups.

$$EF = \frac{\sum \text{mass of the wastes}}{\text{mass of the product}}$$

EF is easily scalable and easy to calculate. It can also include yields, as long as the final product is quantifiable. If we stick to the reductive amination, we can see how easily it is to adapt the EF calculations to different approaches or necessities:

1. During the reaction, only one molecule of water is produced as waste, so the EF for the ideal case is only 0.17.
2. As discussed in a following chapter, the real synthesis was carried out using 100 μL of benzylamine in 5 mL of aqueous ammonia (32 %). In this case the consumption of ammonia and the release of water has a negligible effect and assuming 100 % yield the EF is of 45, mostly due to the excess of reactive solvent.
3. Since the boiling point of benzylamine is much higher than that of aqueous ammonia, the latter can be removed under vacuum and recycled. If we add this additional step to the calculations, then the EF becomes virtually zero.

EF is a potent metric that unites simplicity and flexibility; however, we should also consider that not all reagents and solvents are born the same: some pose a far major hazard than others even when used in the same quantity or less. For example, a reaction run in the same amount of water or benzene have far different environmental impact and pose different dangers to the operators.

A possible approach to address also this topic is using the effective mass yield (EMY) as metric, which is the ratio between the mass of the product and the mass of “nonbenign” reagents used.

$$EMY = \frac{\textit{mass of the product}}{\textit{mass of hazardous reagents}}$$

EMY should not be thought of as an alternative to EF, but more as a complement. Indeed, it does not account for the use of possibly huge quantities of safe substances like water but helps in underlying the consumption of hazardous materials relatively to the product. This is also useful to compare different alternatives for the same reaction. If we again consider the reductive amination of benzylamine, if the reduction step is performed with NaBH_4 the EMY is of 1.95, since benzaldehyde is a safe reagent. If we somehow use isopropanol (*i*PrOH) as a H-donor, since it is safe and non-toxic it does not fall in the calculation even being more massive than NaBH_4 , and so EMY rises to 6.3. Of course, this approach leaves room for interpretation on what is benign and what is not, since sometimes the definition is blurred.

It is clear that different metrics highlight different properties of the same synthesis or process and a certain degree of freedom for the user is unavoidable, so it is recommended to use more than one when designing a process to aim for a true green protocol. In this thesis green metrics will be calculated for the developed synthesis and, when possible, compared to previous works on the topic.

1.1.2 Green solvents

Solvents play a crucial role in the performance of a reaction, and they often compose the most part of its volume or mass, up to 80-90 wt.%¹¹ as shown in **Fig. 4**.

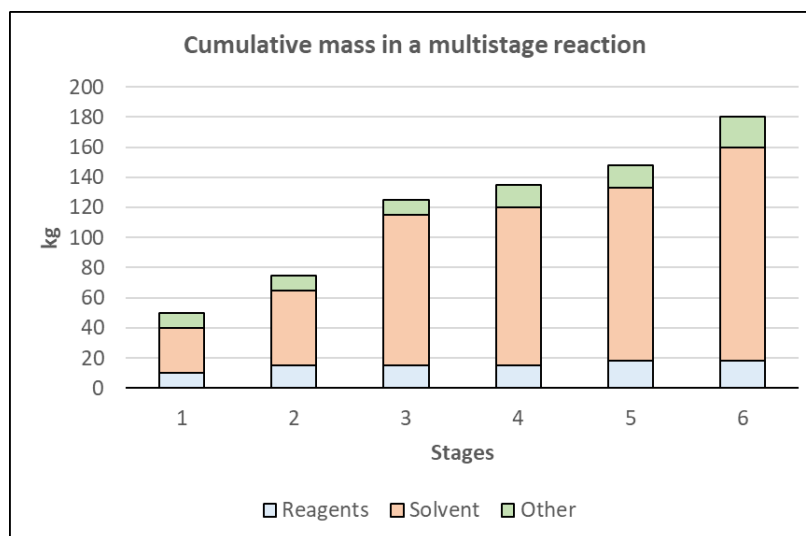


Figure 4: mass composition of a pharmaceutical multistep synthesis¹¹.

Traditional organic chemistry solvents such as methylene chloride or dimethylformamide are often toxic or hazardous¹²⁻¹⁴ and, despite the existence of greener alternatives, they are still widely employed in research work nowadays (**Fig. 5**).

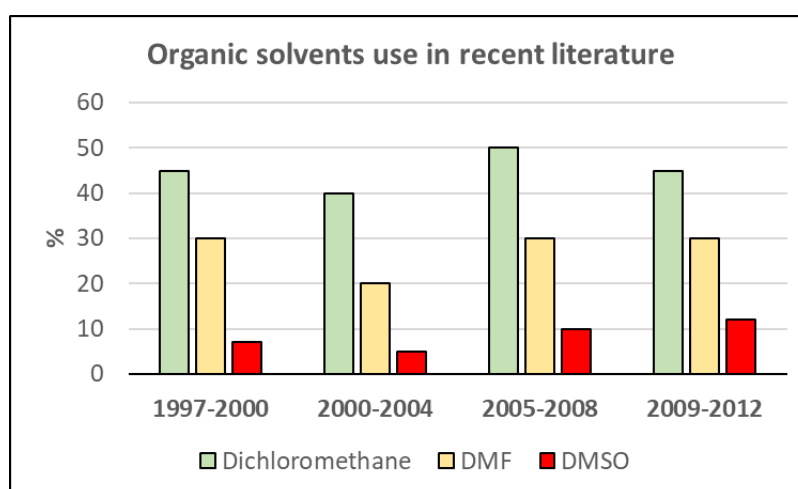


Figure 5: percentage of papers using solvents of concern from a 2015 survey¹².

This is not to say that in recent no effort was taken to shift towards greener solvents: since solvent consumption is a topic of concern for pharmaceutical industries, now many big players such as Pfizer or Astrazeneca have created tables and guidelines to avoid undesired solvents and substitute them with sustainable and safe ones^{15,16}. In general, a “green” solvent should be safe, non-toxic and biocompatible. Also, its volatility should be low both for safety and to reduce its dispersal in the environment.

Water is often regarded as the ideal green solvent: its abundant, cheap, safe to use (it is extremely hard to set it ablaze) and non-polluting¹⁷⁻¹⁹. A number of researches are focused on running organic chemistry in aqueous environment^{20,21}, often through the clever use of

micelles: micelles allow the suspension of lipophilic molecules in water, while the proper reaction takes place in a hydrophobic environment; this breakthrough allowed the substitution of DMF with water for a number of classic organic syntheses²²⁻²⁴. The sustainability of the solvent of choice is also important: ethanol, ethyl acetate and acetone are all examples of organic solvents derived from third generation biomasses and their use is preferred to other solvents derived from the oil industry. In recent years even more green solvents have been derived from biomasses and applied to organic syntheses or chemical conversions, some notable examples are: γ -valerolactone²⁵, 2-methyl tetrahydrofuran²⁶, dimethyl isosorbide^{27,28}, cyclopentyl methyl ether^{29,30}. These improvements are much needed to move away from oil refinery, from which many common organic solvents are derived.

In the works presented in this thesis, efforts to use green solvents have been made and the substitution of organic solvents of concern with greener alternatives will be underlined.

1.1.3 Renewable feedstocks

Many chemical building blocks that feed the chemical and pharmaceutical industry derive from oil. Oil is a precious resource and our society learned to exploit the most of it with refineries that separate it in all its components and send them in their specific market: solvent, fuels, base chemicals, and others. Though efficient, this production is not sustainable since oil is scarce and has a high environmental impact foresting our dependence on it. It is possible instead to derive many base chemicals from renewable feedstocks such as biomasses³¹.

Biomasses are categorized in three generations that also define their derivatives (**Fig. 6**). First generation biomasses are derived directly from food industries and are often edible like sugarcane or corn to produce bioethanol³². These biomasses create a competition with food applications with the risk of cultivations being devoted to fuel instead of feeding people, and the consumption of soil to create new crops; for these reasons they have mostly been surpassed. Second generation biomasses are non-food derived or even wastes. Lignocellulosic biomasses are such an example: they are mostly composed of cellulose, hemicellulose and lignin and they are cheap³³⁻³⁵. Their complex composition is both a challenge and an opportunity. From their cellulose and hemicellulose portion we can derive both biofuels, via fermentation³⁶, and hexose and pentose sugars, from hydrolysis^{37,38}. Such sugars can then be used as platform chemicals for further conversions. Then comes the lignin fraction. Lignin is a complex polymer with no fixed structure, but mostly made up of three components rearranged: *p*-coumaryl alcohol, coniferyl alcohol and sinapyl alcohol³⁹⁻⁴¹. These three base-components vary in relative quantity between hardwood, softwood and grasses. From lignin a number of aromatic compounds can be derived, paving an alternative way than oil refinement^{42,43}. Finally, third generation biomasses involve biotechnology: they are microorganisms specifically studied and grown to produce chemicals or fuels^{44,45}.

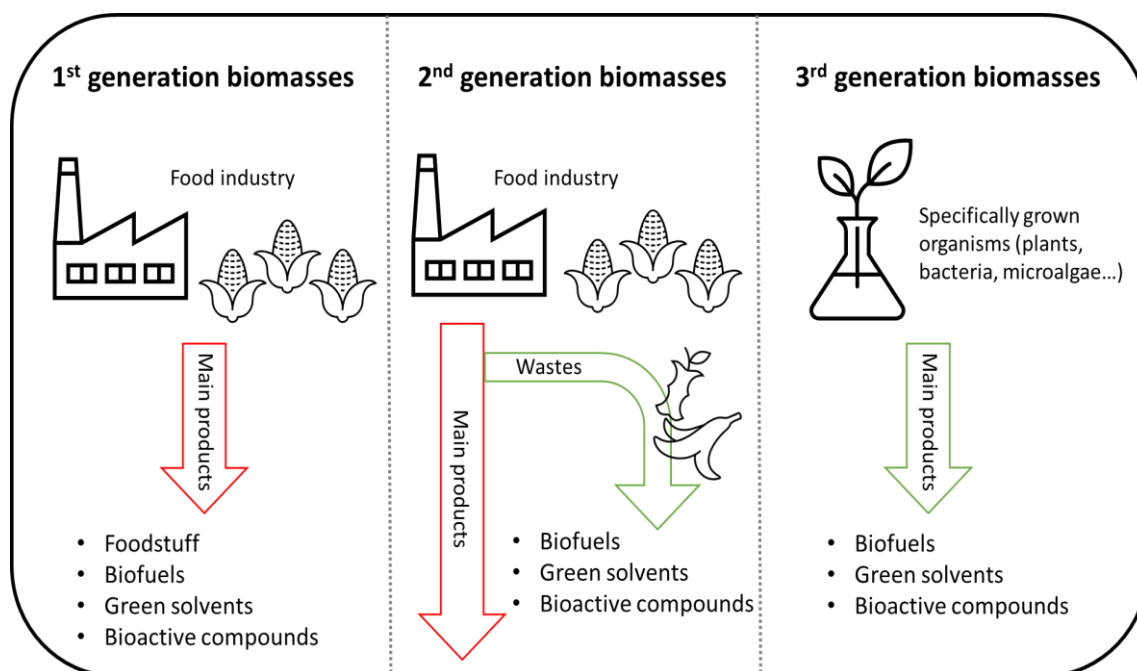


Figure 6: scheme of the three biomass generations.

For the moment, lignocellulosic biomasses are the most interesting for chemical research. Scientific research is trying to apply a biorefinery approach to obtain high added value compounds from this cheap and renewable source⁴⁶⁻⁴⁸. To be effective and comparable to oil-refineries, biorefineries should be able to produce a wide spectrum of products: from fine chemicals to base chemicals to the thermal treatment of the final wastes. So far this approach has been difficult to implement, both because of current technological limitations and the intrinsic variability in biomass feedstocks, so it is important to continue the research in effective biomass conversion; however there are examples of successful and economically sustainable biorefineries, as in the case of citrus peels from which it is possible to obtain fine chemicals (essential oils, polyphenols...), base products (cattle feed) and energy sources (methane and syngas)⁴⁹⁻⁵¹.

The use of renewable feedstocks for chemical conversion is a topic of paramount importance for the future of green chemistry, and the only way for a sustainable process. In 2004 a list of the most promising products (**Table 1**) from integrated biorefineries was published by the US Department of Energy and has guided the research in this field ever since^{52,53}. In this thesis, a careful approach in the choice of solvents and reagents has been taken, with the intent of starting from cheap bio-derived compounds and convert them to fine chemicals through green methods to help the progression to widespread biorefinery integration with chemical and pharmaceutical industry.

Table 1: the DOE top chemicals from carbohydrates.

Succinic, fumaric and malic acid	Itaconic acid
2,5-Furan dicarboxylic acid	Levulinic acid
3-Hydroxypropionic acid	3-Hydroxybutyrolactone
Aspartic acid	Glycerol
Glucaric acid	Sorbitol
Glutamic acid	Xylitol

1.1.4 Heterogeneous catalysis

A catalyst is a substance that lowers the activation energy of a reaction without being consumed in the process. This speeds up the reaction rate and also allows milder reaction conditions often resulting in better selectivity and yield. A catalyst can be as simple as the addition of an acid in Fischer's esterification or something more complicated as a Ru complex for the hydrogenation of artemisinic acid⁵⁴. These two, however, are both examples of homogeneous catalysts: a homogeneous catalyst is already a liquid or can be dissolved in the solvent of choice. Though effective they can be difficult to remove from the reaction mixture often needing a liquid phase extraction that consumes organic solvents.

A greener alternative is the use of heterogeneous catalysts, which is a solid insoluble substance that remains as a separate phase during the reaction. One kind of solid catalysts are metallic nanoparticles supported on porous materials. Transition metals are often used as catalysts for a wide number of organic reactions⁵⁵⁻⁵⁷. The preparation methods of metal nanoparticles can be classified firstly as top-down or bottom-up: top-down techniques start from a bulk material and break it into smaller elements, whereas bottom-up techniques build nanoparticles from scratch via nucleation processes^{58,59}. Another classification is possible on their phase: liquid, gaseous or solid. The most common procedures for liquid phase syntheses include the wet impregnation of the support with a soluble salt followed by a chemical reduction or the precipitation-deposition of the metal hydroxide followed by the chemical reduction^{60,61}. The size and dispersion of the nanoparticles can be controlled by the operative parameters (stirring rate, temperature, concentration...) or the addition of surfactants that later need to be removed by careful washing or pyrolysis⁶².

The advantages of heterogeneous catalyst are their easy removal and recycle. For laboratory scale reactions, powder catalysts are common, while for pilot or production scale processes often the solid catalysts are employed as pellets or porous blocks. Either way, at the end of the reaction they can be removed by filtration or centrifugation, avoiding the contamination of the products; this without the employment of further organic solvent. A minimal amount of solvent is of course necessary to wash them before their recycle⁶³⁻⁶⁵. The possibility to easy recover and reuse them make heterogeneous catalyst both economically and environmentally sustainable. Another advantage for the works presented later in this thesis is the synergistic interaction between metal nanoparticles and MW radiation, as previously discussed. The only true problematics with metal-based heterogeneous catalysts are the reduced mass transfer compared to homogeneous catalysts (which needs to be compensated by vigorous stirring) and the possible metal leaching to the liquid solution.

In this thesis, heterogeneous catalysis has been extensively employed both with commercial and with newly synthesized catalysts. This was both to develop sustainable syntheses and to exploit the hotspot formation under MW heating to promote the studied chemical reactions.

1.2 Process intensification

Process intensification (PI) is another broad term that intersects with green chemistry. As a general definition, PI involves the design for smaller, safer and more efficient processes. This can happen through different paths and technologies; from a strictly scientific point of view an improvement in process efficiency needs to maximize the driving force of the reaction

and the rate of intra and intermolecular events. Kinetic and thermodynamic studies are needed and can then be used for the design of new technological equipment: we can safely state that PI is an integrated approach that aims for efficiency and technological improvement⁶⁶. In particular, it has been proposed to classify four different PI approaches that, alone or together, can achieve the set objective: structure and special domain, energy and thermodynamic domain, synergy and functional domain, time and temporal domain⁶⁷.

An European roadmap for PI exist, targeting petrochemical (PETCHEM) and fine chemical (FINEPHARM) industries as high importance sectors for new technologies to improve energy savings, selectivity of the processes and reduce waste production⁶⁸. As an example, the shift from stirred tank reactors to reactors for fine chemicals was predicted to lead to improve selectivity and yield by 20 % (as an average) maintaining the production output. The reduction in volumes makes a process intrinsically more controllable and safer and the increase in efficiency and selectivity leads to less waste production and so to a greener reaction. Even though at its core PI primarily deals with the reduction of working volumes this does not mean, of course, to produce less *product*, but instead producing the same amount or more with less solvent and in smaller reactors. This of course is a challenging quest and new technologies are needed together with the research for greener and faster chemical reactions.

In this roadmap, enabling technologies are mentioned as tools to improve the industry efficiency. Such technologies are also referred to in the European Horizon 2020 program, a formidable tool of public funding destined for research facilities and industries alike⁶⁹. Such technologies are characterized by sharp advantages respect to conventional ones but often need capital investment and a careful optimization to be competitive. They are however established as the future to aim to, and their application is studied in applied research to be then scaled to pilot scale and finally plant scale.

1.2.1 PI and scalability of a reaction

As aforementioned, the downsizing of a reactor does not mean downsizing the product output. To be successful outside the laboratory, a reaction must be easily scalable. This means that the same result that a Ph.D. student obtains on the mL scale must be reproduced, if not improved, on the litre and then the hundreds of litre scale. This is where many project fail and are abandoned for not being economically feasible.

The most intuitive way to scale a reaction up is to build a larger reactor. Often a “true” scale-up is considered when a tenfold increase in working volume is accomplished: if the reaction is successful is then considered promising for a real-life application. This approach leaves unaltered the ratios of the reaction component, however is not always in line with the PI guidelines and can result in cumbersome, unsafe production plants. An alternative is a numbering-up of small process units to work in parallel. Small-scale reactors are intrinsically safer and easier to control and from the economic point of view it can be more advantageous to use mor smaller units instead of a bigger one: the cost of scaling-up an equipment is usually exponentially correlated to its size, while the installation costs of more units follow a linear progression⁷⁰. Of course this approach is not without its challenges, mainly due to the correct redistribution of fluids and phases in the different reactors⁷¹.

Finally, one can also improve the productivity of a process without making it substantially bigger. This can be accomplished with the application of enabling technologies or the use of flow reactors instead of batch reactors of similar size.

1.2.2 Enabling technologies for PI

Enabling technologies are new technological tools to improve efficiency and efficacy of a process. There are many examples applied to chemistry but two of them will be presented in detail having been used in many experiments in this thesis: MW and ultrasound (US). These technologies can also help to reduce the energy consumption of a reaction, which is an important factor in moving from a fume hood to a factory line. A primary goal should be the use of mild reaction conditions with the ideal being room temperature and atmospheric pressure. Often running a successful reaction in these conditions is not possible, so the focus should be finding the “sweet spot” that maximizes yield at the lowest temperature and pressure possible, so a screening of the experimental space is needed. If available, design of experiment software can be a huge help reducing the necessary experiments using mathematical predictions starting from real data points. In this thesis extensive screening of reaction conditions were applied in all syntheses to move towards the mildest possible.

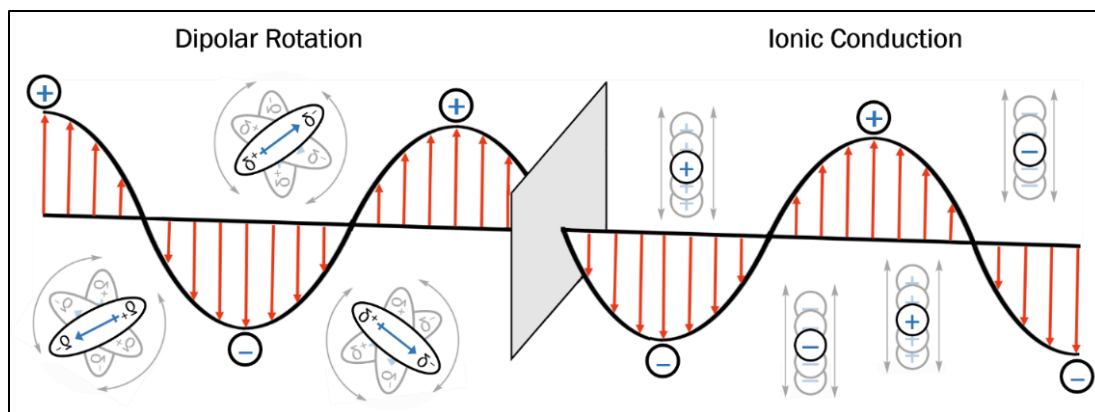


Figure 7: MW heating through dipole rotation and ionic conduction (from CEM.com).

A great portion of the energetic consumption of a reaction goes into heating. In this regard, microwaves (MW) offer a significant advantage over conventional heating. Instead of transferring heat through convection, MW work with the interaction of dipoles with the electromagnetic field generated by a magnetron (**Fig. 7**). MW are electromagnetic waves with frequencies between 0.3 to 300 GHz, but most of the equipment are set to 2.45 GHz, to avoid interferences with telecommunications. The efficiency of MW heating depends on the dielectric properties of the heated materials: the ability of a material to convert MW radiation to heat is defined by its loss factor $(\tan\delta)^{72}$.

$$\tan \delta = \frac{\epsilon''}{\epsilon'}$$

In the equation, ϵ'' represents the dielectric loss or the efficiency of the conversion between MW and heat, while ϵ' is the dielectric constant that indicates the tendency of the material to be polarized by an electric field. The higher the loss factor, the better a material is heated by MW radiation. The values for some common solvents are listed below in **Table 2**.

Table 2: loss factor for some common solvents⁷³

Solvent	$\tan\delta$
Water	0.12
Methanol	0.66
Ethanol	0.94
Isopropanol	0.80
Chloroform	0.09
Toluene	0.04
Hexane	0.02

The physical phenomenon at the base of MW heating is the oscillation of dipoles as they try to follow the oscillating electromagnetic field. This re-alignment to the field is never perfect, and energy is lost in form of heat: we can think of it as a drag generated by the oscillation of polar molecules. MW effects are generally described as thermal and non-thermal⁷⁴. Thermal effects include for example the creation of an inverse thermal gradient respect to conventional heating: dielectric heating is volumetric, and the irradiated sample starts to heat up from inside, instead than from the external walls (**Fig. 8**).

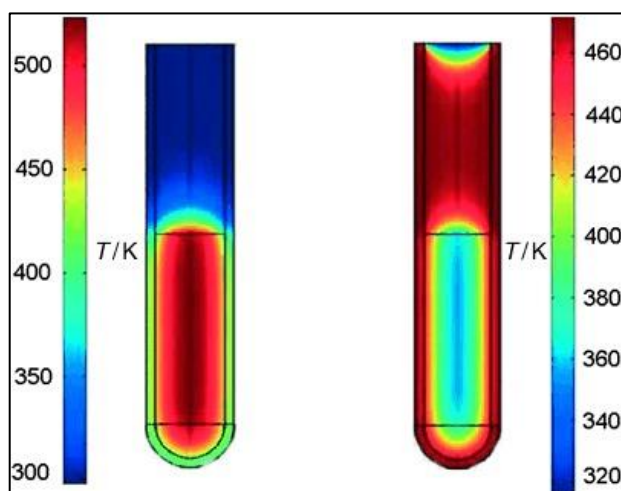


Figure 8: MW induced inverse thermal gradient (left) versus conventional heating (right)⁷⁵.

Also, since dielectric heating is highly selective it is possible to create hotspots at a higher temperature than the bulk: this is often the case when heterogeneous catalysts are used, and this can enhance the catalytic activity and activate reaction paths at lower overall temperatures. This phenomenon was well reported by Bogdal *et al.* with the use of a CrO_2 catalyst for the oxidation of alcohol using toluene as solvent (**Fig. 9**): the catalyst rapidly reached a 140 °C temperature, superior to that of the bulk solution⁷⁶. This effect can be further enhanced using strongly absorbing materials to induce a rapid heating of the less-absorbing bulk, or to speed up the reaction or decomposition on their surfaces⁷⁷.

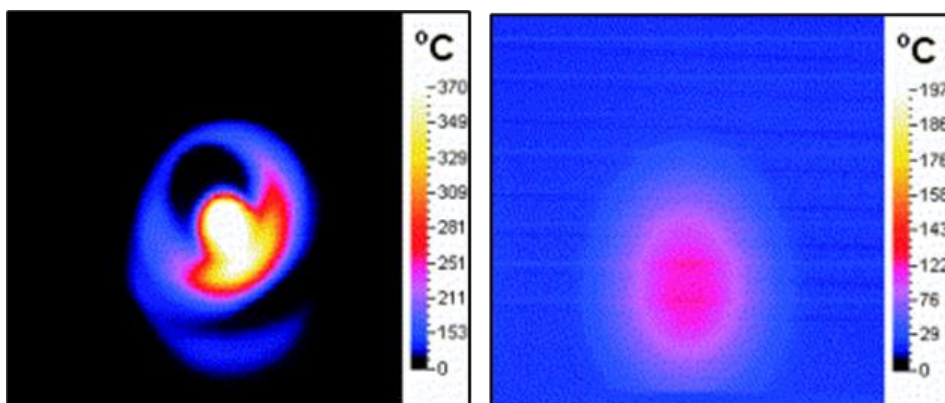


Figure 9: hotspots formed over CrO₂ under MW heating, without (left) and with solvent (right)⁷⁶.

MW can also be used in biphasic systems to selectively heat only the polar phase. One excellent example is the reactive extraction performed by Ricciardi and co-workers, where a bi-phasic system of water and toluene was used to convert xylose to furfural and immediately extract it to avoid its decomposition, allowing a higher yield and a 50 % reduction in side-products compared to convective heating⁷⁸. MW heating dependence on the characteristic of the irradiated material can also cascade in energy savings: the fact that some materials, like Teflon, are transparent to MW allow a direct heating of the sample, without wasting energy on the walls of the reactor. Also, MW can often shorter reaction times from hours to minutes: this was proven for a number of organic reactions in literature and can have an enormous impact on productivity and energy savings⁷⁹. Different studies have compared the energy efficiency of MW reactors to conventional ones for common organic syntheses of the litre scale, finding that MW could indeed lead to improved energy efficiency, though this also depend on the scale and the reaction itself so it is not a general assumption^{80,81}. Even when the energy efficiency of MW, strictly in heating effect, is less than the conventional methods, they more than made up to it with short reaction times⁸².

On practical terms, a MW reactor is composed of three fundamental parts: a magnetron, a waveguide and a reaction chamber. The magnetron is the source of MW, which are produced by a red-hot filament under vacuum that emits electrons: the path of the electrons and the size of the magnetron influence the final frequency of the MW. The MW are captured by a metal spire and travel through a metal pipe (the waveguide) to the reaction chamber, where the sample is exposed to the radiation. The distribution of MW in the chamber separates the reactors into two categories as represented in **Fig. 10**: multimodal and monomodal. In a multimodal reactor MW bounce randomly between the walls of the chamber, ideally creating a homogeneous irradiation which is useful for multiple or massive samples. In a monomodal reactor a static wave fills the chamber and the sample is posed in correspondence of its antinode, where the radiation intensity is maximized⁸³.

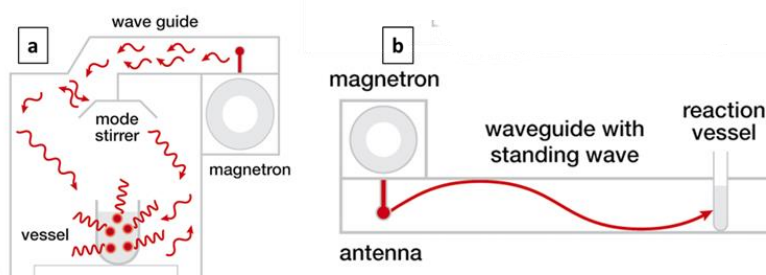


Figure 10: multimodal (a) and monomodal (b) MW reactor scheme (from Anton-Paar.com).

Surprisingly few industrial scale MW reactors exist for chemical conversions. Even though MW offer significant advantages compared to convective heating, they have proven difficult to scale up; on one hand the MW efficiency is higher the more massive is the sample (since small samples will not interact with the electromagnetic waves) but on the other as the reactor size increase it becomes difficult to control the temperature of the process. This is mainly due to the limited penetration depth of MW in polar solvent, since it is inversely proportional to its dielectric constant: for big scale reactors this means that only few centimetres of liquid will be properly heated. Proper mixing can reduce these inhomogeneities, however if the process is not well designed it can happen that the bulk of the solvent is cold while the solvent next to the waveguide gets overheated.

This is not to say that a scale up is impossible, but many factors must be taken into consideration: the materials, the geometry of the reactor, the stirring rate⁸⁴. Sometimes, computational modelling can be helpful in the design of industrial scale reactors⁸⁵. Another possibility is to transition from batch to flow reactors: flow reactors have a higher productivity and can work with smaller volumes, essentially eliminating all the problems deriving from the bulk of the reaction. The applicability of flow chemistry for MW-assisted reactions has been extensively proven even at production scale^{86,87}. The influence on the temperature gradient with or without a stirring system is visualized in **Fig. 11**.

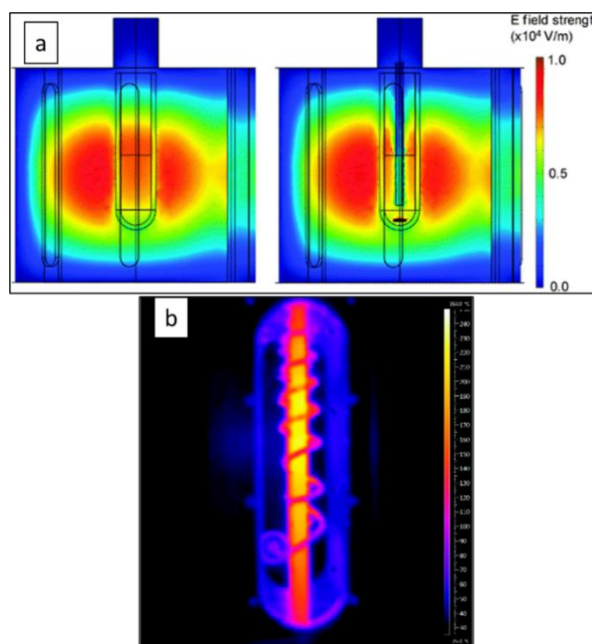


Figure 11: effect of an internal stirrer on field distribution (a)⁸⁴ and homogeneous temperature distribution in a flow MW reactor (b)⁸⁸.

In this thesis, MW have been extensively applied for chemical syntheses and conversions. This approach often led to a significant reduction in reaction time and in the working temperature, with a synergistic effect with the use of metallic catalysts. This further allowed the application of green chemistry principles in the studied reactions, paving the way to the creation of greener protocols compared to literature.

Another key enabling technology for chemical processes are US. US are sound waves above 20 kHz of frequency. Depending on their exact frequency they find different application: from medicine to material science to sonochemistry. Usually, US are applied for sonochemistry mainly in the range between 20-150 kHz. They derive most of their properties to the phenomena of cavitation: the formation and energetic collapse of vapour bubbles inside the liquid they travel. The propagation of US creates zones of compression and decompression in the medium (**Fig. 12**); the decompression allows the formation of microbubbles that grow and collapse in the span of few microseconds. This collapse releases a great amount of energy in a small volume, creating a hotspot of high temperature and pressure while the bulk of the solvent remains at the same temperature. These hotspots can kickstart chemical reactions, release radicals and the turbulence of cavitation dramatically improves the mass transfer compared to mechanical stirring^{89,90}.

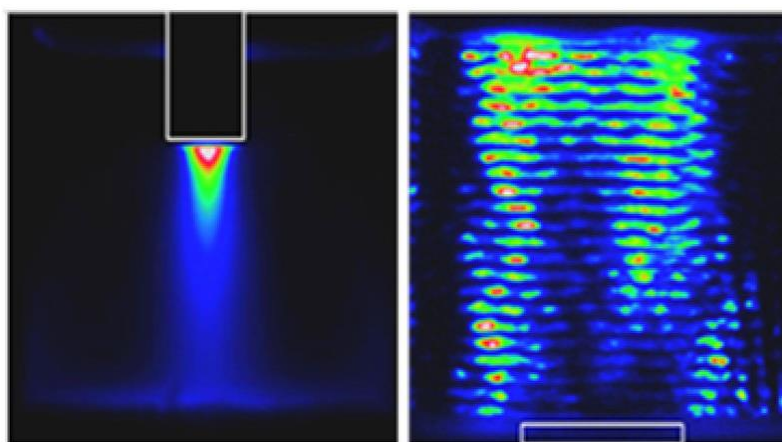


Figure 12: cavitation and US propagation differences between a ultrasonic horn (left) and plate (right)⁹¹.

How efficient cavitation is depends on different factors. Firstly, the frequency and intensity of the applied US. Then one must also consider the solvent: US are best used with high-boiling solvents like water, otherwise the microbubbles will be too stable and release little energy. Temperature is also a factor: over time also the bulk temperature will increase at a rate depending on the thermal capacity of the solvent and the intensity of US. As temperature increases the vapour phase becomes more favoured and cavitation is hindered.

Another interesting field of application of US is sonocrystallization. The compression waves can indeed induce nucleation in a supersaturated solution at a faster rate than most conventional methods, reducing the induction time. Also, the energy transfer of US is so efficient that the metastable zone is reduced, allowing crystallization processes at lower concentrations and/or at higher temperatures compared to classical protocols. Also, as crystals grow, they are subjected to sonofragmentation, and this often leads to smaller and more homogeneous crystals respect to other methods⁹²⁻⁹⁴. Another possible application for

US is the rapid oxidation of pollutants in wastewaters: since high frequency US produce a large amount of radicals they can be exploited to remove dangerous molecules from water solution, potentially without using other reagents but more often than not they are used in tandem with ozone and UV light to enhance the oxidizing effects^{95,96}. US can be applied via ultrasonic plates or, more common on the larger scales, ultrasonic horns. Ultrasonic horns work starting from a generator that creates an electric signal of the needed frequency and is then translated into mechanical vibrations by a piezoelectric crystal connected to the body of the horn. The horn must be of a length that can resonate with the frequency and transmits the US from its tip; horns are usually made of ceramics, glass or more commonly titanium⁹⁷⁻⁹⁹.

As for MW, cavitation can only travel so far in a liquid so once again the miniaturization of the system is recommended. For US however this is less of a problem since they can be generated directly inside the operative unit and multi-nodal ultrasonic horn exist to maximise the homogeneity of cavitation offering competitive performances on production scale.

1.2.3 Flow chemistry

Flow chemistry operates in small tubular reactors instead of cumbersome batch ones which are often seen in chemical plants. A flow reactor has intrinsically higher productivity respect to a batch one, since it eliminates charge, discharge, heating, cooling and cleaning steps. This allows production of large quantities of products in a relatively small working volume, accordingly to PI principles. However, flow chemistry provides much more than a simple increase in productivity, although that is certainly appealing on its own. Flow chemistry allows industries to exploit hazardous chemistry that would be too difficult to control in large batches: nitrations, organometallic reactions, functionalization of diazo compounds and more¹⁰⁰⁻¹⁰².

Flow chemistry offers advantages when it comes to speed, safety and selectivity as reactions are run in smaller volumes (without sacrificing productivity), and thus parameters such as residence time, temperature and concentrations can be carefully controlled. Moreover, as residence time and ambient conditions can be tailored, handling reactive intermediates becomes much easier and more selective than in batch chemistry¹⁰³. Temperature is a key parameter for successful syntheses and safe processes, and can be determined using thermocouples, infrared (IR) sensors or optical fibres. As we have discussed, large differences can exist from the surface and the bulk of a reaction vessel, however with flow equipment the bulk becomes less and less relevant allowing for finer measurements. Also, flow chemistry becomes even more appealing when coupled with the short-penetrating MW and US¹⁰⁴.

It is clear that flow chemistry offers many advantages for industrial production and interfaces well with green chemistry and process intensification. Efforts should be made to switch from batch to flow both in laboratory and in production scale.

References

1. Anastas P, Warner J *Green Chemistry: Theory and Practice*. 1st ed. Oxford: Oxford University Press.
2. Anastas P, Eghbali N. *Chemical Society Reviews*, 2010, **39**, 301-312.

3. Calvo-Flores FG. *ChemSusChem*, 2009, **2**, 905–919.
4. Thulasi KM, Manikoth ST, Ranjusha MK, et al. In: *Green Chemistry and Applications*. CRC Press, pp. 5–36.
5. Lim FPL, Dolzhenko A V. In: *Green Sustainable Process for Chemical and Environmental Engineering and Science*. Amsterdam: Elsevier, 2020, pp. 1–12.
6. Molloy JJ, Morack T, Gilmour R. *Angew Chemie - Int Ed*, 2019, **58**, 13654–13664.
7. Trost BM. *Science*, 1991, **254**, 1471–1477.
8. Trost BM. *Angew Chemie Int Ed English*, 1995, **34**, 259–281.
9. Eissen M, Mazur R, Quebbemann HG, et al. *Helv Chim Acta*, 2004, **87**, 524–535.
10. Sheldon RA. *Green Chem*, 2017, **19**, 18–43.
11. Constable DJC, Jimenez-Gonzalez C, Henderson RK. *Org Process Res Dev*, 2007, **11**, 133–137.
12. Ashcroft CP, Dunn PJ, Hayler JD, et al. *Organic Process Research and Development*, 2015, **19**, 740–747.
13. Slater CS, Savelski MJ, Carole WA, et al. In: *Green Chemistry in the Pharmaceutical Industry*. John Wiley & Sons, Ltd, pp. 49–82.
14. Joshi DR, Adhikari N. *J Pharm Res Int*, 2019, **28**, 1–18.
15. Byrne FP, Jin S, Paggiola G, et al. *Sustain Chem Process*, 2016, **4**, 1–24.
16. Hargreaves CR, Manley JBACS GCI Pharmaceutical Roundtable Collaboration to Deliver a Solvent Selection Guide for the Pharmaceutical Industry, www.acs.org/gcipharmarroundtable.
17. Breslow R. In: *Handbook of Green Chemistry*. American Cancer Society, pp. 1–29.
18. Hartonen K, Riekkola ML. In: *The Application of Green Solvents in Separation Processes*. Elsevier, 2017, pp. 19–55.
19. Castro-Puyana M, Marina ML, Plaza M. *Curr Opin Green Sustain Chem*, 2017, **5**, 31–36.
20. Lipshutz BH, Ghorai S, Cortes-Clerget M. *Chem - A Eur J*, 2018, **24**, 6672–6695.
21. Cortes-Clerget M, Yu J, Kincaid JRA, et al. *Chem Sci*, 2021, **12**, 4237–4266.
22. Gallou F, Guo P, Parmentier M, et al. *Org Process Res Dev*, 2016, **20**, 1388–1391.
23. Isley NA, Linstadt RTH, Kelly SM, et al. *Org Lett*, 2015, **17**, 4734–4737.
24. Parmentier M, Wagner MK, Magra K, et al. *Org Process Res Dev*, 2016, **20**, 1104–1107.
25. Kumar A, Thompson-Adewumi A, Nandhini KP, et al. *Org Process Res Dev*, 2019, **23**, 1096–1100.
26. Pace V, Hoyos P, Castoldi L, et al. *ChemSusChem*, 2012, **5**, 1369–1379.
27. Russo F, Galiano F, Pedace F, et al. *ACS Sustain Chem Eng*, 2020, **8**, 659–668.
28. Aricò F, Tundo P. *Beilstein J Org Chem* 12218, 2016, **12**, 2256–2266.
29. de Gonzalo G, Alcántara AR, Domínguez de María P. *ChemSusChem*, 2019, **12**, 2083–2097.
30. Azzena U, Carraro M, Pisano L, et al. *ChemSusChem*, 2019, **12**, 40–70.
31. Zhang XS, Yang GX, Jiang H, et al. *Sci Rep*, 2013, **3**, 1–7.
32. Canilha L, Chandel AK, Suzane Dos Santos Milessi T, et al. *J Biomed Biotechnol*, **2012**. Epub ahead

- of print 2012. DOI: 10.1155/2012/989572.
33. Isikgor FH, Becer CR. *Polym Chem*, 2015, **6**, 4497–4559.
 34. Tayyab M, Noman A, Islam W, et al. *Appl Ecol Environ Res*, 2018, **16**, 225–249.
 35. Zoghلامي A, Paës G. *Front Chem*, 2019, **7**, 874.
 36. Sabiha-Hanim S, Asyikin Abd Halim N. In: *Fuel Ethanol Production from Sugarcane*. IntechOpen. Epub ahead of print 5 November 2019. DOI: 10.5772/intechopen.81656.
 37. Qin L, Li W-C, Zhu J-Q, et al. Springer, Singapore, pp. 3–41.
 38. Binder JB, Raines RT. *Proc Natl Acad Sci U S A*, 2010, **107**, 4516–4521.
 39. Rencoret J, Gutiérrez A, Nieto L, et al. *Plant Physiol*, 2011, **155**, 667–682.
 40. Lourenço A, Pereira H. In: *Lignin - Trends and Applications*. IntechOpen. Epub ahead of print 20 December 2018. DOI: 10.5772/intechopen.71208.
 41. Patil ND, Tanguy NR, Yan N. In: *Lignin in Polymer Composites*. William Andrew Publishing, 2016, pp. 27–47.
 42. Kim SR, Ko JK, Kim K, et al. In: *Biomass, Biofuels, Biochemicals*. Elsevier, 2021, pp. 15–32.
 43. Wen J-L, Wang H-M, Ma C-Y, et al. In: *Biomass, Biofuels, Biochemicals*. Elsevier, 2021, pp. 33–55.
 44. Raheem A, Prinsen P, Vuppaladadiyam AK, et al. *J Clean Prod*, 2018, **181**, 42–59.
 45. Jabeen N, Majid I, Nayik GA. *Cogent Food Agric*, 2015, **1**, 1117749.
 46. Cheng H, Wang L. *Biomass Now - Sustain Growth Use*. Epub ahead of print 30 April 2013. DOI: 10.5772/51491.
 47. Saini R, Osorio-Gonzalez CS, Hegde K, et al. *Curr Sustain Energy Reports 2020 74*, 2020, **7**, 122–136.
 48. Saini JK, Gupta R, Hemansi, et al. 2019, 25–46.
 49. Patsalou M, Chrysargyris A, Tzortzakis N, et al. *Waste Manag*, 2020, **113**, 469–477.
 50. González-Rivera J, Spepi A, Ferrari C, et al. *Green Chem*, 2016, **18**, 6482–6492.
 51. Joglekar SN, Pathak PD, Mandavgane SA, et al. *Environ Sci Pollut Res*, 2019, **26**, 34713–34722.
 52. Bozell JJ, Petersen GR. *Green Chem*, 2010, **12**, 539–55.
 53. Werpy T, Petersen G. *Top Value Added Chemicals from Biomass Volume I*. Epub ahead of print 1 August 2004. DOI: 10.2172/15008859.
 54. Li J, Shen J, Xia C, et al. *Org Lett*, 2016, **18**, 2122–2125.
 55. Jagtap RA, Punji B. *Asian J Org Chem*, 2020, **9**, 326–342.
 56. Fanourakis A, Docherty PJ, Chuentragool P, et al. *ACS Catal*, 2020, **10**, 10672–10714.
 57. Colonna P, Bezenine S, Gil R, et al. *Adv Synth Catal*, 2020, **362**, 1550–1563.
 58. Irvani S. In: *Metal Nanoparticles*. John Wiley & Sons, Ltd, pp. 15–31.
 59. Marinescu L, Fikai D, Oprea O, et al. *J Nanomater*, 2020. Epub ahead of print 2020. DOI: 10.1155/2020/6651207.
 60. Barkhuizen D, Mabaso I, Viljoen E, et al. *Pure Appl Chem*, 2006, **78**, 1759–1769.

61. White RJ, Luque R, Budarin VL, et al. *Chem Soc Rev*, 2009, **38**, 481–494.
62. An K, Somorjai GA. *ChemCatChem*, 2012, **4**, 1512–1524.
63. Bhanage BM, Arai M. *Catal Rev - Sci Eng*, 2001, **43**, 315–344.
64. Arai M, Zhao F. *Catalysts*, 2015, **5**, 868–870.
65. Sheldon RA, Van Bekkum H *Fine Chemicals through Heterogeneous Catalysis*. Wiley-VCH, 2007. Epub ahead of print 2007. DOI: 10.1002/9783527612963.
66. Boffito DC, Fernandez Rivas D. *Can J Chem Eng*, 2020, **98**, 2489–2506.
67. Van Gerven T, Stankiewicz A. *Ind Eng Chem Res*, 2009, **48**, 2465–2474.
68. Dopfer JG, van Luijk GJ, van Harten GA, et al. *European Roadmap for Process Intensification*. 2000.
69. Butter M, Fischer N, Gijsberg G, et al. *Horizon 2020: Key Enabling Technologies (KETs), Booster for European Leadership in the Manufacturing Sector*. 2014.
70. Weber RS, Askander JA, Barclay JA. *J Adv Manuf Process*, 2021, **3**, e10074.
71. Shen Q, Zhang C, Tahir MF, et al. *Chem Eng Process - Process Intensif*, 2018, **132**, 148–159.
72. Gabriel C, Gabriel S, Grant EH, et al. *Chem Soc Rev*, 1998, **27**, 213–223.
73. Hayes BL *Microwave synthesis: chemistry at the speed of light*. 1st ed. CEM Pub, 2003. Epub ahead of print 2003. DOI: 10.5860/choice.40-4619.
74. de la Hoz A, Díaz-Ortiz À, Moreno A. *Chem Soc Rev*, 2005, **34**, 164–178.
75. Schanche JS. *Mol Divers*, 2003, **7**, 293–300.
76. Bogdal D, Lukasiewicz M, Pielichowski J, et al. *Tetrahedron*, 2003, **59**, 649–653.
77. Katsuki H, Kamochi N, Komarneni S. *Chem Mater*, 2008, **20**, 4803–4807.
78. Ricciardi L, Verboom W, Lange JP, et al. *ChemSusChem*, 2020, **13**, 3589–3593.
79. Kappe CO. *Angewandte Chemie - International Edition*, 2004, **43**, 6250–6284.
80. Devine WG, Leadbeater NE. *Arkivoc*, 2011, **2011**, 127–143.
81. Moseley JD, Woodman EK. *Energy and Fuels*, 2009, **23**, 5438–5447.
82. Kappe CO. *Chem Soc Rev*, 2008, **37**, 1127–1139.
83. Rana KK, Rana S. *OALib*, 2014, **01**, 1–20.
84. Robinson J, Kingman S, Irvine D, et al. *Phys Chem Chem Phys*, 2010, **12**, 4750–4758.
85. Goyal H, Mehdad A, Lobo RF, et al. *Ind Eng Chem Res*, 2020, **59**, 2516–2523.
86. Martina K, Cravotto G, Varma RS. *J Org Chem*. Epub ahead of print 2021. DOI: 10.1021/acs.joc.1c00865.
87. Estel L, Poux M, Benamara N, et al. *Chem Eng Process - Process Intensif*, 2017, **113**, 56–64.
88. Öhrngren P, Fardost A, Russo F, et al. *Org Process Res Dev*, 2012, **16**, 1053–1063.
89. Wu TY, Guo N, Teh CY, et al. In: *Advances in Ultrasound Technology for Environmental Remediation*. Dordrecht: Springer, Dordrecht, pp. 5–12.
90. Wu Z, Tagliapietra S, Giraudo A, et al. *Ultrason Sonochem*, 2019, **52**, 530–546.

91. Lee J, Yang S. *Crystals*, 2018, **8**, 320.
92. Kim H, Suslick K. *Crystals*, 2018, **8**, 280.
93. Ramisetty KA, Kumar KV, Rasmuson AC. *Org Process Res Dev*, 2019, **23**, 935–944.
94. Castillo-Peinado L de los S, Luque de Castro MD. *J Pharm Pharmacol*, 2016, **68**, 1249–1267.
95. Babu SG, Ashokkumar M, Neppolian B. *Top Curr Chem*, 2016, **374**, 375–407.
96. Mahamuni NN, Adewuyi YG. *Ultrason Sonochem*, 2010, **17**, 990–1003.
97. Campos-Pozuelo C, Granger C, Vanhille C, et al. *Ultrason Sonochem*, 2005, **12**, 79–84.
98. Peshkovsky SL, Peshkovsky AS. *Ultrason Sonochem*, 2007, **14**, 314–322.
99. Nalesso S, Bussemaker MJ, Sear RP, et al. *Ultrasonics Sonochemistry*. Epub ahead of print 2019. DOI: 10.1016/j.ultsonch.2019.04.020.
100. Noël T, Su Y, Hessel V. *Top Organomet Chem*, 2016, **57**, 1–41.
101. Brocklehurst CE, Lehmann H, La Vecchia L. *Org Process Res Dev*, 2011, **15**, 1447–1453.
102. Greb A, Poh JS, Greed S, et al. *Angew Chemie - Int Ed*, 2017, **56**, 16602–16605.
103. Mándity IM, Ötvös SB, Fülöp F. *ChemistryOpen*, 2015, **4**, 212–223.
104. Koyama E, Ito N, Sugiyama J ichi, et al. *J Flow Chem*, 2018, **8**, 147–156.

2.0 Synthesis of new heterogeneous materials

This chapter presents the experimental preparation and characterization of new heterogeneous materials for different purposes: adsorption of organic molecules, antimicrobial applications, and catalysis. In this and the following experimental sections our empiric tests and their results are presented after a short dissertation about the state of the art. Each sub-chapter deals with the preparation of a different kind of material with its own set of experiments. Enabling technologies such as high-energy ball milling and US have been used in the synthetic process and compared to conventional methods. After these materials were characterized, they were tested in real applications to see how well they could perform compared to literature or commercial equivalents.

2.1 Synthesis and application of cyclodextrin-based insoluble polymers

2.1.1 Introduction and state of the art

Cyclodextrins (CD) are natural-occurring donut-shaped molecules made of glucose (glucopyranose) units connected through 1,4 glycosidic bonds. They can be pre-produced, and were firstly discovered, from starch via biological digestion^{105,106}. They are classified by their numbers of glucose subunits: α -CD have six units, β -CD have seven and γ -CD have eight (**Fig. 13**). CD are characterized by a hydrophobic cavity and a hydrophilic surface; this duality grants them a partial solubility in water and the possibility of forming host-guest complexes with organic, hydrophobic molecules. These complexes do not involve the formation of covalent bonds, but are only due to weak interactions, with the driving force being the substitution of complexed water with more energetically favoured guests^{107,108}. CD are non-toxic, since they cannot penetrate most organic barriers¹⁰⁹, biodegradable¹¹⁰ and cheap, so it is not surprising that they have many different applications.

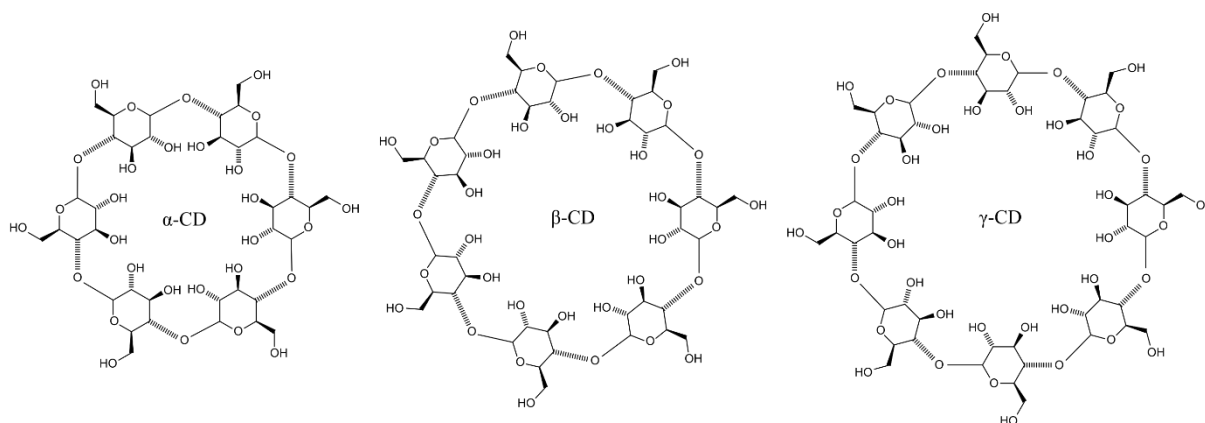


Figure 13: α , β and γ -cyclodextrin structure compared (from Wikipedia).

In pharmaceuticals, CD are used to improve the water solubility of API and as drug-delivery agents. Itraconazole is an antifungal agent with poor water solubility, however a clear 10 mg/mL solution can be made using CD¹¹¹. Lipophilic molecules such as testosterone, cholesterol or hydrocortisone can form soluble complexes with natural CD and their derivatives^{112–114}. CD can behave as true carriers for API: given their size and hydrophilicity, CD cannot permeate through cellular membranes, however they can allow the permeation of lipophilic molecules from their cavity to the membrane^{115,116}. In food, they can be used to

inhibit bad tastes and smells¹¹⁷. In the analytical field, CD are used as a stationary phase for chromatography to discriminate between enantiomers^{118,119}.

Table 3: properties of natural CD¹²⁰.

Property	α CD	β CD	γ CD
Glucose units	6	7	8
MW (g/mol)	972	1135	1297
Water solubility 25 °C (wt.%)	14.5	1.8	23.2
Cavity diameter (Å)	4.7-5.3	6.0-6.5	7.5-8.3

Among CD, β CD are the most widely used; some of their properties compared to other natural CD are listed in **Table 3**. They are the cheapest and their cavity is wide enough to host many common organic reagents. β CD solubility in water is temperature-dependent and it varies roughly from 2 wt.% at room temperature to 20 wt.% in boiling water¹²¹. Their solubility is limited because of the rigidity of their ring-structure that impedes the formation of H-bonds with water and, especially for β CD, favours intra-molecular interactions. Albeit low, solubility is not zero and it is common for the formed complexes to have a higher water solubility than their components. This can be an advantage to solubilize an organic reagent, but it is a problem when we want to recover a target compound from a solution. This is an application better suited for insoluble CD polymers (CDPIS).

Different classes of such polymers exist, depending on their synthesis that of course cascades into their structure, properties and possible applications: cross-linked, linear, immobilized and hyperbranched¹²². Cross-linked polymers are formed with the addition of a cross-linking agent containing multiple functional groups to form a solid network between CD reacting with the available hydroxyls. The higher the reticulation, the lower the solubility, until an insoluble solid is formed. Common cross-linking agents can be citric acid¹²³ or epichlorohydrin^{124–126}. CDPIS are useful for the adsorption of pollutants in water solution, given their insoluble nature they minimize losses and ensure an easy separation from the liquid. Many applications of CDPIS are reported for the removal of dyes, pharmaceuticals and pesticides from water^{127–130}.

A. Alsaiee *et al.* reported the synthesis of a cross-linked β CD polymer for the removal of pollutants from water¹³¹. In their tests, the polymer outperformed Norit® activated carbon (a common commercial adsorbent) for the adsorption of different aromatics, pesticides and pharmaceuticals in flow (9 mL/min). They stressed the importance of obtaining a porous structure, confirmed by BET measurements with N₂, since the polymer had greater adsorption efficacy and speed compared to non-porous equivalents. G. Crini *et al.* tested different CD-based cross-linked polymers, synthesized with epichlorohydrin, for the batch adsorption of five different triazoles fungicides¹³². All CD polymers outperformed commercial activated carbons for the adsorption of such pollutants from water. All polymers behaved similarly, with a removal efficacy that spanned from 30-90 % depending on the adsorbate, however average better results were obtained with mixed CD and hydroxypropyl β CD polymers. Although high removals are needed for all target compounds in a real-life application, studies like this show the applicability of CDPIS for the treatment of complex organic mixtures. Another interesting example of a successful application of CDPIS for wastewater treatment is the study by E. Fenyvesi *et al.* where a commercial bead β CDP from CycloLab Ltd. was used for the

simultaneous removal of nine pollutants from municipal wastewaters¹³³. Nine target compounds were added to the treated wastewater to ensure a concentration of 5 µg each. A total of 300 L of wastewater could be purified over 1 kg of bead polymer (65 wt.% βCD), working in loop with a 120 L/min flow in a fluid-bed setup. GC analysis showed a total removal of bisphenol A and hormones, and 85 % removal for ibuprofen and diclofenac, with the equilibrium reached after only 5 min of contact time. This was comparable with results obtained with commercial activated carbons.

2.1.2 Preparation and purification

During this thesis, two cross-linked CDPIS were synthesized with the same procedure (**Fig. 14**): one from standard βCD and one from randomly methylated βCD (RAMEB). Epichlorohydrin was used as a cross-linking agent for its high reactivity and because its use is widely reported, and the reaction mechanism is and reproducible. As previously described, βCD are the most widely used and studied among natural CD, so they were the natural choice as a substrate; RAMEB are the most common CD derivative: they are obtained by the partial (12 out of 21) substitution of hydroxyls with methoxy groups, giving them higher lipophilicity but also greater water solubility, thanks to the decrease in intra-molecular H-bonding. The objective was the synthesis of an insoluble material to use for the adsorption of organics from aqueous solutions, but also to use as a support for heterogeneous catalysis. To avoid the use of solvents, both for green chemistry purposes and an easier recover of the product, the polymerization was run in a high energy ball mill using mechanochemical activation as the driving force. Mechanochemistry allows for a solventless reaction that reduces the working volume and simplifies the recovery of the product and this allows a further scalability of the reaction^{134,135}. A planetary high energy ball mill (Retsch PM100) was used for the synthesis, run in a stainless-steel jar with stainless-steel balls. In a planetary ball mill, the jar containing the sample rotates around the central axis of the instrument, while also rotating on itself. The rotation is usually reversed after some time to ensure a homogeneous treatment. During the reaction, temperature was monitored at 15 min intervals with an IR sensor on the top of the jar.

At first, a 2 g scale protocol was developed for the βCD: 2.3 g (2 mmol) of dried βCD are firstly reacted with 0.84 g (20 mmol) of NaOH for 15 min. This first step forms the sodium salts of the CD hydroxyls: this is an activation for the subsequent step. This first step releases water: since the presence of water, in our experience, leads to a hardening and darkening of the material, it is better to start from dried CD to minimize the moisture. After this, the jar was removed and cooled to -30 °C before the addition of the very reactive epichlorohydrin (1.6 mL, 20 mmol) as the cross-linker. The 1:10 CD to epichlorohydrin ratio was chosen after previous trials established that up to 1:5 ratio predominantly resulted in soluble polymers. In alkaline media, three reactions occur: cross-linking between CD monomers, polymerization between glyceryl units of the linker and hydrolysis to sodium salts (which leads to soluble impurities). Since these reactions proceed in parallel, an excess of cross-linker is needed to ensure the formation of the wanted insoluble structure¹³⁶: the reaction is not controlled and occurs randomly, but the C-6 hydroxyls are the main target since they are the most reactive and accessible. The polymerization step is then run for 9 h, during which the temperature may increase between 50-60 °C before dropping to 40 °C again, a sign that the reaction is over. As it reacts, epichlorohydrin releases HCl as a by-product, this however is readily consumed to

NaCl by the CD salts previously formed and the excess of NaOH. All steps were performed at 650 rpm, inverting the rotation every 15 min.

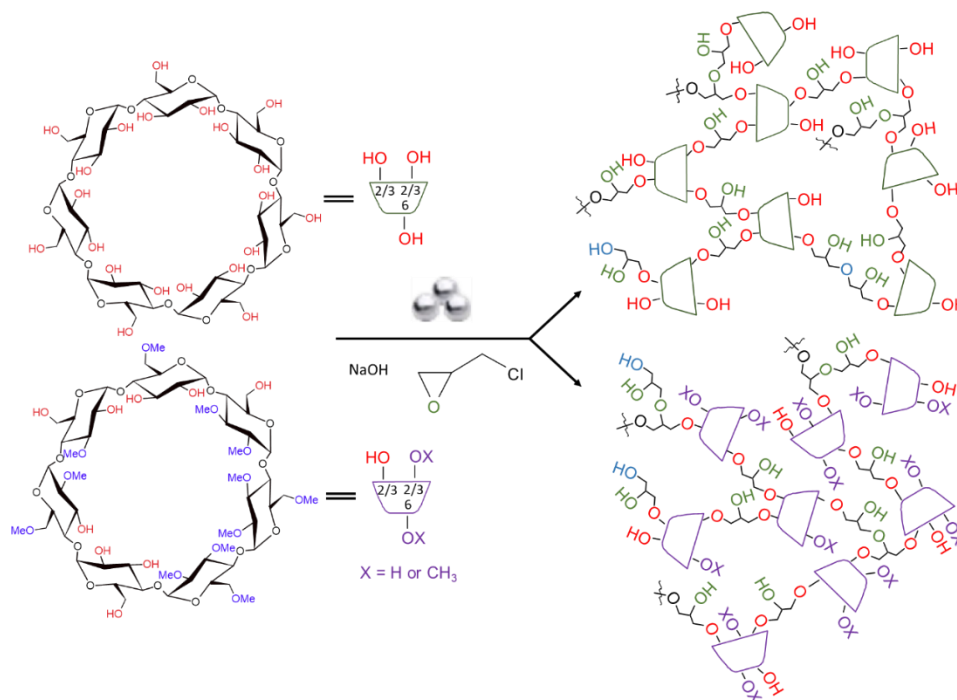


Figure 14: graphical representation of the polymeric structure of β CDPIS and Me β CDPIS¹³⁷.

The reaction resulted in a yellowish powder, which was sieved and collected. Firstly, the solid is suspended in water and neutralized with HCl 0.1 N, then the suspension is centrifuged at 4000 rpm for 10 min and the supernatant is wasted. The suspension and centrifugation are repeated 3 times to remove the salts and the soluble fractions of the polymer. After the third step, a small sample of the supernatant is collected and a drop of AgNO₃ solution is added to check for residual chlorides: if chlorides are present, AgCl forms leading to a white precipitate. If needed, a fourth washing step is performed, otherwise the deposited solid is dried overnight at 80 °C in oven. Finally, the dried solid is milled one last time at 300 rpm for 2 min to obtain a fine white powder.

This first protocol resulted in an average yield of 96 %. The reaction was subsequently scaled-up, processing 70 g of β CD with the same protocol. This resulted in an average yield of 91.6 % and it was possible to isolate a total of 200 g of product (β CDPIS). Having established a successful synthesis, we also applied it to RAMEB as substrate. RAMEB, however, presents a smaller number of reactive hydroxyls, so salt formation is hindered: the first step was then prolonged to 25 min, after that, however, 6 h were sufficient to consume the epichlorohydrin for the polymerization step. The RAMEB polymerizations (Me β CDPIS) were run in the 3 g scale only, resulting in an average yield of 76 %.

2.1.3 Characterization

The morphology of the synthesized polymers was investigated via field emission scanning electron microscope (FESEM) analysis (**Fig. 15**). The FESEM study reveals a similar structure for the two materials, composed of irregular and inflated cloud-like formations. This irregularity and the superposition of the particles resulted in a high variance in their measure

diameter, however it can be stated that the β CDPIS is composed of slightly smaller structures (501 ± 466 nm) compared to Me β CDPIS (676 ± 473 nm).

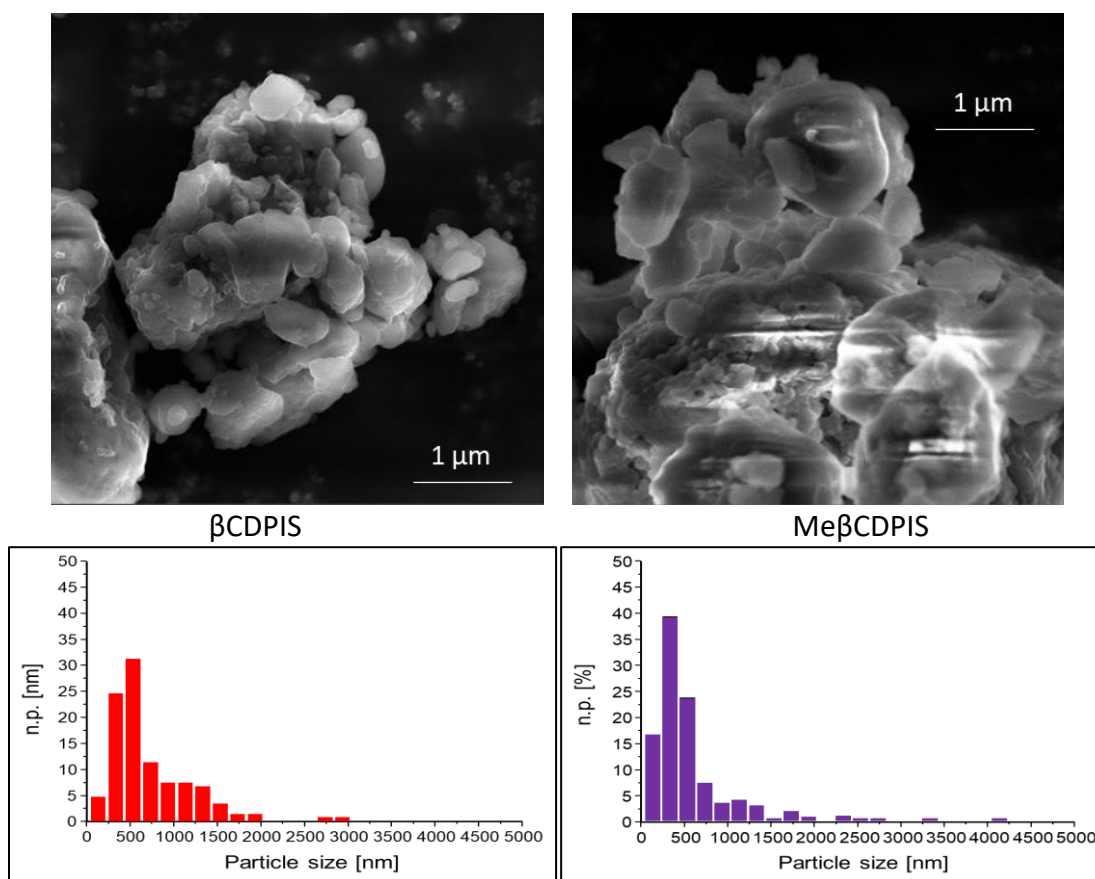


Figure 15: FESEM images and particle size distribution. β CDPIS: mag. 55.0 Kx, FOV 5.15 μ m, det. In-beam SE, 5 KeV. Me β CDPIS: mag. 50.0 Kx, FOV 5.66 μ m, det. In-beam SE, 5 KeV.

To investigate the polymers particle size in solution a dynamic light scattering (DLS) analysis was used (**Table 4**). The instrument was also used to measure their Z-potential (**Table 5**). The Z-potential of a particle is the electric potential of the thin layer of liquid on its surface and it reflects its tendency to aggregate: a high potential, positive or negative, cause the particles to repel and the suspension to be stable, whereas a small potential may be overcome by non-covalent interactions and lead to aggregation and flocculation. For the particle size measurement, a 1 mg/mL suspension of polymer was prepared in the chosen solvent. The measurements were repeated over time to measure the possible swelling of the materials (**Fig. 16**). A selection of solvent of different polarity was used to spot the influence over the aggregation of the suspended particles.

Table 4: particle size^a in nm of CDPIS in freshly prepared suspensions at 1 mg/ml concentration.

	H ₂ O	Gly-H ₂ O ^b	MeOH	Abs. EtOH	nPrOH	iPrOH	Acetone	Dichloro methane	Toluene
β CDPIS	1561.2	481.4	914.3	837.5	511.8	562.2	1423.3	613.8	2133.6
	± 112.4	± 73.6	± 61.9	± 47.8	± 89.2	± 127.7	± 136.4	± 83.2	± 274.7
Me β CDPIS	1471.9	704.6	1184.5	854.5	739.4	559.5	1357.4	1170.8	1796.8
	± 181.4	± 104.2	± 90.5	± 84.9	± 94.3	± 121.1	± 88.3	± 114.3	± 285.4

^a effective diameter (hydrodynamic diameter), calculated from the lognormal intensity distribution, ^b 60:40 w/w mixture of glycerin and water.

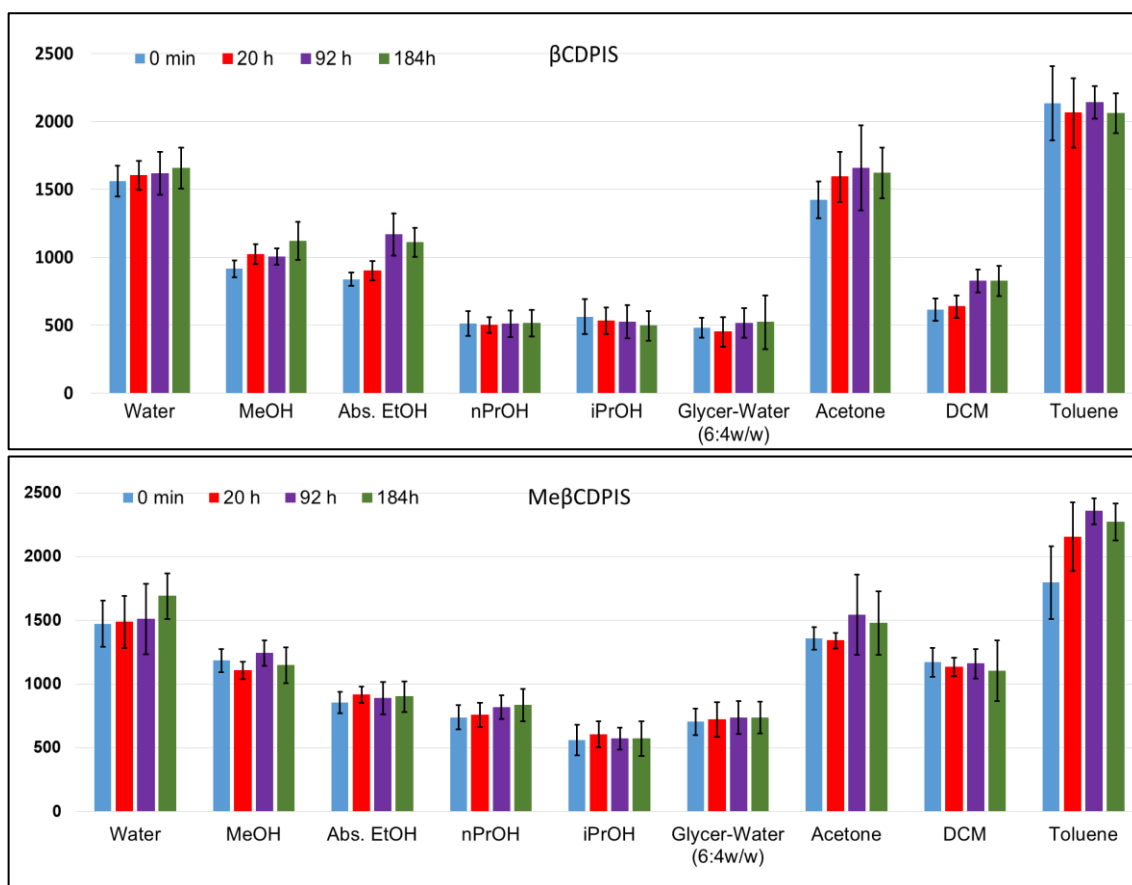


Figure 66: swelling of β CDPIS (up) and Me β CDPIS (down) in different solvents over time.

Despite being composed of smaller particles, β CDPIS tends to form bigger aggregates than Me β CDPIS in solution. For both polymer, aggregation is stronger in highly polar solvents (water) or highly lipophilic solvents (toluene). Swelling is relatively small, resulting on average in a 15-20 % increase in effective diameter over a week period. In low polarity environments however, this becomes less predictable. Notably, the different number of free hydroxyls between β CDPIS and Me β CDPIS does not translate in meaningful differences in their particle size not in their swelling.

Even the Z-potential resulted to be similar between the two, as listed in **Table 5**. In water their potential only grants a short-time stability, which indicated the need of an efficient stirring to keep the polymers in suspension. This is true also for the other tested solvents, except in *i*PrOH where the potentials are above 30 mV thus indicating a moderate stability over time.

Table 5: Measured zeta-potentials in mV of BM prepared polymers in various solvents.

	Water	Glycerin-water	MeOH	Abs. EtOH	nPrOH
βCDPIS	-16.2 \pm 2.0	-16.2 \pm 2.0	13.3 \pm 3.4	13.0 \pm 5.3	34.0 \pm 10.3
MeβCDPIS	-13.3 \pm 1.5	-16.2 \pm 2.0	9.6 \pm 2.4	10.8 \pm 3.6	32.2 \pm 8.0

2.1.4 Adsorption of dyes as model compounds

Adsorption processes are common downstream treatment of wastewaters. They can be used both to recover valuable chemicals and to diminish the concentration of pollutant in the outputs. In pharmaceutical industries in particular, the removal of bioactive compounds and heavy metals from leaked catalysts is a matter of dire importance^{138,139}. Common adsorbents are activated charcoals and zeolites^{140,141}, however innovative materials such as chitosan, MOF, and CD polymers are gaining interest for the adsorption of organics in diluted water solutions^{142,143}. One advantage that CD hold over commercial activated carbons is that they can be easily modified to be selective and are easy to clean, usually EtOH:water mixtures are more than enough: this is particularly useful if the adsorbates are valuable molecules.

To study the possible application of the synthesized CD polymers three steps were needed: the measurement of the adsorption isotherms, kinetic studies and finally flow adsorption experiments.

At first, the adsorption properties of the two polymers were investigated and compared using two reference compounds: methylene blue and methyl violet, two common commercial dyes. Methylene blue can be used for medical application or in textiles, furthermore it is often used to compare different adsorptive materials, for example the methylene blue uptake is often found in the certificate of analysis of activated carbons. Methyl violet also finds application both in textiles and in medicine; it can be used as a mixture or it can be classified ad 2B, 6B or 10B depending on the methyl substituents bonded to the amino group.

To begin with, the room temperature adsorption isotherms of the two dyes over the synthesised materials needed to be recorded. The shape of the isotherm gives information about the interaction between the adsorbate and the surface of the adsorbing material as well as the possible formation of multilayers. With enough points and repetitions is possible to apply mathematical models to predict the maximum adsorption capacity and the shape and distribution of pores on the sample, however even without such manipulations the isotherm reflects the affinity between the adsorbent and the adsorbate. A UV-Vis calibration curve was built for methylene blue and methyl violet; both compounds registered an absorbance around 1 at 0.02 mM, so that was set as the maximum concentration for the future analysis.

There are two ways of recording an adsorption isotherm: keeping the quantity of adsorbent material constant and changing the concentration of the adsorbate or doing the opposite. If the operator is careful, the two will result in the same isotherm. For the sake of simplicity, it was decided to prepare a stock solution of the adsorbates to use while changing the quantity of the polymer for every experiment (**Fig. 17**). A first attempt was made with 1.0 mM solutions; six experimental points were recorded using 30, 50, 80, 100, 120 and 150 mg of polymer for 15 mL of solution. The materials were put in 15 mL glass test tubes and vigorously shaken to suspend the solid. An oscillating plate (Heidolph Synthesis 1) at 450 rpm was used to keep the suspension stirred during the adsorption, which took place overnight to ensure equilibrium. After that, the tubes were centrifuged at 4000 rpm, the supernatant collected, diluted 1:50 and filtered through an HPLC Teflon filter.

The MV spectra were recorded and lead to a satisfactory adsorption isotherm, the MB adsorption was negligible instead and the experiments were repeated at 0.02 mM.

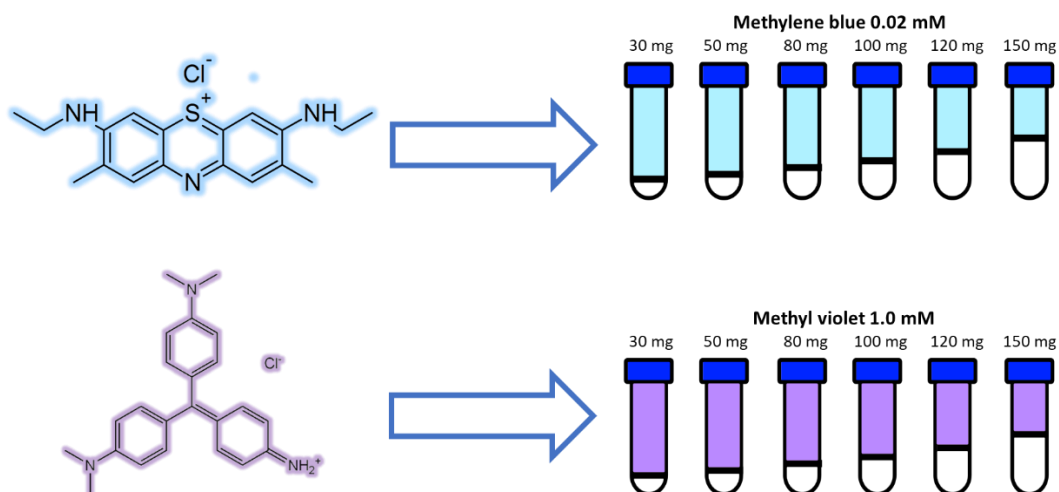


Figure 77: procedure for the record of the adsorption isotherms with MB and MV.

With MB both polymers gave a L type isotherm (**Fig. 18**). L curves are typical langmuirian isotherms: at first the adsorbate uptake is proportional to its concentration, following Henry's law, but a higher concentration a plateau is reached: this corresponds to the formation of a monolayer of adsorbate molecules on the surface of the adsorbent. L curves are common in aqueous solution and usually indicate that the molecules are adsorbed flat on the surface. In these conditions, β CDPIS showed a higher affinity for MB than Me β CDPIS.

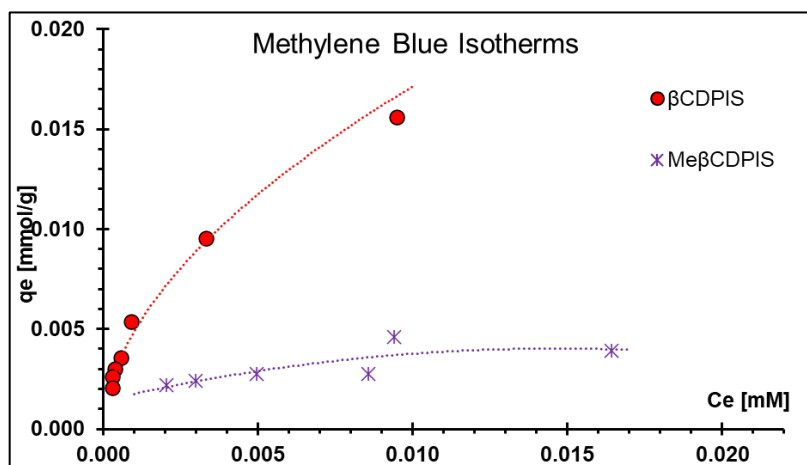


Figure 18: MB adsorption isotherms.

Things changed with MV. MV adsorption resulted in a S curve over β CDPIS and a H curve over Me β CDPIS instead (**Fig. 19**). Once again, however, β CDPIS showed a greater affinity for the compound. S curves are often the result of competition over the adsorption sites and the presence of intermolecular attraction between the adsorbates: this can be the result of the higher concentration used which enhanced both the interaction between the MV and the polymer and those between MV molecules. Similarly, the H curve over Me β CDPIS may indicate that the interactions between MV and the polymer are weak and disrupted by the association of MV in solution.

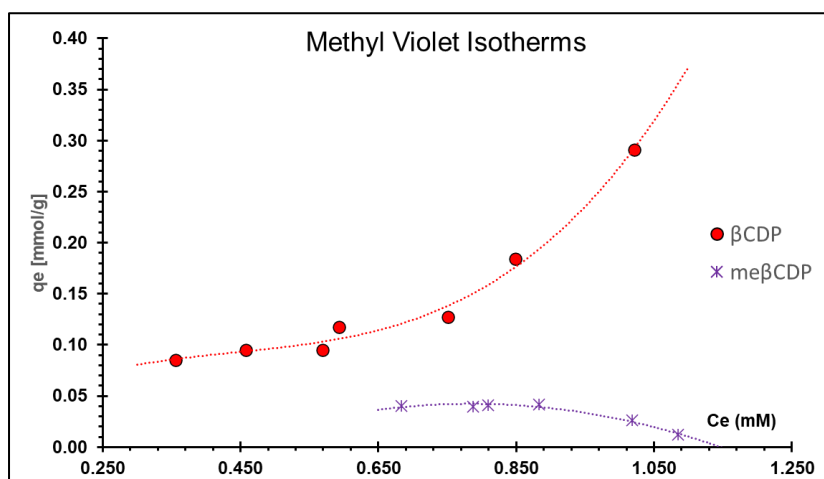


Figure 19: MV adsorption isotherms.

With these data it is possible to conclude that β CDPIS is the better adsorbent for the reference compounds. When MB is used a monolayer is formed for both polymers, in accordance with Langmuir's model. When MV is used the intermolecular interaction improves the adsorption over β CDPIS creating a multilayer, instead over Me β CDPIS the high MV concentration can disrupt the adsorption.

After these preliminary experiments, we moved on to obtain the kinetic curves of the adsorption; this would give information about the speed of adsorption and the experimental maximum uptake. The experiments were run with 0.5 g of polymer in 200 mL of solution 0.02 mM both for MB and MV. The solution was stirred at 450 rpm and samples were taken from 2 min to 2 h. Samples (3 mL) were centrifuged at 4000 rpm, filtered, and analysed with a UV-Vis spectrophotometer (Agilent Cary 60). The resulting curves are shown in Fig. 20.

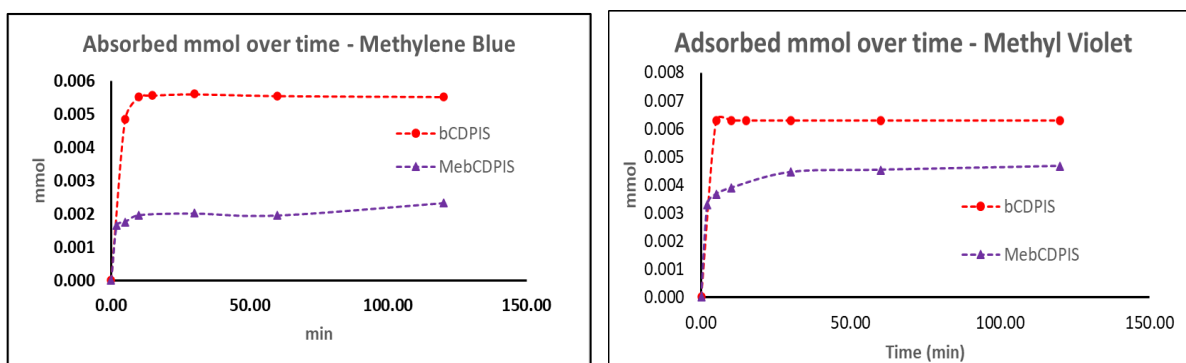


Figure 20: MB and MV adsorption kinetic curves.

For both compounds, uptake was fast, and a plateau was reached within few minutes. Also, for both dyes β CDPIS was the better adsorbent, especially in the case of MB adsorption. A linearization with a pseudo-second order kinetic model found good accordance with the data, meaning that in these conditions the rate-limiting step is the adsorption on the surface and the overall speed of the process depends on the availability of sorption sites rather than the concentration of the solute. The k_2 constant represents the equilibrium rate constant and reflects the speed at which the system reaches equilibrium. The acquired kinetic data are listed in Table 6.

Table 6: kinetic parameters for MB and MV adsorption.

	Adsorbate	Max uptake (mmol/g)	Max uptake (mg/g)	Lin. R ²	k ₂ (g/mg*min)
βCDPIS	MB	0.011	3.5	0.99	0.28
	MV	0.013	5.1	0.99	0.13
MeβCDPIS	MB	0.005	1.6	0.99	0.66
	MV	0.009	3.5	0.99	0.26

Finally, the breakthrough curve was constructed. Most of the industrial equipment for adsorption consists of packed columns or compacted disks of adsorbent material, designed to work in flow. The wastewater flows through the adsorbent and is purified: as the first layers of adsorbent are filled with adsorbates, the concentration of pollutants in the output rises through the length of the column: the concentration profile inside the column is the breakthrough curve, and it moves towards the end of the column as the mass transfer zone becomes saturated. The time/volume after which the concentration of adsorbate in the output becomes greater than zero, or greater than the accepted limit, is the working time/volume of the column. When the concentration in the output equals the concentration in the input, the breakpoint is reached, and the column is completely saturated. Of course, the breakpoint has only theoretical value and the column must be changed or regenerate much earlier than that. In this sense, the working time or working volume is the parameter of interest for a real-life process.

Knowing the maximum expected uptake, it was possible to plan the flow adsorption experiments. Unfortunately, it was not possible to set up an equipment to directly apply a pressurized flow through a cartridge of polymer, so vacuum (<0.01 MPa) was applied instead. A portion of 1 g of polymer was used for the adsorption; the polymer was put inside a 10 mL glass syringe with a small quantity of clean cotton on the bottom and gently pressed: for both materials 1 g (dry) resulted in 2 mL of volume. Knowing the CV (2 mL) and the maximum uptake, it was possible to predict the CV before the breakthrough. Using 0.02 mM solution would have been ideal for analysis since one would simply collect the samples and record the UV-Vis adsorption until 1 Abs was reached; however, this would require a volume of roughly 500 mL (250 CV) to exhaust the polymers. Expecting a slow flow, this was not feasible, so 0.2 mM solutions were prepared instead. The resulting curves for MV and MB over the two polymers are shown in **Fig. 21**.

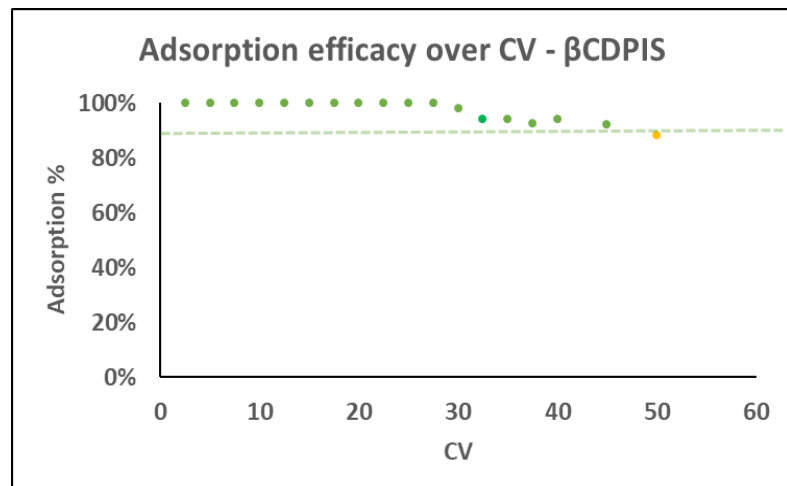
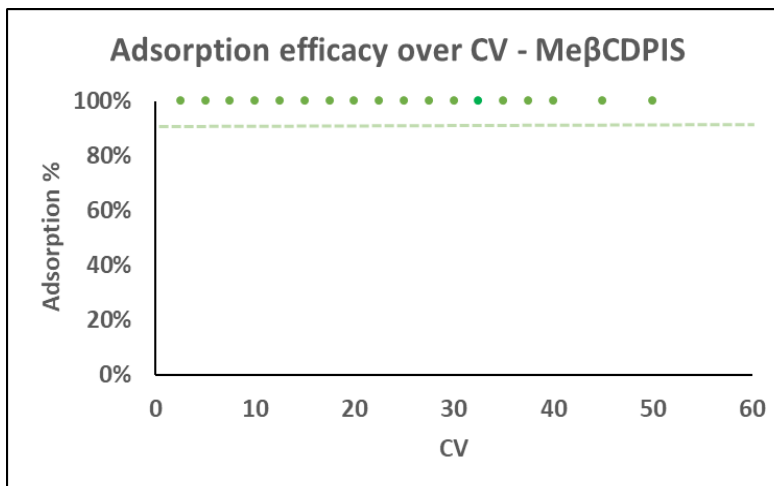
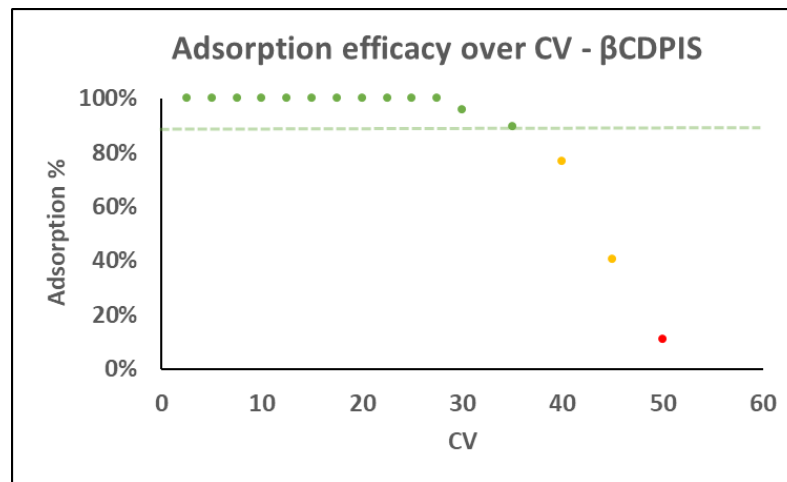
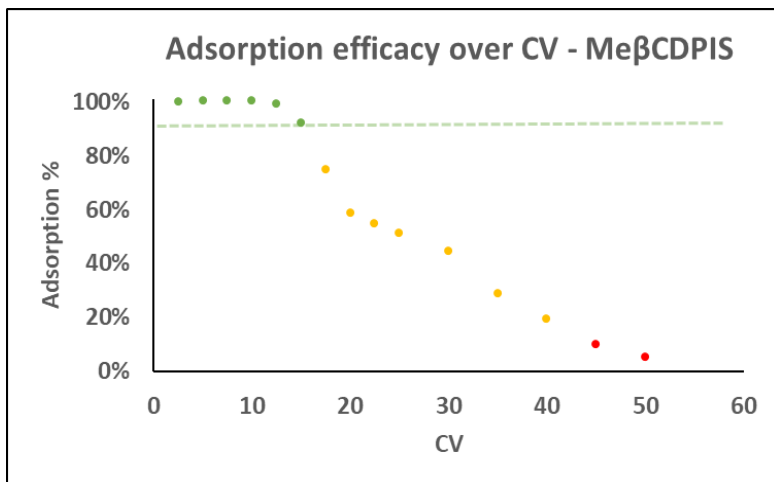


Figure 21: adsorption efficacy over CV for MB (top) and MV (bottom).

The results show a remarkable difference between the batch and the flow experiments (**Table 7**), since in all cases the polymer performed better than the predictions based on the kinetic experiments. We considered the 90 % removal as the minimum acceptable: the CV interval where the efficacy was higher was considered as the working range of the column. On the opposite, when the efficacy dropped to 10 % or below, the breakthrough was considered reached. For the MB adsorption, breakthrough was expected after 27.5 CV over β CDPIS and 12.5 over Me β CDPIS, however both polymers outperformed the calculations. Apart small oscillation, β CDPIS had a working range of 30 CV but breakthrough arrived only after 50 CV; Me β CDPIS had a working range of 15 CV instead, and it reached breakthrough after 45 CV. Same with MV, where breakthrough was expected after 32.5 and 22.5 CV for β CDPIS and Me β CDPIS respectively, but both polymers never reached it during the experiments and only β CDPIS dropped below 90 % efficacy after 50 CV. One explanation might be the aggregation of adsorbates on the surface of the solids: this phenomenon may have been enhanced in the flow experiments because of the higher concentration and the slow flux, whereas magnetic stirring would have disrupted such weak interactions. Another possibility is that in these conditions not only the surface is available for the adsorption, but also a diffusion in the bulk of the polymer occurs. Indeed, the predicted breakthroughs are close to the working range of the polymers: the kinetic experiments may have predicted the surface capacity of the materials, however secondary mechanisms may have extended the adsorption capacity in flow tests. Nonetheless, this allowed us to treat a good amount of CV before exhausting the material and this makes for a promising first step in the application of such polymers for the adsorption of pollutants. A set of experiments at lower concentration would be advised, however, without the possibility to apply pressure to maintain a faster flux this was not a possibility for now.

Table 7: predicted and experimental parameters for MV and MB flow adsorption.

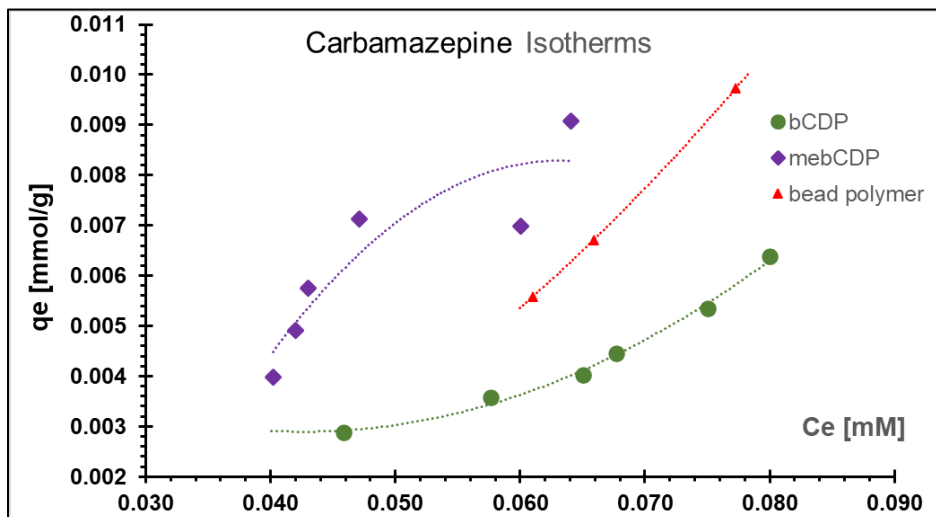
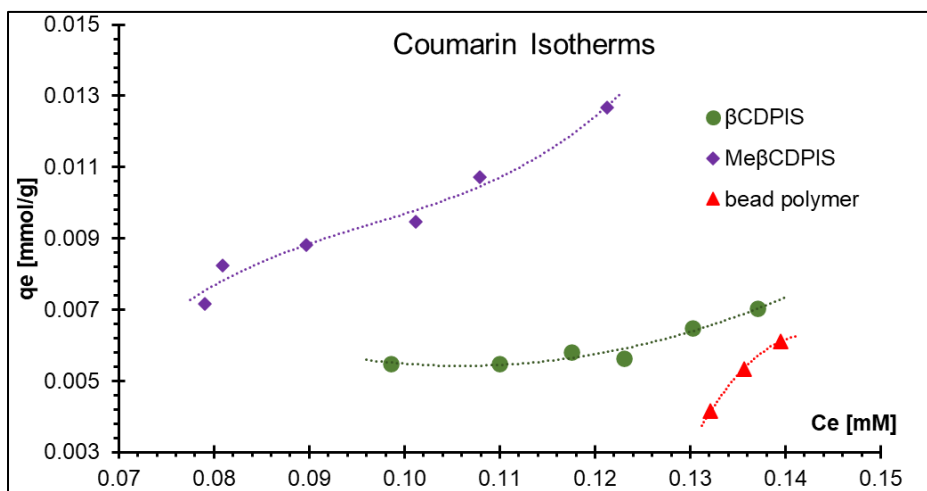
	Dye	Max CV (predicted)	Max CV (experimental)	Working range (CV)
β CDPIS	MB	27.5	50	30
	MV	12.5	>50	45
Me β CDPIS	MB	32.5	45	15
	MV	22.5	>50	>50

2.1.5 Adsorption of pharmaceuticals and bioactive compounds

Having completed the experiments with the model compounds and having established a good adsorption capability and applicability for the polymers, we went on to test them on some real-life target compounds. Organic pollutants of medical and pharmaceutical application were selected, since the production of wastewater from pharmaceutical productions and consequently their purification is a topic of huge importance. Another requirement was for them to have a good UV-Vis adsorption for their detection. Our goal was to prove that the synthesized polymers could be applied for the adsorptions of such organic pollutants from diluted aqueous solutions. We selected the following molecules for the first screening:

- Coumarin (0.10 mM) ✓
- Carbamazepine (0.10 mM) ✓
- Oxytetracycline HCl (0.08 mM)
- Doxycycline HCl (0.08 mM)
- Tetracycline HCl (0.08 mM)
- Caffeine (0.10 mM)
- Hydrocortisone (0.10 mM) ✓
- Clenbuterol (0.10 mM)
- Ractopamine HCl (0.35 mM) ✓

Of these, only those marked with the ✓ sign on the list showed significant adsorption onto the polymers and were selected to further experimentation. Their adsorption isotherms are showed below (**Fig. 22**), compared with those obtained from a commercial β CD-based polymer from Cyclolab, in bead form:



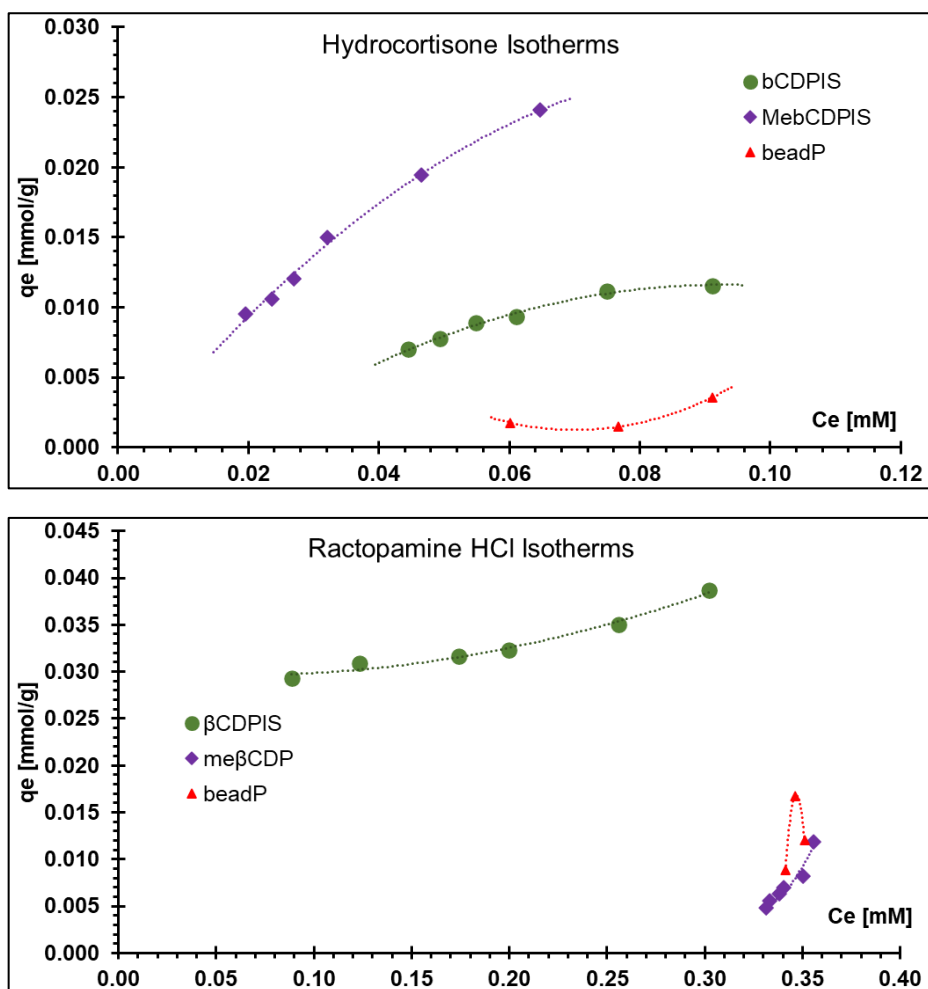


Figure 22: adsorption isotherms of coumarin, carbamazepine, hydrocortisone and ractopamine HCl.

In all cases except hydrocortisone the behaviour of the synthesized polymers was similar and comparable to the commercial one; for hydrocortisone the bead polymer isotherm is not shown because the experiment resulted in ten times more adsorption than with the use of our polymers and so the curves were not comparable. The isotherms established that hydrocortisone, coumarin and carbamazepine are best adsorbed over Me β CDPIS, while ractopamine is more affine to β CDPIS. This way we recorded the kinetic curves of adsorption on the appropriate polymer for each compound (**Fig. 23**). All adsorptions followed a pseudo-second order kinetic, but this time they were somewhat slower than the dyes and the plateau was reached between 30-60 min, with only small variations afterwards. Interestingly, ractopamine showed a significantly greater depletion from solution respect to the other compounds, while coumarin and carbamazepine resulted in practically identical trends. Kinetic data are listed in **Table 8**.

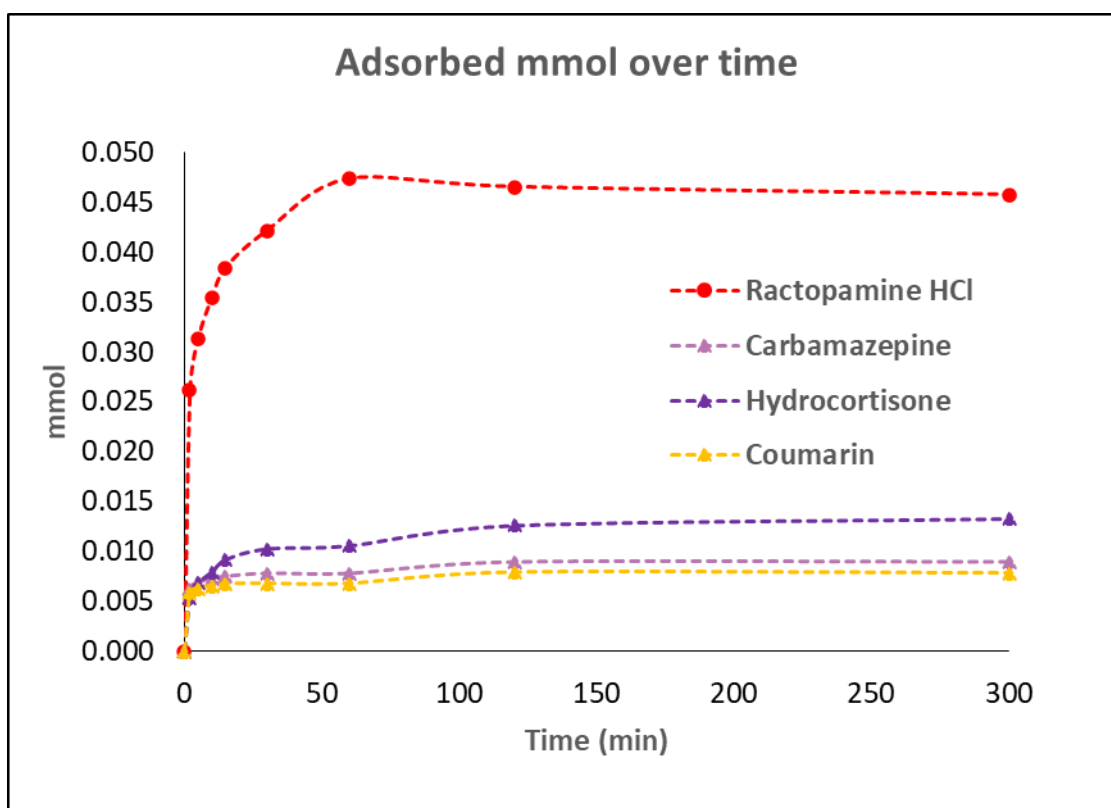


Figure 23: adsorption kinetic curves of ractopamine HCl, carbamazepine, hydrocortisone and coumarin.

As before, for the flow experiments the concentration were increased to reduce the needed amount of CV to exhaustion. This led to the prediction of 13 CV before the breakthrough for ractopamine, 27 CV for hydrocortisone and 16 CV for both coumarin and carbamazepine.

Table 8: adsorption kinetic parameters for the target compounds.

	Adsorbate	Max uptake (mmol/g)	Max uptake (mg/g)	Lin. R ²	k ₂ (g/mg*min)
βCDPIS	Ractopamine HCl	0.091	30.7	0.99	0.003
MeβCDPIS	Coumarin	0.016	2.3	0.99	0.09
	Hydrocortisone	0.027	9.8	0.99	0.13
	Carbamazepine	0.016	4.2	0.99	0.15

The flow adsorptions were executed with the same setup as before, using vacuum as driving force. From the UV-Vis analysis of the samples, the adsorption efficacy curves were obtained (**Fig. 24**): coumarin and carbamazepine behaved as predicted, while ractopamine reached the breakthrough point before expected and hydrocortisone on the opposite had a working interval of 40 CV, far better than the 16 predicted.

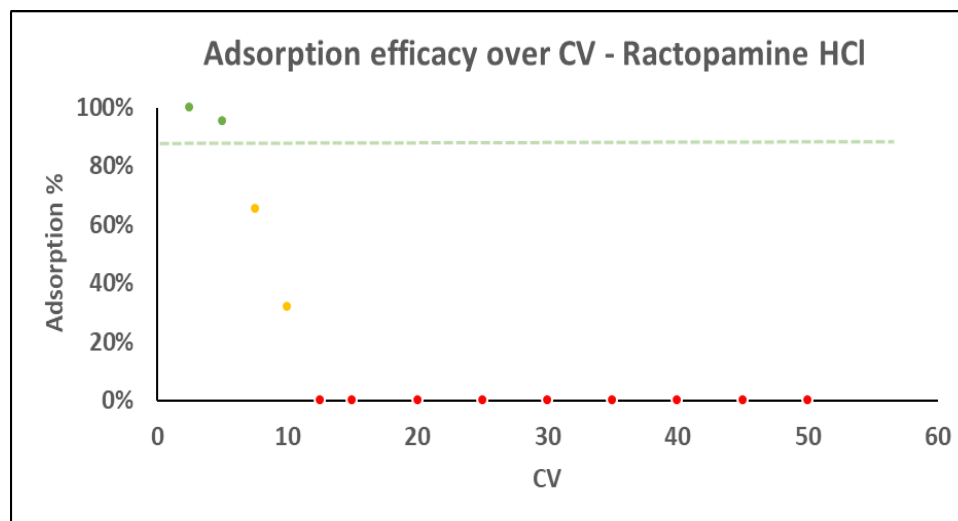
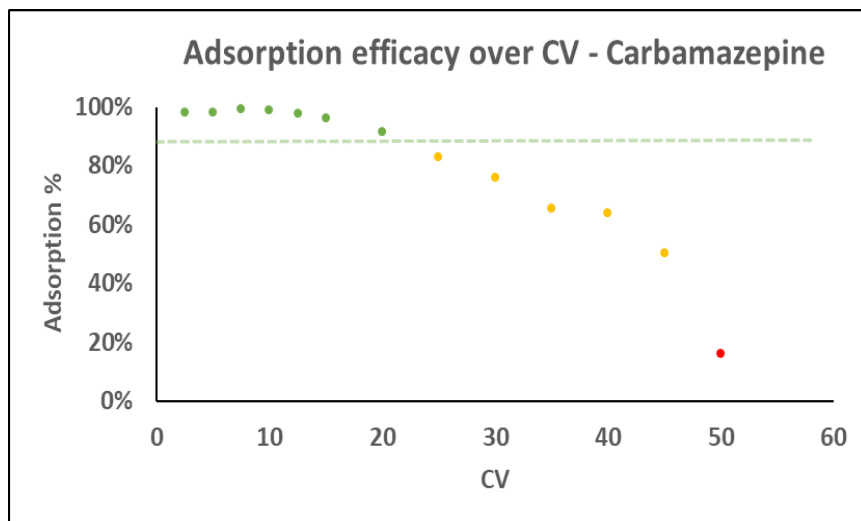
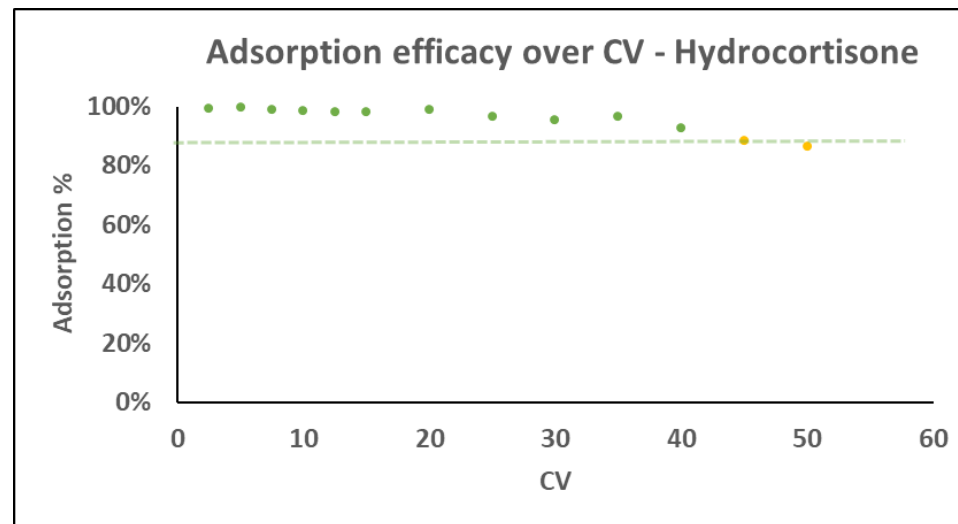
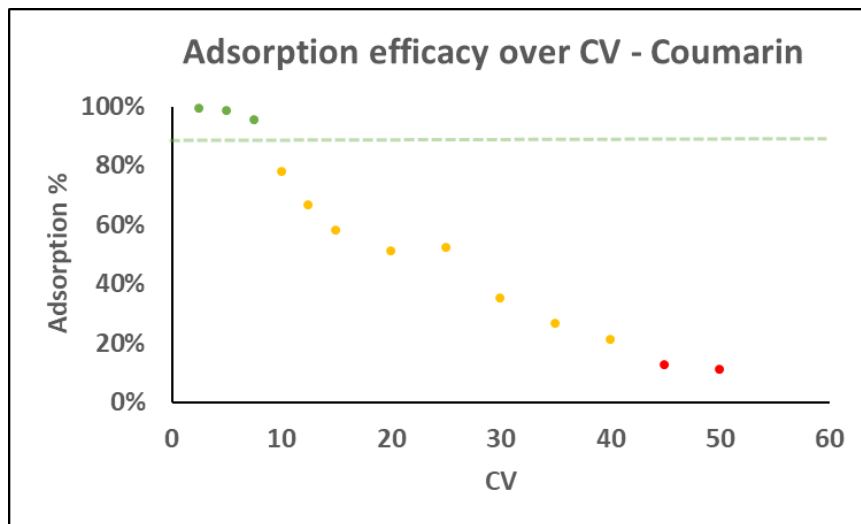


Figure 24: adsorption efficiency curves for coumarin, carbamazepine, hydrocortisone and ractopamine HCl.

2.1.5 Conclusion

The preliminary adsorption experiments using diluted solutions of methylene blue and methyl violet showed high adsorption capability for both polymers. Starting from adsorption isotherms and kinetic curves flow experiments were performed using a packed syringe and vacuum as driving force: the results were not only reproduced but improved. The improvement in adsorption capacity may be linked both to the different setup (flow instead of stirred tank) but also in the conditions, since a higher concentration and a slow flow were applied, giving the chance for secondary adsorption mechanism to apply.

When we tested the polymers for the adsorptions of pharmaceuticals from water the kinetic data from the diluted solutions successfully predicted the working range of the column, except for hydrocortisone (1.0 mM) which outperformed the stirred tank results (**Table 9**). However, for all adsorbates except ractopamine HCl the breakthrough points were reached far after the maximum adsorption reached in the kinetic experiments. This may suggest that the gentle flow and the higher concentration of target compounds favoured the diffusion inside the bulk of the polymer powder and/or the inter-molecular forces between the adsorbate leading to a multi-layered adsorption. Kinetic tests at higher concentrations may be needed to discern the two contributions.

Table 9: Flow adsorptions parameters and results.

Entry	Polymer	Adsorbate	Working Conc. (mM)	Predicted Max CV	Working range (CV)	Breakthrough point (CV)
1	β CDPIS	Methylene Blue	0.2	27.5	35.0	50.0
2	β CDPIS	Methyl Violet	0.2	32.5	45.0	>50
3	β CDPIS	Ractopamine HCl	3.5	13.0	5.0	12.5
4	Me β CDPIS	Methylene Blue	0.2	12.5	15.0	45.0
5	Me β CDPIS	Methyl Violet	0.2	22.5	>50	>>50
6	Me β CDPIS	Coumarin	1.2	5.0	7.5	45.0
7	Me β CDPIS	Carbamazepine	0.5	16.0	20.0	50
8	Me β CDPIS	Hydrocortisone	1.5	13.5	40.0	>>50

These results prove the applicability of the newly synthesized polymers for the adsorption of pollutants in wastewaters, starting from a benign substrate and with a green and innovative synthesis. A different array of compounds was tested and the results were successfully scaled and translated from batch to flow. Of course, since pollutants can be present in low concentration (traces), future tests over diluted solutions are needed for a complete assessment of the materials.

2.2 US-assisted preparation of Au and Ag nanoparticles over pectin

2.2.1 Introduction and state of the art

US can be used to improve mass transfer in a liquid and to create or disrupt emulsions, depending on the conditions. Also, they can interact with microscopic particles homogenizing their size via sonofragmentation: a tool often used to regulate crystal size distribution during sonocrystallization. Given the proven interaction between US and nanoparticles, both in their formation and dispersion, we decided to investigate their role in the synthesis on metal nanoparticle and their deposition onto solid supports. In this chapter the preparation of different materials is presented: Au- and Ag-doped citrus pectin for antimicrobial application and a series of heterogeneous catalysts based on Rh, Au and Co nanoparticles for hydrogenation and oxidation reactions. Characterization and experimental testing of the materials are also given; the results confronted with commercial or conventional equivalents to spot the influence of US on their performance.

Pectin is natural polymer (**Fig. 25**) found in fruit peels and is a key constituent of plant cells walls. Its composition may vary from specimen but commonly it is mostly (≈ 70 wt.%) made of galacturonic acid units bonded via α -(1-4) bonds. Along this linear backbone many ramifications can branch, with monosaccharides such as rhamnose, fructose or glucose as pending groups¹⁴⁴. This gives pectin a strong hydrophilicity and leads to formation of gelatinous emulsion with water: indeed, pectin is mostly known for its use as thickener in foods like marmalade.

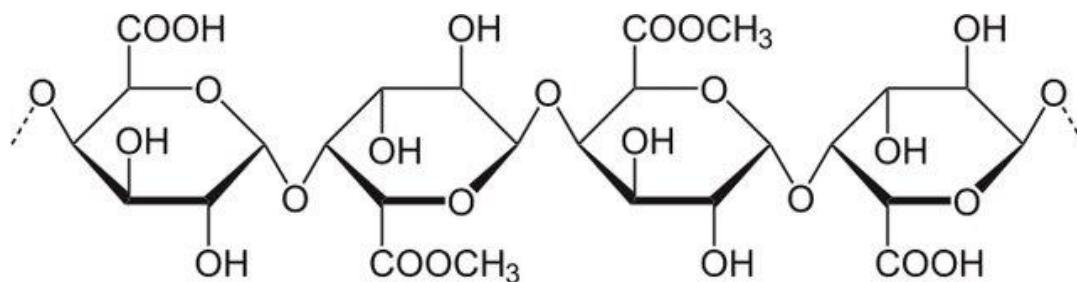


Figure 258: schematic representation of pectin chemical structure¹⁴⁵.

Pectin is a benign material, cheap, derived from renewable feedstock, biodegradable and with no risk for human health^{146–148}. Pectin can be classified also via its degree of esterification, but a portion of free carboxylic moieties is always present. Such free carboxylic groups can interact with polar substrates and possibly coordinate them^{149,150}. A recent publication by Haddada *et al.* investigated the interaction between Au^{3+} cations and the carboxylic residues of PEG 600 diacid for the creation of dispersed gold nanoparticles¹⁵¹. The synthesized material was also doped with doxycycline to obtain an antimicrobial gel, bonding the antibiotic to the same carboxylic groups via carbodiimide chemistry. In the age of antibiotic-resistance spreading, these new antibacterial materials that enhance or substitute current drugs are of high interest and potential for real-life applications. Our goals were to replicate the synthesis using pectin as a substrate, being it cheaper and greener, testing not only Au but also Ag deposition through the same process, since both metals have renown antifungal and antimicrobial activities^{152–157}. Au nanoparticles show good chemical stability and biocompatibility in humans¹⁵⁸, however they are able to disrupt bacteria cell membranes causing damages. This property has been exploited for drug-delivery with antibiotic-functionalized gold

nanoparticles, leading to higher antibacterial activities respect to antibiotics alone^{159–161}. Some research suggests that silver nanoparticles antimicrobial activity is mainly related to the release of silver ions; however, some studies showed how immobilized Ag nanoparticles were more effective against certain strains than dispersed Ag ions (colloidal silver)^{162,163}. The mechanism of action of both Au and Ag nanoparticles is linked to their contact with bacteria cell membrane, and antibacterial activity is strongly connected to their size and dispersion¹⁶⁴. For this reason, US that could improve both the dispersion and size distribution of the metal nanoparticles were applied and compared and compared to magnetic stirring for the dispersion of metal nanoparticles on the support, with the objective of improving dispersion and size distributions.

Aside from antimicrobial activity, Au and Ag nanoparticles have interesting optical properties. Some studies have linked their size and shape to their SERS (Surface-Enhanced Raman Scattering) efficiency, which could also be increased preparing core-shell bimetallic particles^{165,166}. This cascades in possible biosensing and nanophotonic applications. Balachandran *et al.* deposited Ag and Au nanoparticles on pectin to study their interaction and the optical properties of the synthesized material¹⁶⁷. They found that size and shape could be easily controlled by varying the concentration of pectin, especially for gold: anisotropic particles were found at low pectin concentration, while triangular crystals and spherical particles appeared at higher concentrations. From SERS studies, Au nanoparticles were found to be mostly inactive, while Ag nanoparticles showed good activity.

2.2.2 Deposition and characterization of the metal nanoparticles

We started with the deposition of gold nanoparticles on pectin. Metallic nanoparticles were prepared via a simple wet impregnation of the solid. A typical preparation used 1 g of commercial citrus pectin in 50 mL of 0.13 mM H₂AuCl₄ solution to obtain an Au content of 1 wt.% at the end of the treatment. For the conventional synthesis, the impregnation was run overnight at room temperature under magnetic stirring at 450 rpm in a 50 mL glass round-bottom flask, while for the US procedure the suspension was put in a 50 mL plastic test tube and left in an ultrasonic bath set at 40 kHz and 200 W for 30 min or 1 h. Surprisingly, this step alone already produced a blue-purple coloration on the pectin, clue of the formation of Au nanoparticles of the distinctive colour. We consequently decided to complete the preparation in three different ways: without the addition of a reducing agent or with the addition of a stoichiometric quantity of NaBH₄ or L-ascorbic acid (L-AA) as reducing agents. This was to investigate the role of the reducing agent on the nanoparticles size and morphology. After the addition of the reducing agent the suspension was left to stir for 1 h and finally it was filtered, washed three times with 50 mL H₂O and freeze-dried. The subsequent analysis of the materials was conducted via FESEM, collecting the back-scattered electrons (BSE mode): the detector collects electrons as they bounce back from dense material, this way Au nanoparticles would appear as bright white spot on a dark surface.

The analysis revealed that the addition of NaBH_4 led to non-homogeneous particles and agglomerates. Most nanoparticles were irregular globules of about 50 nm in diameter, but bigger hexagonal and triangular crystals were also observed (**Fig. 26**).

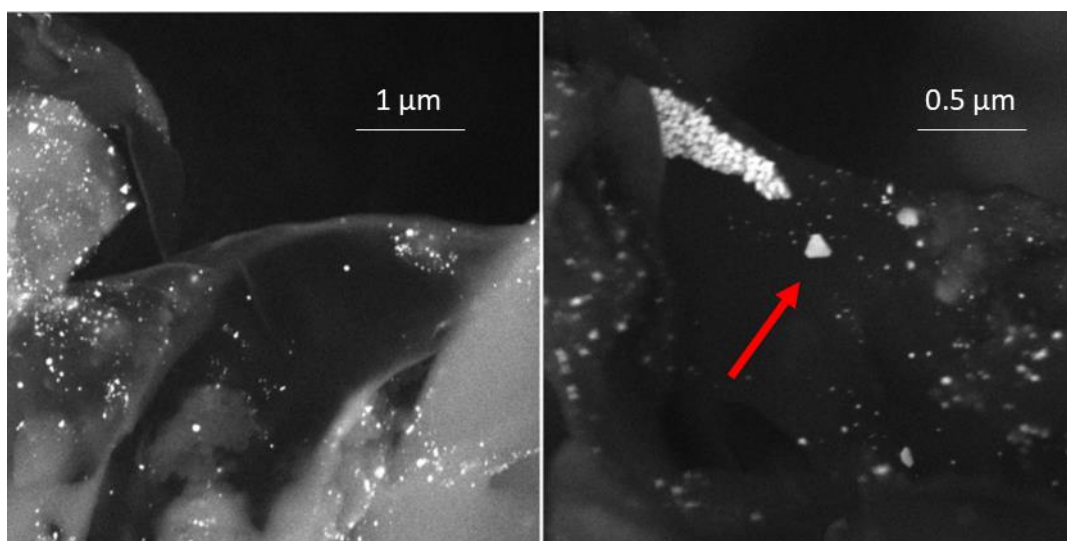


Figure 26: Au nanoparticles reduced with NaBH_4 . A gold crystal highlighted on the right. Left: 70.0 Kx, FOV 3.32 μm , BSE, 15 KeV. Right: 130.0 Kx, FOV 2.18 μm , BSE, 5 KeV.

This did not change with the time of the impregnation, since an attempt of adding NaBH_4 immediately after the coloration started to show (around 30 min) with no differences (**Fig.27**), or the kind of reductant, since the L-AA gave the same result.

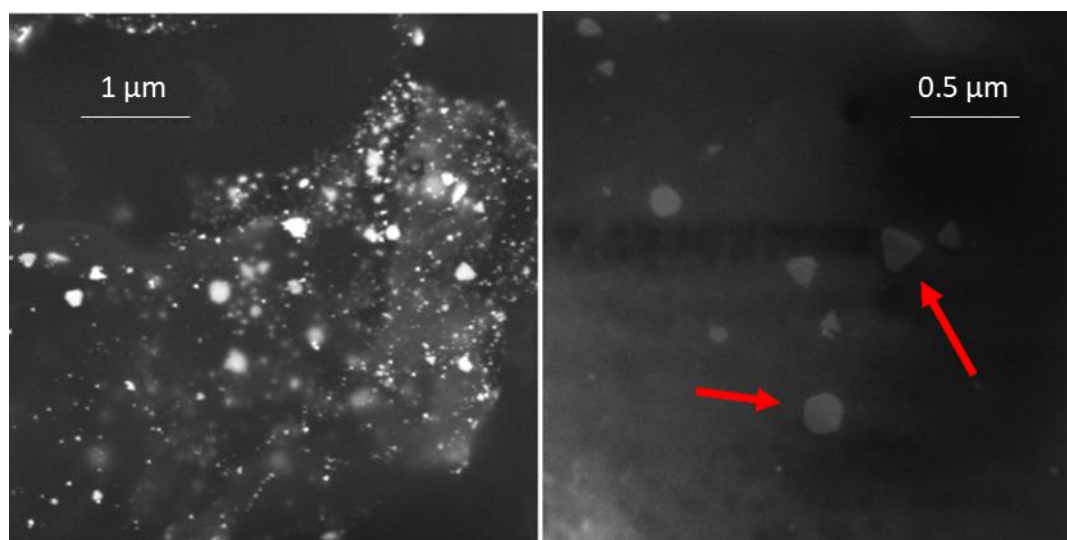


Figure 27: Au nanoparticles reduced with NaBH_4 after 30 min of stirring. Gold crystals highlighted on the right. Left: 50.0 Kx, FOV 5.66 μm , BSE, 10 KeV. Right: 100.0 Kx, FOV 2.83 μm , SE, 10 KeV.

A significant difference was found when no reducing agent was added to the suspension, thus relying on the intrinsic reducing properties of pectin (in our case, possibly due to ascorbic acid impurities). With this procedure, even though the particles shifted to higher diameters, they appeared more dispersed, with no significant agglomeration, and more homogeneous in size distribution (**Fig. 28**). No crystals were observed in the samples.

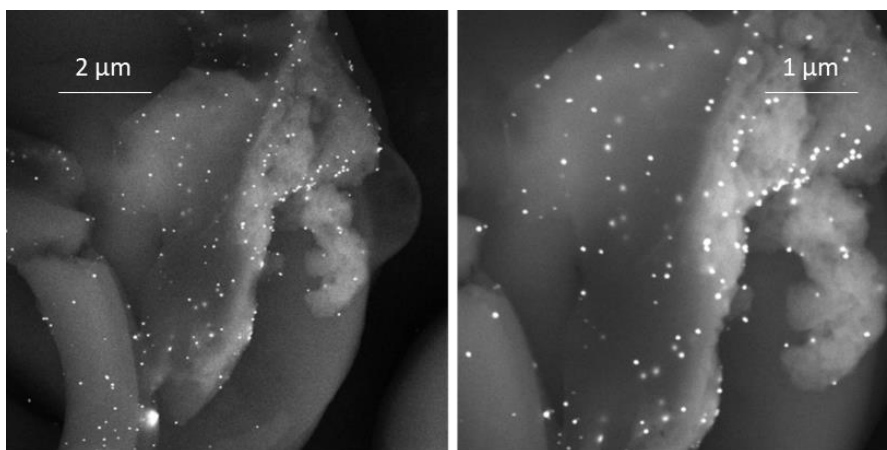


Figure 28: Au nanoparticles without reducing agents. Left: 30.0 Kx, FOV 9.44 μm , BSE, 15 KeV. Right: 50.0 Kx, FOV 2.66 μm , BSE, 15 KeV.

The use of US instead of mechanical stirring was tested with or without NaBH_4 and for 30 min or 1 h of impregnation (**Fig. 29**). When NaBH_4 is used, bigger particles are observed; also, 30 min showed insufficient for a quantitative gold uptake as the nanoparticles were barely observed in the samples, so 1 h was considered for future tests.

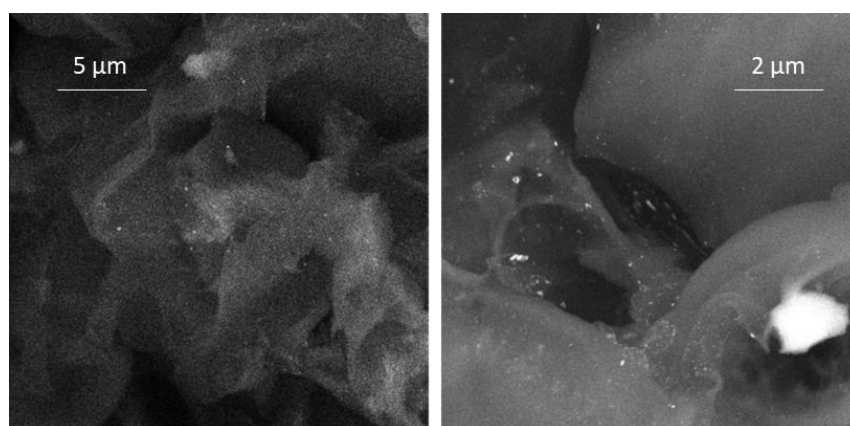


Figure 29: Au nanoparticles after 30 min of US with NaBH_4 . Left: 12.0 Kx, FOV 23.6 μm , BSE, 15 KeV. Right: 30.0 Kx, FOV 9.44 μm , BSE, 15 KeV.

Without NaBH_4 the use of US improved dispersion and reduced the nanoparticle size. Also, a number of Au crystals was observed (**Fig. 30**).

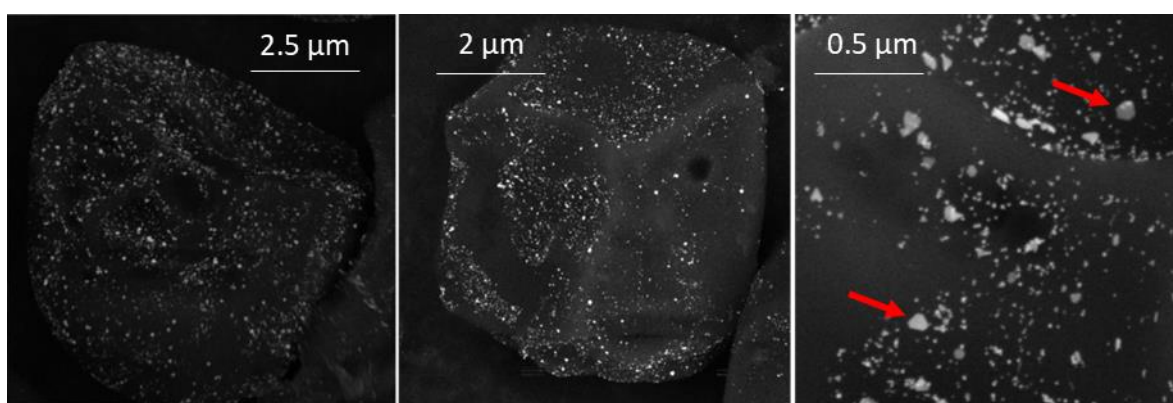


Figure 30: Au nanoparticles after 30 min of US without NaBH_4 . Left: 10.0 Kx, FOV 25.6 μm , BSE, 10 KeV. Centre: 20.0 Kx, FOV 14.2 μm , BSE, 10 KeV. Right: 100.0 Kx, FOV 2.83 μm , BSE, 15 KeV.

The comparison of the size distributions (**Table 10**) shows that the presence of a reducing agent has the greatest influence on the material, however the use of US led to smaller nanoparticles in both cases. The calculation for NaBH_4 treated samples is not reported since the population was too heterogeneous both with US and with conventional stirring.

Table 10: size distribution of Au nanoparticles.

	Reducing agent	Average size (nm)	Distribution (nm)
Conventional	L-AA	54.6	± 45.5
	-	43.0	± 15.0
US	-	35.3	± 17.7

Au nanoparticles have a distinct absorption band at around 20000 cm^{-1} (500 nm); its position is indicative of the nanoparticles' mean size (smaller nanoparticles result in a blueshift and *vice versa*) while its length represents how widely their size-distribution ranges. For these reasons, the Au-doped samples were also analysed with a UV-Vis spectrophotometer recording their diffuse reflectance (DR) spectra (**Fig. 31**).

When the conventional samples are compared, it can be seen how pectin has no absorption in the region so gold plasmonic band is clearly seen. The conventional samples are quite similar, even though the immediate (after 30 min) addition of NaBH_4 results in a broader band, meaning a more non-homogeneous sample: this is correct as no addition of reducing agents results in the thinner adsorption band. A later addition of NaBH_4 has less result on the plasmon (and the nanoparticles creating it) since most of the nanoparticles are already formed. Also, the immediate addition leads to a higher intensity at around 12000 cm^{-1} , a region which may be linked to Au agglomerates absorption. When US samples are compared the differences are less evident. It can be observed, however, how 1 h of US thins the plasmon band and reduces the adsorption at lower wavenumbers.

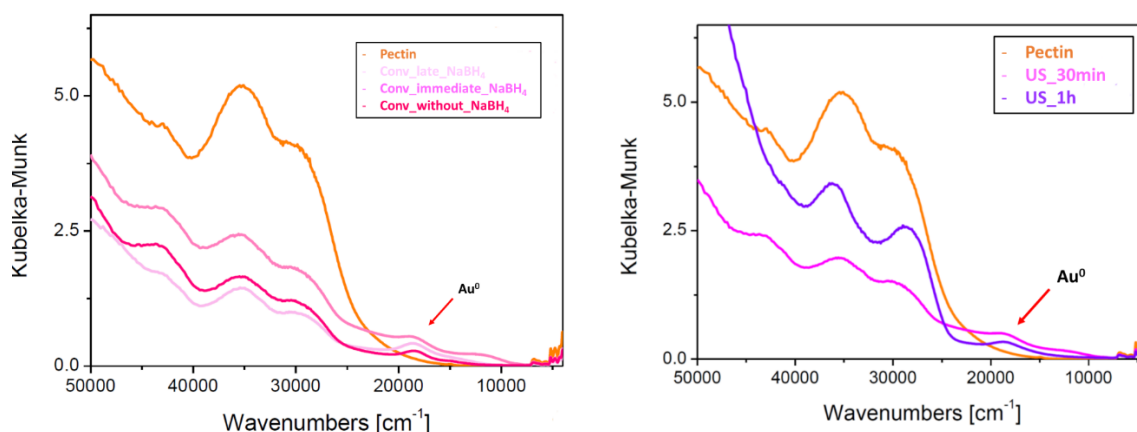


Figure 31: DR-UV-Vis analysis of the Au nanoparticles, with the Au⁰ plasmonic band highlighted.

For the preparation of Ag nanoparticles, the same procedures were followed. However, since the use of NaBH_4 or L-AA did not make any difference in previous tests, only L-AA was used for these samples. However, it was observed that if no reducing agent was used the formation of nanoparticles resulted insufficient. An interesting result was also the observation of many elongated wired formations when reducing agents were used (**Fig. 32**). They fell in the μm scale, however their true size was difficult to determine due to the irregular shape and they also varied a lot in dimensions, so no size distribution was calculated.

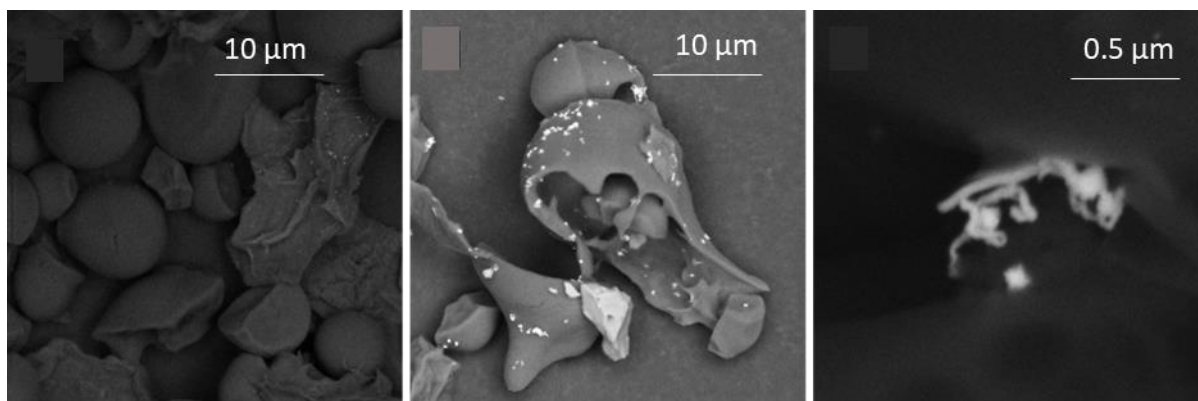


Figure 32: Ag nanoparticles reduced with L-AA under mechanical stirring. Left: 5.0 Kx, FOV 56.6 μm , BSE, 10 KeV. Centre: 6.0 Kx, FOV 47.2 μm , BSE, 10 KeV. Right: 113.0 Kx, FOV 2.52 μm , BSE, 10 KeV.

For Ag nanoparticles, the use of US had a dramatic influence over their shape and size (**Fig. 33**). Indeed, when US were used together with L-AA only few wired structures formed, while instead well dispersed rounded nanoparticles were predominantly observed, which was a desired result.

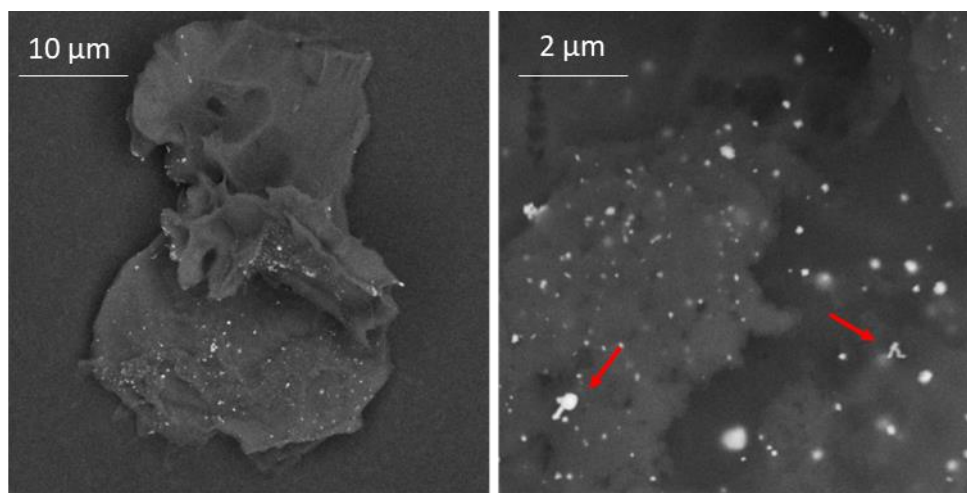


Figure 33: Ag nanoparticles reduced with L-AA under US. Residual wired structures highlighted on the right. Left: 5.0 Kx, FOV 56.6 μm , BSE, 10 KeV. Right: 30.0 Kx, FOV 9.44 μm , BSE, 10 KeV.

The use of US resulted in a size distribution of 106.6 ± 44.7 nm: a huge improvement respect to the conventional synthesis. Both for Au and Ag samples, the use of US resulted in a strong improvement in nanoparticle size distribution, however the best result was achieved with Au nanoparticles.

2.2.3 Doping with tetracycline derivatives

After the preparation of the nanoparticles, we moved on to the coupling of antibiotics to the carboxylic residues of the pectin. Au@pectin synthesized without reducing agents and Ag@pectin reduced with L-AA were selected for this further step. Both doxycycline (DOXY) and oxytetracycline (OXY), two common broad-spectrum antibiotics for human and veterinary use, were used for the coupling. We followed the procedure reported by M.B. Haddada *et al.* with only slight adjustments: 1 g of Au@pectin or Ag@pectin was suspended in 30 mL of water under magnetic stirring, 15.5 mg of EDC·HCl (0.1 mmol) and 4 mg of hydroxy succinimide (HSM, 0.025 mmol) were added together with 15 μ L of triethylamine (TEA, 0.1 mmol). After 1 h of stirring, during which the activation of the carboxylic groups with EDC happened, 10 mg of the chosen antibiotic were dissolved in 20 mL of water and added to the suspension. This new suspension was left to stir for 1 h at room temperature, then it was filtered and washed 3 times with 50 mL H₂O to be freeze-dried. The antibiotic uptake was calculated via UV-Vis analysis of the collected wastewaters from the washing: the antibiotic concentration was calculated and the uptake resulted in the difference between the starting 10 mg and the quantity in the washings (**Fig. 34**).

It was found that only OXY led to an appreciable uptake, whereas DOXY did not couple with the materials (**Table 11**). Both pectin treated under magnetic stirring and US were coupled with OXY to be later confronted in antimicrobial tests.

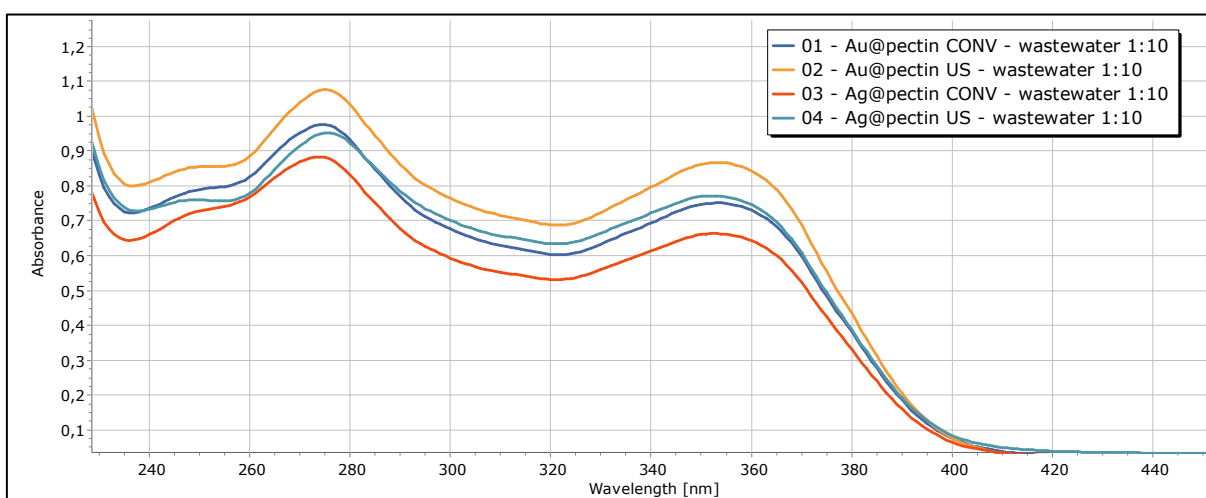


Figure 349: oxytetracycline content in the wastewaters for the different pectin.

Table 11: oxytetracycline uptake.

Sample	Conc. (mg/mL)	Uptake (%)	Wt. (%)
Au@pectin conv	0.050	6.0	0.04
Au@pectin US	0.060	5.2	0.04
Ag@pectin conv	0.042	6.6	0.06
Ag@pectin US	0.052	5.9	0.05

2.2.4 Antimicrobial tests and results

The antimicrobial activity of the prepared materials was assessed by a zone of inhibition test: it consists in measuring or comparing the radius of inhibition around a substance, placed in a culture medium. These experiments were performed in collaboration with Professor Di Nardo's group from the Department of Biological Sciences of University of Turin. Two separate bacteria strains were used: *Staphylococcus epidermidis* (gram positive) and *Escherichia coli* DH5 α (gram negative). The pectin was suspended and diluted to the concentrations of 6.75, 12.5, 25 and 50 $\mu\text{L/mL}$. Pure oxytetracycline and non-treated pectin were also tested as reference.

The samples are labelled as reported in **table 12**.

Table 12: list of the labels for the tested samples.

1	Au@pectin conv OXY	5	Au@pectin conv
2	Au@pectin US OXY	6	Au@pectin US
3	Ag@pectin conv OXY	7	Ag@pectin conv
4	Ag@pectin US OXY	8	Ag@pectin US

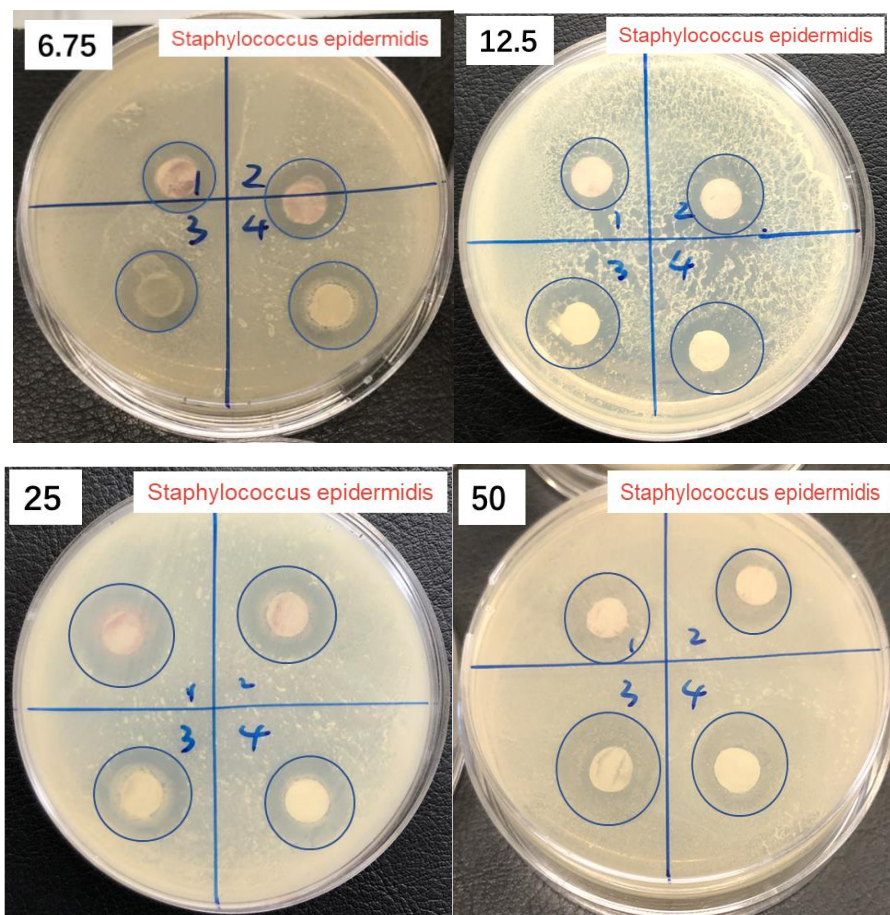


Figure 35: zone of inhibition tests over *S. epidermidis* at different antibiotic concentrations.

For the pectin doped with both metal nanoparticles and oxytetracycline the antimicrobial activity against *Staphylococcus epidermidis* is high even at the lowest concentration and it rises with concentration although not dramatically (**Fig. 35**). The two metal seems to have

similar activities, suggesting that oxytetracycline concentration is the dominant factor, and indeed pectin without antibiotic have a reduced activity (**Fig. 36**). Compared to the pure antibiotic we can see a clear improvement, however, so a possible explanation might be that both metal act as carriers of the drug, while not having strong antimicrobial activity on their own.

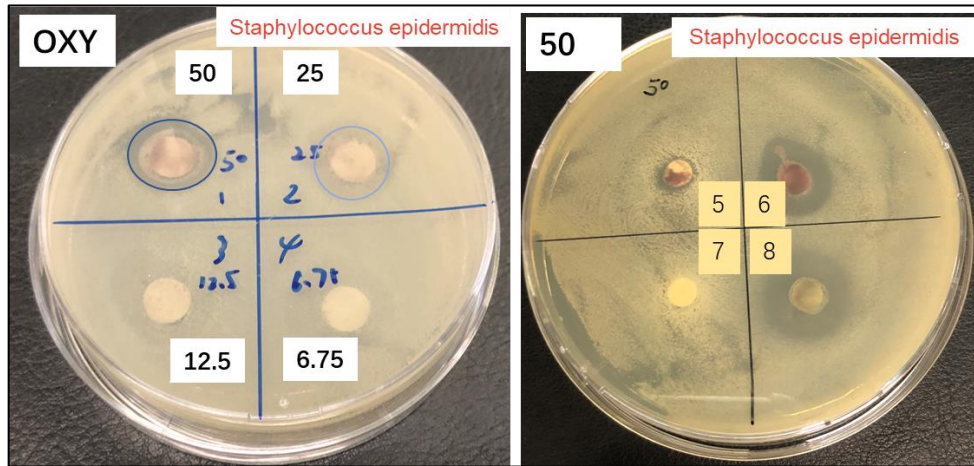


Figure 36: zone of inhibition tests over *S. epidermidis* for pure oxytetracycline and antibiotic-free pectin.

Against *E. coli* the antimicrobial activity was even greater (**Fig. 37**).

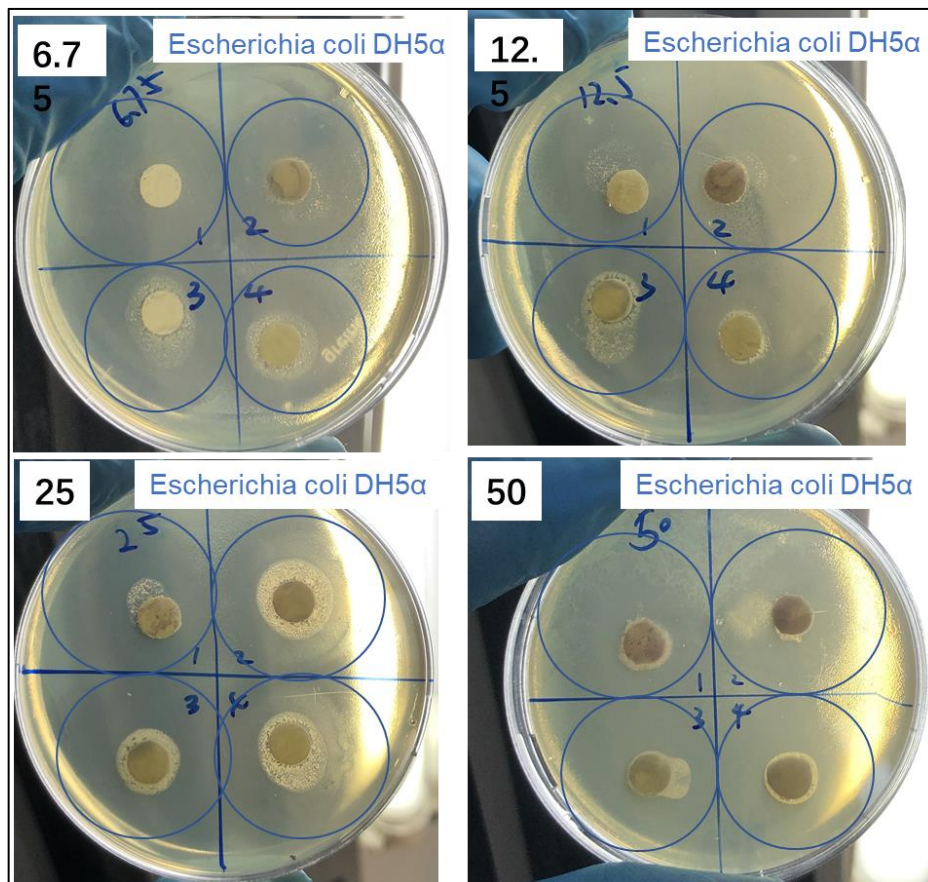


Figure 37: zone of inhibition tests over *E. coli* at different antibiotic concentrations.

Both Au and Ag-based pectin showed great inhibition against the microorganism. This time, though, it is not clear if the activity is enhanced or not respect to pure oxytetracycline (**Fig. 38**), but it is clearly improved compared to pectin without antibiotic. For *E. coli* it may be useful to repeat the test at lower concentration of oxytetracycline to have a clear comparison between the samples.

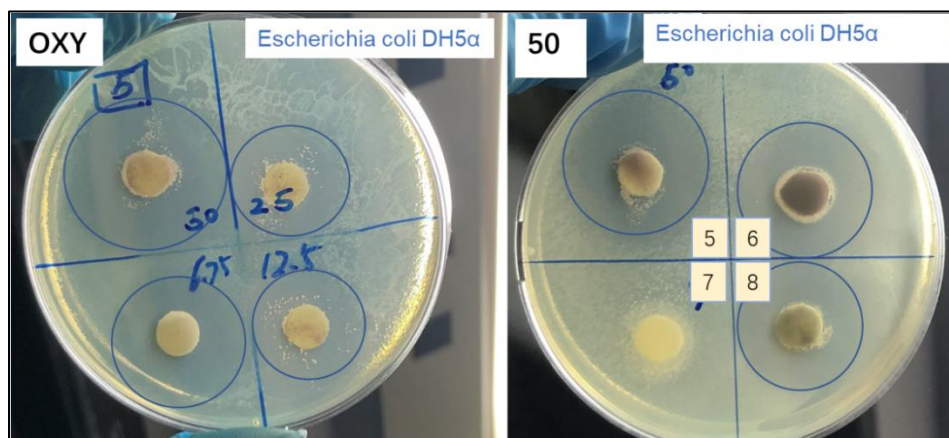


Figure 38: zone of inhibition tests over *E. coli* for pure oxytetracycline and antibiotic-free pectin.

2.2.5 Conclusion

The synthesis and characterization of novel Au and Ag nanoparticles supported over citrus pectin were proposed. The role of US application was demonstrated on the deposition of metal nanoparticles upon FESEM analysis: both with Au and Ag the US improved the dispersion and homogeneity, also allowing smaller nanoparticles on average. US had a huge impact over Ag nanoparticles in particular, since with conventional stirring irregular elongated particles formed, while with US dispersed spheres of regular shape and size appeared. For Au nanoparticles the role of US was measured but it was the reducing agent which had the greatest effect: avoiding the use of reducing chemicals and relying only on the reducing activity of natural pectin allowed more regular and dispersed nanoparticles. US enhanced this effect synergically, but if NaBH_4 was used the result was unsatisfactory even with US.

Upon coupling with the antibiotic oxytetracycline the supported nanoparticles were tested against *E. coli* and *S. epidermidis* in some zone of inhibition experiments. The tests showed that the coupled materials had greater antibacterial activity than both the supported nanoparticles without antibiotic and the pure oxytetracycline (although results are less clear for *S. epidermidis*). The antibiotic and the metal nanoparticles showed a synergistic effect, possibly explained by the role of the nanoparticles as drug carriers.

These positive results demonstrate the feasibility of US for tailored nanoparticle synthesis over a benign support as pectin, and the possible synthesis of new antimicrobial materials with green and efficient protocols.

2.3 US-assisted preparation and characterization of metallic heterogeneous catalysts

2.3.1 Introduction

As previously discussed, heterogeneous catalysis is a fundamental tool for green chemistry. A heterogeneous catalyst can be easily filtered, washed, and recycled, while homogeneous catalysts often need to be extracted with great expense of organic solvents. Transition metals are often used for catalytic purposes in synthesis and conversions. One possibility to prepare a metal-based heterogeneous catalyst is to support metallic nanoparticles onto another material. High surface area materials such as activated carbons or zeolites are often the choice to disperse the metal and host the substrate for the reaction^{168,169}. The support can also have more active roles in the reaction, for example the use of TiO₂ to support Au nanoparticles for the hydrogenation of LA to 1,4-pentanediol proved crucial in the activation of the intermediate GVL and in the formation of highly active hydrogen species thanks to the spill-over from the Au to the support¹⁷⁰. Different supports do not only lead to different dispersion of the nanoparticles, but may also influence their charge or shape, leading to different properties for the same metal¹⁷¹.

Since a focus on the conversion of chemicals through hydrogenation and oxidation was an objective of this thesis, we decided to prepare metal-based catalysts for the scope. Rh was initially chosen as many hydrogenation reactions require it as a catalyst¹⁷²⁻¹⁷⁴ and it was possible to compare the obtained catalysts with commercial equivalents. Co was also used to provide a possible cheaper alternative for Rh catalysis. Au-based catalysts were mainly prepared for oxidation reactions. Activated carbon Norit® and carbon nanofibers of high graphitization degree (HHT) were used as carbonaceous supports for the catalysts. Activated carbons are cheap porous materials that are commonly used as supports for heterogeneous catalysts, however their properties and structure are often difficult to control and determine. Carbon nanofibers offer a possible alternative: their structure is more regular and composed of stacked sheets of graphene. They present a high porosity coupled with tensile strength, useful for their recycling after the reaction. Examples exist of highly dispersed Rh nanoparticles on such support, with good catalytic activity for hydrogenation reactions^{175,176}. Carbon nanofibers were synthesized and provided us by prof. Alberto Villa's group at University of Milan. It was their experience that such material improved catalytic activity compared to normal activated carbon for Pd catalysts¹⁷⁷ and were also able to prepare bimetallic Pd-Rh catalysts for formic acid dehydrogenation, which proved more stable and active than monometallic Pd¹⁷⁸. We also decided to test our synthesized β CDPIS as a support for catalysis. Cyclodextrins have been used for the preparation of catalyst thanks to their ability to coordinate metal ions in liquid medium. These "immobilized" ions can act as catalyst themselves or be reduced to metal nanoparticles. Cu^{II} ions were successfully coordinated by β CD grafted onto silica to prepare a heterogeneous catalyst for alkyne azide reactions¹⁷⁹. Supported Pd catalysts were also prepared using β CD as solid support: firstly, the metal ions were coordinated in solution and then reduced¹⁸⁰. US application proved useful in increasing the dispersion of the nanoparticles, and so the catalytic activity¹⁸¹. Since US have proven useful in obtaining highly dispersed metal nanoparticles onto solid supports¹⁸²⁻¹⁸⁴, we studied their application to improve the catalytic performances of our materials as well.

2.3.2 Preparation of Rh-based catalysts

For Rh-based catalyst RhCl_3 was used as precursor. We aimed for 1 wt.% and 5 wt.% catalyst for a direct comparison with commercial products so, for 1 g of support, 20.3 mg RhCl_3 (0.1 mmol) were needed for the 1 wt.%, or 101.5 mg of RhCl_3 (0.5 mmol) for the 5 wt.%. Different ways exist to deposit metal nanoparticles onto solid supports. The precipitation-deposition method usually leads to small nanoparticle precipitates: this consists in starting from a soluble salt and transforming it into an insoluble one, usually a hydroxide. This requires a strong alkaline solution. After the precipitation the hydroxides can be reduced to metal via chemical reduction. In our case, however, even at pH above 12 both in water or MeOH a complete precipitation of $\text{Rh}(\text{OH})_3$ was not achieved, so a simple impregnation with RhCl_3 followed by a chemical reduction was chosen instead.

In a typical preparation, a 0.025 mM stock solution of RhCl_3 was diluted as needed to a volume of 50 mL of aqueous solution. In these 50 mL, 1 g of support was suspended, and US were applied. Both an ultrasonic plate and an ultrasonic horn were tested for the Rh/C catalysts. The ultrasonic plate used (Weber MG 200) could be set to 40, 80 or 120 kHz with a power of 200 W. The ultrasonic horn worked at 20 kHz with a generator (Heinertec Shozou) working at 50 W. When the ultrasonic plate was used, sonication was applied for 1 h using a cooling serpentine inside the bath to control the temperature. With the horn instead, only a total of 30 min of sonication was applied since the US application via a horn is generally more effective. After 10 min the sonication was stopped, and the sample allowed to cool in an ice bath for 5 min before restarting: this kept the working temperature between 10-40 °C.

After the impregnation step, the suspension was cooled to room temperature and put to stir. A stoichiometric amount of NaBH_4 was added to reduce Rh^{3+} to Rh^0 , stirring for 1 h. After that, the solid was filtered, washed three times with 50 mL of distilled water and dried in oven (80 °C) overnight.

2.3.3 Preparation of Co-based catalysts

Co is a precious metal of the 9th group, just like Rh but part of the 4th period instead. Transition metals of the same group tend to have similar properties, such is the case for Cu and Au or Pt and Pd, so Co may be a good candidate in replacing Rh in some reaction given the latter's prohibitive cost¹⁸⁵⁻¹⁸⁷. For this reason, we also prepared a supported Co-based catalyst to test in hydrogenation reactions.

We repeated the wet impregnation procedure as with RhCl_3 but using $\text{Co}(\text{CH}_3\text{COO})_2$ as precursor instead, so a 0.028 mM stock solution was prepared. Aiming for a 5 wt.% catalyst, 150.2 mg of $\text{Co}(\text{CH}_3\text{COO})_2$ (0.85 mmol) were necessary for 1 g of support (activated carbon Norit®). US were applied through an ultrasonic horn working at 20 kHz and 50 W power. After the impregnation, a stoichiometric amount of NaBH_4 was added to the suspension and stirred for 1 h. The solid was then filtered, washed three times with 50 mL of distilled water and dried in oven (80 °C) overnight. Thus, the catalyst Co/C US 5% was obtained.

2.3.4 Deposition of Rh and Au nanoparticles over cyclodextrin-based polymer

Previously was discussed the synthesis of new β CD insoluble polymers (β CDPIS and Me β CDPIS) for adsorption processes. However, given the resilience of cyclodextrins to reaction conditions, these polymers can be also useful as green, easy to recover supports for metal nanoparticles. We decided to investigate this possibility starting with the β CDPIS polymer, since it is prepared from a green and natural occurring monomer and has the simplest composition. We selected once again Rh for hydrogenation reactions and Au for oxidations. Examples exist in literature of heterogeneous catalysts based on CD polymers¹⁸⁸. Recently, Tabasso *et al.* demonstrated the synergy between MW radiation and a Pd-based catalyst supported onto a cross-linked β CD polymer for the functionalization of thiophenes¹⁸⁹. The catalyst showed excellent flexibility and robustness, being successfully applied for the conversion of numerous substrates using GVL as a solvent and showing negligible leaching. Huang *et al.* described the synthesis of sub-nanometric metal nanoparticles of various noble metals over a cross-linked β CD polymer¹⁹⁰. Per-(6-azido-6-deoxy)- β -cyclodextrins were used as monomers in a click-chemistry synthesis; the excellent coordination properties of the polymer allowed the formation of small and dispersed particles with a simple wet impregnation followed by a chemical reduction. The catalysts were successfully applied for the hydrogenation of nitro-compounds and Suzuki-Miura coupling reaction in mild conditions.

Metal nanoparticles were prepared by simple wet impregnation of the support, as previously described, with or without US. Aiming for a 5 wt.% catalyst, in a typical preparation, a 0.025 mM stock solution of RhCl_3 or 0.015 mM of HAuCl_4 was diluted as needed to a volume of 50 mL in distilled water. Secondly, 1 g of β CDPIS was added to the mixture. For the conventional process, the suspension was stirred at 450 rpm overnight, otherwise 30 min of US at 20 kHz were applied. After the impregnation step, a stoichiometric amount of NaBH_4 (for the Rh-based) or L-AA (for the Au-based) was added, and the suspension was stirred for an additional hour, otherwise 10 min of US application was followed by 1 h of stirring. Finally, the solid was filtered washed three times with 50 mL of distilled water and freeze-dried. The catalysts so obtained were labelled Au/ β CDPIS 5%, Au/ β CDPIS US 5%, Rh/ β CDPIS 5% and Rh/ β CDPIS US 5%. Also, since the materials were firstly prepared by ball milling, we also tested the possibility of preparing a heterogeneous catalyst by a dry impregnation followed by the addition of the reducing agent, all in ball mill. For these preparations 1 g of β CDPIS and 101.5 mg of RhCl_3 or 76.6 mg of AuCl_3 were added together in a stainless-steel jar. 35 g of stainless-steel balls were added. First a "dry impregnation" is performed at 300 rpm for 90 min: this step dispersed the metallic precursor inside the polymeric matrix and a homogeneous coloration could be appreciated at the end. Next was the reduction step: for Rh a stoichiometric quantity of NaBH_4 was added, while L-AA was used for Au instead. This second step, which implied a true chemical reaction, was performed at 550 rpm for 90 min. A dark-coloured powder was visible at the end. The powder was sieved and suspended in 50 mL of water, for the usual 3x50 mL of washings and freeze-drying. The so obtained materials were labelled Au/ β CDPIS 5% BM and Rh/ β CDPIS 5% BM.

2.3.5 Model reactions over the β CDPIS-based catalysts

In order to study the catalytic activity of the prepared catalysts we selected some model reactions to run. The objective was not the reaction itself, but the compared results at the end. For the Rh-based catalysts we tested the benzene ring hydrogenation reaction using toluene and hydroquinone as substrates; since Au catalysts can be used both for oxidation and hydrogenation reaction, we tested the oxidation of benzyl alcohol to benzaldehyde and the reverse hydrogenation of benzaldehyde to its alcohol.

For the benzene ring hydrogenation reactions 100 μ L of toluene (0.95 mmol) or 100 mg of hydroquinone (0.91 mmol) were dissolved in 5 mL of ethyl acetate in a glass vial. 10 mg of the chosen catalyst were added, and the reaction was run under H₂ pressure in a MW multimodal autoclave (SynthWave, Milestone srl.).

Table 13: hydrogenation reactions over the Rh-based catalysts.

Entry	Substrate	Catalyst	T (°C)	Conversion (%)	Selectivity (%)	Yield (%)
1	Toluene	Rh/ β CDPIS conv.	80	100	100	100
2		Rh/ β CDPIS conv.	60	10.5	100	10.5
3		Rh/ β CDPIS US	60	100	100	100
4		Rh/ β CDPIS BM	60	8.7	100	8.7
5	Hydroquinone	Rh/ β CDPIS conv.	80	100	61.4	61.4
6		Rh/ β CDPIS conv.	60	10.7	100	10.7
7		Rh/ β CDPIS US	60	63.4	74.1	47.0
8		Rh/ β CDPIS BM	60	3.3	100	3.3

Reaction conditions: 100 μ L of toluene or 100 mg of hydroquinone, 5 mL EtOAc, 10 bar H₂, 4 h, 10 mg of catalyst (5 wt.%).

Toluene was always converted to methyl cyclohexane with complete selectivity, however the conventional catalyst needed 80 °C to obtain complete conversion, while with the US catalyst 100 % yield was obtained even at 60 °C (**Table 13, entries 1 and 3**). No significant difference in catalytic activity was found between the BM catalyst and the conventional one (**Table 13, entries 2 and 4**). For hydroquinone complete conversion to 1,4-cyclohexandiol was only observed at 80 °C, however a higher temperature also led to the formation of 4-hydroxycyclohexanone, lowering the yield to 61.4 % (**Table 13, entry 5**). At 60 °C selectivity was complete, but conversion dropped for the conventional catalyst achieving only a 10.7 % yield. At the same temperature the US catalyst achieved a 47.0 % yield with a high albeit not complete selectivity (**Table 13, entry 7**) while the BM catalyst hardly converted the substrate at all.

The results suggest a strong correlation between the US impregnation procedure and the catalytic activity, while BM treatment does not seem to offer any advantage to the conventional impregnation, except for the avoidance of solvent during the synthesis. The results were good enough to justify a comparison between Rh/ β CDPIS US and a commercial Rh/C 5 wt.%. The Rh/ β CDPIS US catalyst outperformed the commercial equivalent for both reactions. The compared results are listed in **Table 14**.

Table 14: comparison between the Rh/ β CDPIS US catalyst and a commercial equivalent.

Entry	Substrate	Catalyst	Conversion (%)	Selectivity (%)	Yield (%)
1	Toluene	Rh/ β CDPIS US	100	100	100
2		Rh/C	88.6	100	88.6
3	Hydroquinone	Rh/ β CDPIS US	63.4	74.1	47.0
4		Rh/C	66.2	32.5	24.8

Reaction conditions: 100 μ L of toluene or 100 mg of hydroquinone, 5 mL EtOAc, 10 bar H₂, 60 °C, 4 h, 10 mg of catalyst (5 wt.%).

For the oxidation of benzyl alcohol to benzaldehyde reaction over the Au-based catalysts 100 μ L of benzyl alcohol (0.93 mmol) were dispersed in 5 mL of water and 10 mg of catalyst (5 wt.%) were added. For the hydrogenation of benzaldehyde to benzyl alcohol 100 μ L of benzaldehyde (0.94 mmol) were dissolved in 5 mL of ethyl acetate and 10 mg of catalyst (5 wt.%) were added. The reactions were both run in the same MW autoclave, under O₂ or H₂ pressure.

Table 15: oxidation and hydrogenation reactions over the Au-based catalysts.

Entry	Substrate	Catalyst	T (°C)	Conversion (%)	Selectivity (%)	Yield (%)
1	Benzyl alcohol	Au/ β CDPIS conv.	80	3.0	100	3.0
2		Au/ β CDPIS conv.	60	0.0	0.0	0.0
3		Au/ β CDPIS US	80	10.3	100	10.3
4		Au/ β CDPIS BM	80	2.7	100	2.7
5	Benzaldehyde	Au/ β CDPIS conv.	80	0.0	0.0	0.0
6		Au/ β CDPIS conv.	120	0.0	0.0	0.0
7		Au/ β CDPIS US	120	0.0	0.0	0.0
8		Au/ β CDPIS BM	120	0.0	0.0	0.0

Reaction conditions: 100 μ L of benzyl alcohol or benzaldehyde, 5 mL H₂O or EtOAc, 10 bar O₂ or H₂, 4 h, 10 mg of catalyst (5 wt.%).

The oxidation of benzyl alcohol to benzaldehyde did not give great result with neither catalyst (**Table 15**). Conversion was only possible at 80 °C; both the conventional and the BM Au catalyst gave \approx 3 % yield while the US catalyst reached a 10.3 % yield in benzaldehyde. The yields were poor overall, however the Au/ β CDPIS US catalyst was clearly the best performing (**Table 14, entry 3**). The poor results might be due to modifications of the support under O₂ atmosphere, however further analysis is needed to confirm this hypothesis, for example ATR analysis of the spent catalyst. Worst yet for the hydrogenations, for which the Au catalysts showed no activity, even when temperature was increased from 80 to 120 °C. This suggest that the catalysts are actually better suited for oxidation purposes, although harsher conditions are needed respect to those tested so far.

2.3.6 Conclusion

A number of catalysts was prepared using US as enabling technology to improve the dispersion of the metallic nanoparticles over the support. Activated carbon and carbon nanofibers were used to support Rh and Co catalyst, prepared both with a conventional impregnation under mechanical stirring and using US generated by ultrasonic plates and horn. These materials will be tested in chemical conversion and organic reactions in the following chapter, allowing a comparison between different metals, support and preparations and their effect over the reaction outcome.

Heterogeneous catalysts were also prepared using our β CDPIS polymer as support for Rh and Au nanoparticles. For these catalysts mechanical stirring, US and BM were used to disperse the precursor, followed by a chemical reduction. The obtained catalysts were then compared for some model reactions. Rh-based catalysts showed remarkable activity for hydrogenations even at low temperature (60 °C) and in particular Rh/ β CDPIS US outperformed the others and even the commercial Rh/C catalyst. The Au-based catalysts were less active overall; they were tested for both oxidation and hydrogenation reactions but only showed activity for the first mechanism. Once again, the catalyst prepared under US (Au/ β CDPIS US) was the best performing, achieving a 10.3 % conversion of benzyl alcohol to benzaldehyde. The results show how US can improve the catalytic performances of heterogeneous catalyst and the possibility to use our β CDPIS polymer as support. Further characterizations will show how the support interacts with the nanoparticles exactly and new catalytic tests will be performed for reactions of true interest.

References

105. Loftsson T, Duchêne D. *International Journal of Pharmaceutics*, 2007, **329**, 1–11.
106. Crini G, Fourmentin S, Fenyvesi É, et al. Springer, Cham, pp. 1–55.
107. Loftsson T, Brewster ME. *J Pharm Sci*, 1996, **85**, 1017–1025.
108. Szejtli J. *Chem Rev*, 1998, **98**, 1743–1753.
109. Irie T, Uekama K. *Journal of Pharmaceutical Sciences*, 1997, **86**, 147–162.
110. Fenyvesi E, Gruiz K, Verstichel S, et al. *Chemosphere*, 2005, **60**, 1001–1008.
111. Stevens DA. *Pharmacotherapy*, 1999, **19**, 603–611.
112. Frank SG, Kavaliunas DR. *J Pharm Sci*, 1983, **72**, 1215–1217.
113. Sigurdsson HH, Magnusdottir A, Másson M, et al. *J Incl Phenom*, 2002, **44**, 163–167.
114. Taylor GT, Weiss J, Pitha J. *Pharm Res An Off J Am Assoc Pharm Sci*, 1989, **6**, 641–646.
115. Matsuda H, Arima H. *Adv Drug Deliv Rev*, 1999, **36**, 81–99.
116. Uekama K, Adachi H, Irie T, et al. *J Pharm Pharmacol*, 1992, **44**, 119–121.
117. Szejtli J, Szenté L. *Eur J Pharm Biopharm*, 2005, **61**, 115–125.
118. Fejős I, Kalydi E, Malanga M, et al. *J Chromatogr A*, 2020, **1627**, 461375.

119. Singh M, Sharma R, Banerjee UC. *Biotechnol Adv*, 2002, **20**, 341–359.
120. Del Valle EMM. *Process Biochem*, 2004, **39**, 1033–1046.
121. Hedges A. In: *Starch*. Academic Press, 2009, pp. 833–851.
122. Liu Y, Lin T, Cheng C, et al. *Molecules*, 2021, **26**, 1090.
123. Ghorpade VS, Yadav AV, Dias RJ, et al. *Int J Biol Macromol*, 2018, **118**, 783–791.
124. Gidwani B, Vyas A. *Colloids Surfaces B Biointerfaces*, 2014, **114**, 130–137.
125. Wang D, Song S, Feng J, et al. *Materials (Basel)*, 2017, **10**, 343.
126. Crini G. *Environ Chem Lett*, 2021, **19**, 2383–2403.
127. Sancey B, Trunfio G, Charles J, et al. *Journal of Inclusion Phenomena and Macrocyclic Chemistry*, 2011, pp. 315–320.
128. Jurecska L, Dobosy P, Barkács K, et al. *J Pharm Biomed Anal*, 2014, **98**, 90–93.
129. Cova TF, Murtinho D, Aguado R, et al. *Polysaccharides*, 2021, **2**, 16–38.
130. Saifi A, Joseph JP, Singh AP, et al. *ACS Omega*, 2021, **6**, 4776–4782.
131. Alsbaiee A, Smith BJ, Xiao L, et al. *Nature*, 2016, **529**, 190–194.
132. Crini G, Exposito SA, Rocchi S, et al. *Heliyon*, 2017, **3**, e00380.
133. Fenyvesi É, Barkács K, Gruiz K, et al. *J Hazard Mater*, 2020, **383**, 121181.
134. Friščić T, Mottillo C, Titi HM. *Angew Chemie - Int Ed*, 2020, **59**, 1018–1029.
135. Do JL, Friščić T. *ACS Cent Sci*, 2017, **3**, 13–19.
136. Renard E, Barnathan G, Deratani A, et al. *Macromol Symp*, 1997, **122**, 229–234.
137. Jicsinszky L, Bucciol F, Manzoli M, et al. *Curr Org Chem*, 2021, **25**, 1923–1936.
138. De Andrade JR, Oliveira MF, Da Silva MGC, et al. *Ind Eng Chem Res*, 2018, **57**, 3103–3127.
139. Grassi M, Kaykioglu G, Belgiorno V, et al. Springer, Dordrecht, pp. 15–37.
140. Chang EE, Wan JC, Kim H, et al. *Sci World J*, **2015**. Epub ahead of print 2015. DOI: 10.1155/2015/186501.
141. Da'na E. *Microporous Mesoporous Mater*, 2017, **247**, 145–157.
142. Liakos E V., Lazaridou M, Michailidou G, et al. *Macromol*, 2021, **1**, 130–154.
143. Huang L, Shen R, Shuai Q. *J Environ Manage*, **277**. Epub ahead of print 1 January 2021. DOI: 10.1016/J.JENVMAN.2020.111389.
144. Mohnen D. *Curr Opin Plant Biol*, 2008, **11**, 266–277.
145. Kitir N, Yildirim E, Şahin Ü, et al. In: *Peat*. IntechOpen. Epub ahead of print 5 November 2018. DOI: 10.5772/intechopen.79171.
146. Bonnin E, Pelloux J. In: *Pectin: Technological and Physiological Properties*. Springer, Cham, pp. 37–60.
147. Abbott DW, Boraston AB. *Microbiol Mol Biol Rev*, 2008, **72**, 301–316.
148. Jonker D, Fowler P, Albers R, et al. *Food Chem Toxicol*, 2020, **139**, 111243.

149. Aleeva S V., Lepilova O V., Koksharov SA. *Prot Met Phys Chem Surfaces*, 2021, **57**, 37–44.
150. Pellerin P, O'Neill MA. *Analisis*, **26**. Epub ahead of print 1998. DOI: 10.1051/analisis:1998143.
151. Haddada M Ben, Jeannot K, Spadavecchia J. *Part Part Syst Charact*, 2019, **36**, 1–11.
152. Tao C. *Lett Appl Microbiol*, 2018, **67**, 537–543.
153. Zhang Y, Shareena Dasari TP, Deng H, et al. *J Environ Sci Heal - Part C Environ Carcinog Ecotoxicol Rev*, 2015, **33**, 286–327.
154. Durán N, Durán M, de Jesus MB, et al. *Nanomedicine: Nanotechnology, Biology, and Medicine*, 2016, **12**, 789–799.
155. Kailasa SK, Park TJ, Rohit J V., et al. In: *Nanoparticles in Pharmacotherapy*. William Andrew Publishing, 2019, pp. 461–484.
156. Kim JS, Kuk E, Yu KN, et al. *Nanomedicine Nanotechnology, Biol Med*, 2007, **3**, 95–101.
157. Gu X, Xu Z, Gu L, et al. *Environ Chem Lett*, 2021, **19**, 167–187.
158. Gupta A, Moyano DF, Parnsubsakul A, et al. *ACS Appl Mater Interfaces*, 2016, **8**, 14096–14101.
159. Zou Y, Xie R, Hu E, et al. *Int J Biol Macromol*, 2020, **148**, 921–931.
160. Zhao X, Jia Y, Li J, et al. *ACS Appl Mater Interfaces*, 2018, **10**, 29398–29406.
161. Khandelwal P, Singh DK, Sadhu S, et al. *Nanoscale*, 2015, **7**, 19985–20002.
162. Said J, Dodoo CC, Walker M, et al. *Int J Pharm*, 2014, **462**, 123–128.
163. Agnihotri S, Mukherji S, Mukherji S. *Nanoscale*, 2013, **5**, 7328–7340.
164. Osonga FJ, Akgul A, Yazgan I, et al. *Molecules*, 2020, **25**, 2682.
165. Yang Y, Shi J, Kawamura G, et al. *Scr Mater*, 2008, **58**, 862–865.
166. Samal AK, Polavarapu L, Rodal-Cedeira S, et al. *Langmuir*, 2013, **29**, 15076–15082.
167. Balachandran YL, Panarin AY, Khodasevich IA, et al. *J Appl Spectrosc*, 2015, **81**, 962–968.
168. Anthonysamy SBI, Afandi SB, Khavarian M, et al. *Beilstein J Nanotechnol*, 2018, **9**, 740–761.
169. Campelo JM, Luna D, Luque R, et al. *ChemSusChem*, 2009, **2**, 18–45.
170. Bucciol F, Tabasso S, Grillo G, et al. *J Catal*, 2019, **380**, 267–277.
171. Sankar M, He Q, Engel R V., et al. *Chem Rev*, 2020, **120**, 3890–3938.
172. Fujiwara H, Ogasawara Y, Kotani M, et al. *Chem - An Asian J*, 2008, **3**, 1715–1721.
173. Cao P, Su L, Li C, et al. *Rubber Chem Technol*, 2015, **88**, 547–559.
174. Saito Y, Kobayashi S. *J Am Chem Soc*, 2020, **142**, 16546–16551.
175. Ros TG, Keller DE, Van Dillen AJ, et al. *J Catal*, 2002, **211**, 85–102.
176. Motoyama Y, Takasaki M, Yoon SH, et al. *Org Lett*, 2009, **11**, 5042–5045.
177. Testolin A, Cattaneo S, Wang W, et al. *Surfaces*, 2019, **2**, 205–215.
178. Barlocco I, Capelli S, Zanella E, et al. *J Energy Chem*, 2020, **52**, 301–309.
179. Martina K, Calsolaro F, Zuliani A, et al. *Molecules*, 2019, **24**, 2490.
180. Zare Asadabadi A, Hoseini SJ, Bahrami M, et al. *New J Chem*, 2019, **43**, 6513–6522.

181. Martina K, Baricco F, Caporaso M, et al. *ChemCatChem*, 2016, **8**, 1176–1184.
182. Perkas N, Rotter H, Vradman L, et al. *Langmuir*, 2006, **22**, 7072–7077.
183. Pol VG, Grisar H, Gedanken A. *Langmuir*, 2005, **21**, 3635–3640.
184. Perkas N, Zhong Z, Chen L, et al. *Catal Letters*, 2005, **103**, 9–14.
185. Knijnenburg Q, Horton AD, Van Der Heijden H, et al. *J Mol Catal A Chem*, 2005, **232**, 151–159.
186. Li YY, Yu SL, Shen WY, et al. *Acc Chem Res*, 2015, **48**, 2587–2598.
187. Khodakov AY, Griboval-Constant A, Bechara R, et al. *J Catal*, 2002, **206**, 230–241.
188. Herbois R, Noël S, Léger B, et al. *Green Chem*, 2015, **17**, 2444–2454.
189. Tabasso S, Calcio Gaudino E, Acciardo E, et al. *Front Chem*, 2020, **8**, 253.
190. Huang T, Sheng G, Manchanda P, et al. *Sci Adv*, **5**. Epub ahead of print 1 November 2019. DOI: 10.1126/sciadv.aax6976.

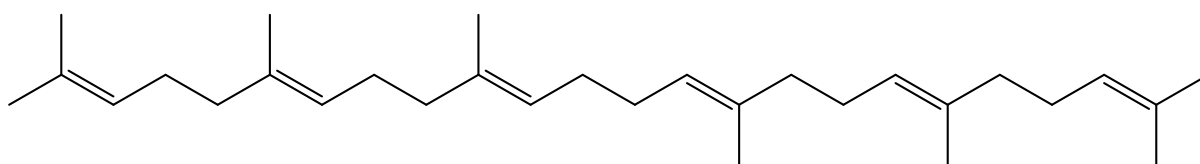
3.0 Enabling technologies for synthesis and PI

Enabling technologies are powerful tool to make chemistry more efficient and greener. In particular, we focused on the application of MW for the conversion of building blocks to high added value molecules. When possible, substrates from renewable feedstocks were chosen such as LA, glucose or furfural. As previously discussed, MW allow fast and selective heating leading to a reduction of reaction time, improved selectivity and energy efficiency. Furthermore, we implemented the use of green solvents for the reactions such as water or alcohols instead of far more polluting DMF, DMSO or CHCl_3 . We also aimed for a one-pot approach, running all the synthetic steps in the same container without intermediate workups: this approach, if met, is important for the scalability of the reaction. A one-pot synthesis improves the productivity of a process and reduces the wasted deriving from washings and filtrations. In general, synthesis on renewable feedstocks using green reagents and solvents were studied to fill the gaps in the bio-refinery approach and apply green chemistry on relevant processes. Also, attention to scalability and PI for the reaction, even in laboratory scale, was given to simplify future real-life applications of the studied synthesis.

3.1 Squalene and FAME recovery from ODD and hydrogenation to squalane

3.1.1 Introduction and state of the art

Squalene is a natural terpenoid (**Fig. 39**) that has a biological activity in humans as precursor of cholesterol and steroid hormones¹⁹¹. It was firstly isolated from shark liver oil¹⁹², however this process has risen ethical concerns for the wellbeing of marine fauna and despite its high yields and purity of the final product (squalene makes up to 40 wt.% of shark liver) it now being abandoned in favour of vegetable sources¹⁹³. Squalene is now commonly extracted from vegetable oils. Squalene content of course varies depending on the specimen: olive oil is the most common source and has a content of ≈ 500 mg/100 g, amaranth is among the richest sources with a content of ≈ 5 g/100 g while other oils such as soybean have only ≈ 10 mg/100 g¹⁹⁴. The extraction procedures vary from mechanical extraction to solvent extraction (often with hexane) or, more recently, with scCO_2 ^{195–197}. The problem with the extraction from vegetable oil is that refining processes lower the yields and this also creates a competition with the food industry. A possible alternative is starting from oil deodorised distillates (ODD) which are the residues of the deodorisation process of exhausted vegetable oils: with vacuum and high temperature (usually above 200 °C) the low-boiling fractions of oils, which contribute to bitterness and unpleasant smell, are removed by a steam current and the regenerated oil is edible again. Squalene is concentrated in this fraction and thus is easier to extract. One common source is soybean ODD (SODD) which are often rich in other useful bioactive molecules^{198,199}. In general, ODD are wastes of the food industry and are cheap and abundant. They are rich in free fatty acids (FFA) but also contain vitamins and terpenoids which, if isolated, have a high value as fine chemicals. Their content depends on the origin of the oil, so it must be determined first.



Squalene

Figure 3910: chemical structure of squalene.

Squalene has many interesting properties: its high unsaturation degree grants it excellent antioxidant properties²⁰⁰, it has cardioprotective properties²⁰¹ and has been tested for drug-delivery applications²⁰²⁻²⁰⁴. Another way to valorise this compound is to hydrogenate it to squalane, which is a high added-value moisturizing and emollient ingredient for cosmetics. Our objective with this work was to isolate squalene from the ODD and hydrogenate it to squalane. Also, FFA in the starting material can be recovered and converted to fatty acid methyl esters (FAME), an essential component in biodiesel. This would lead to a zero-waste approach, giving a purpose to each fraction of the substrate which would have been a waste otherwise.

3.1.2 Conversion of FFA to FAME

The first step in the valorisation of ODD was the conversion of FFA to FAME. Beforehand, the FFA content was to be determined for the two substrates we handled: soybean ODD (SOY) and mixed oils ODD (MIX). A protocol used for the determination of FFA in olive oils was followed: 10 g of ODD were dissolved in 50 mL of a 3:1 diethyl ether-EtOH mixture and kept in slow stirring with a magnetic stirrer. Phenolphthalein 1.0 mM in EtOH was added as pH indicator. A standard 0.1 N NaOH aqueous solution was added dropwise until the turning point was reached and the solution turned pale pink. The process was repeated three times for each substrate, the results shown in **Table 16**.

Table 16: FFA content for SOY and MIX.

	Titration 1 (mmol/g)	Titration 2 (mmol/g)	Titration 3 (mmol/g)	Mean (mmol/g)	Interval (95 %)
MIX	2.8	3.1	3.1	3.0	± 0.11
SOY	2.2	2.3	2.2	2.2	± 0.01

10 g of sample in 50 mL diethyl ether-EtOH (3:1), phenolphthalein. Titration with 0.1 N NaOH.

The FFA content was similar, but slightly higher for MIX. We then moved on to the conversion itself, which was achieved through a simple acid-catalysed esterification in MeOH under MW. As a reference, the reaction was firstly run with *p*-toluene sulfonic acid (PTSA), a common homogeneous acid catalyst, in a ratio of 2.5 mg (0.015 mmol) per mmol of FFA in the substrate. The reactions were performed in 5 mL of MeOH over 1 g of substrate at 100 °C for 1 h under 7 bars of N₂. After the reaction, MeOH was removed under vacuum. The crude was dissolved in 10 mL hexane and washed three times with 10 mL of distilled water to remove the PTSA. Finally, hexane was removed under vacuum before the analysis.

$^1\text{H-NMR}$ of the mixtures were taken before and after the reaction and a sharp methyl ester peak showed at 3.5 ppm. A GC-MS analysis also only revealed FAME with no residual FFA (**Fig. 40**).

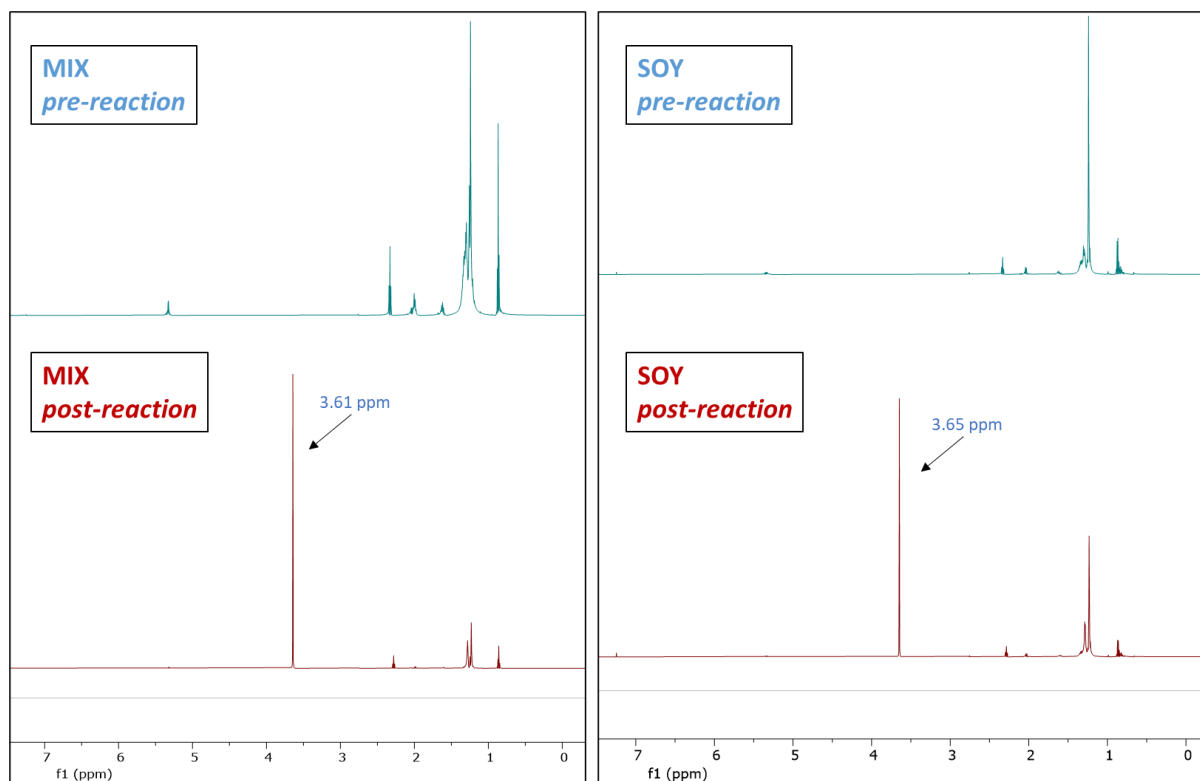


Figure 40: ^1H NMR analysis of the ODD pre and post treatment, with the methyl ester peak highlighted.

No increase in the ratio between the methyl esters peak and the CH peaks at 1.2 ppm (used as a reference) was found doubling the reaction time nor the PTSA amount, so complete conversion was assumed. We decided to test different heterogeneous catalysts to replace PTSA for the reaction: three acid zeolites and two acid silicas, as listed in **Table 17**.

Table 17: properties of the tested zeolites and silica.

	$\text{SiO}_2:\text{Al}_2\text{O}_3$ (mol/mol)	Acid sites (meq/g)	Surface area (m^2/g)	Max T ($^\circ\text{C}$)
Zeolite HY 30	30	0.03	780	>200
Zeolite HY 5.1	5.1	0.14	730	>200
Zeolite Hβ	360	-	620	>200
SiO_2 – propyl sulfonic acid	-	0.80	480-550	120
SiO_2 – tosic acid	-	0.84	480-550	120

The use of a heterogeneous catalyst dramatically simplified the workup, since only filtration was necessary to recover the catalyst. Vacuum was still necessary to remove MeOH before the analysis. Reaction conditions were tuned to obtain complete conversion. All catalysts achieved complete conversion except for zeolite HY 5.1 which did not show any conversion in the experiments. It was speculated that the highly polar cavities of the zeolite, the most acidic

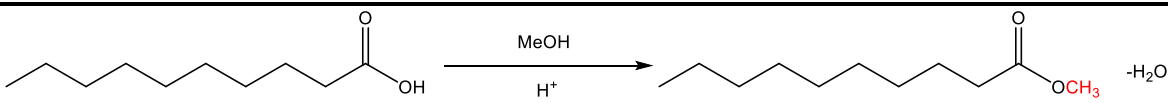
of the tested, could not properly host the FFA for the esterification. On the other hand, Zeolite H β was able to convert the FFA even with its low acidity, possibly for the same but opposite reason. Silicas performed better, possibly because of the strength of their acidic sites respect to zeolites. For all, a bigger mass of catalyst was needed respect to PTSA, since the acidic equivalents were more diluted in the bulk material. For silicas, approximately 0.15 meq of acid were necessary to treat 1 g of substrate, instead of 0.045 of PTSA: this increase is likely due to the reduced mass transfer in the heterogeneous system, however the catalytic amount is still small and reasonable. With these results (**Table 18**) it can be stated that a replacement of PTSA with a solid acid catalyst is possible in mild reaction conditions. Green metrics for the studied reaction are shown in **Table 19**.

Table 18: conditions to obtain complete conversion over different acid catalysts.

	Cat/FFA (mg/mmol)	Cat/FFA (meq/mmol)	Time (h)
PTSA	2.5	0.015	1
Zeolite Hy 30	100	0.003	2
Zeolite H β	100	-	2
SiO ₂ – propyl sulfonic acid	55	0.045	2
SiO ₂ – tosic acid	55	0.047	1

Reaction conditions: 100 °C, 5 bar N₂.

Table 19: Scheme of the reaction and green metrics. Decanoic acid is used as an example, the metrics are independent from the catalysts. The EMY high value is influenced by the excess of MeOH.

	AE	EF	EMY
Stoichiometric	0.92	0.08	0.15
Actual	0.92	0.10	4.63

3.1.3 Squalene and FAME isolation

GC-MS analysis of the substrates revealed a content of 1.6 % in squalene for MIX and 2.1 % for SOY. The rest of MIX was composed of FFA, especially oleic acid (78.3 %) while SOY also contained γ -tocopherol (7.8 %), α -tocopherol (1.4 %) and campesterol (3.4 %).

We firstly tried to separate FAME from the rest using high temperature vacuum distillation in a kugelrohr: the instrument is composed of a glass bubble-tube that rotates inside a heating mantle while connected to a high-vacuum pump. At the end of the tube the sample (1 g) stays in a 10 mL round-bottom flask: the temperature gradient along the tube separates the components in the different glass bubbles. For technical limitations it was only possible to work at 200 °C, however at this temperature prolonged treatment made the sample boil and smoke so it was not possible to work for more than 1 h, after which only 30 mg of FAME were recovered. Unfortunately, this was not a feasible way to recover the FAME. The alternative way was to separate the fractions of the post-esterification crudes via flash-chromatography (CombiFlash Rf200) over an inverse-phase C18 silica column (RediSep). From literature, gradients of H₂O and *i*PrOH were suggested. We then optimized the gradient using 100 mg of

sample over a 36 g C18 column until a fine separation of the components was achieved (**Table 20**).

Table 20: composition of the different elution fraction.

	Fraction	FAME %	Squalene %	Tocopherols %
MIX	A	100	0	0
	B	54.0	46.0	0
SOY	A	100	0	0
	B	23.4	6.3	70.4
	C	8.8	42.6	48.6

In order to isolate sufficient squalene for the hydrogenation experiments we repeated the separation over a 64 g column treating 1 g of sample at a time (**Fig. 41**). Surprisingly, this also led to an improvement in squalene separation: fraction B from MIX resulted in 87.4 % squalene content and fraction C from SOY contained 89.0 % squalene. However, the recovery after the chromatography was only around 55 % of the expected material. Having isolated FAME and squalene, we moved to the last step of the process: the hydrogenation to squalane.

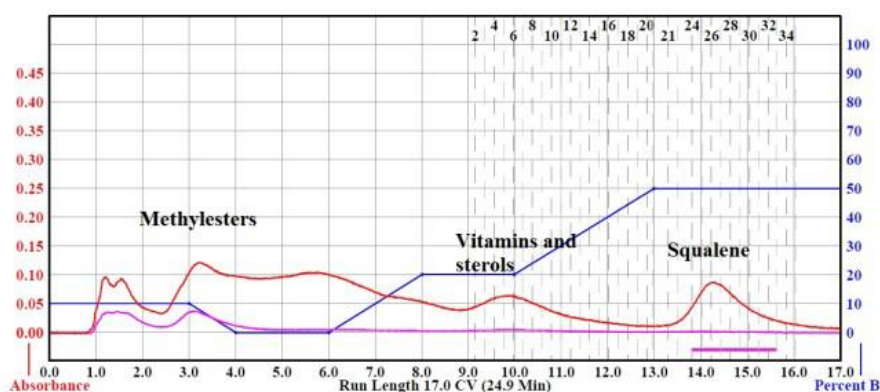


Figure 41: chromatogram of the separation of an ODD into methyl esters, vitamins, sterols and squalene.

3.1.4 Squalene hydrogenation to squalane

With the objective being the hydrogenation of the extracted squalene, we firstly optimized the reaction conditions on a commercial standard. Since squalene is a high-boiling liquid we tested the possibility for a neat reaction, without the addition of a solvent. The hydrogenation was run in a MW reactor under H₂ pressure using a commercial Pd/C 5 wt.% as catalyst. After the reaction the sample was filtered on paper and diluted in CHCl₃ for GC-MS analysis. Results are listed in **Table 21**.

Table 21: Hydrogenation of commercial squalene in neat conditions.

Entry	Catalyst (mg)	Time (h)	H ₂ (bar)	Conversion (%)	Selectivity (%)
1	10	4	10	100	100
2	5	4	10	100	100
3 ^a	5	4	10	98.3	25.0
4	5	4	5	100	15.5
5	5	2	10	100	91.3
6	5	2	5	100	30.9

Reaction conditions: 500 μL squalene (1 mmol), 150 °C. ^a100°C.

As showed, conversion and selectivity were optimal at 150 °C and 10 bar H₂. When the temperature was dropped to 100 °C (**Table 21, entry 3**) conversion was still high, but selectivity dropped to 25 % due to an only partial hydrogenation of the double bonds of squalene. A similar drop happened when only 5 bars were used (**Table 21, entries 4 and 6**), instead the reaction time had only little influence on the selectivity which was almost complete even after 2 h (**Table 21, entry 5**). Since the use of EtOH as a solvent can reduce the viscosity of the system and improve the dissolution of H₂ in the liquid phase. Being EtOH a benign solvent we decided to test this hypothesis adding 2 mL for the reaction (**Table 22**). Indeed, the solvent allowed a better mass transfer and so every parameter could be reduced to milder conditions maintaining an excellent conversion and selectivity (**Table 22, entry 2**).

Table 22: optimization of the reaction condition for commercial squalene.

Entry	Catalyst (mg)	T (°C)	Time (h)	H ₂ (bar)	Conversion (%)	Selectivity (%)
1	5	120	2	5	100	100
2	5	100	2	5	100	100
3	5	100	1	5	100	98.4

Reaction conditions for 500 μL of squalene in 2 mL EtOH, 5 mg Pt/C 5 wt.%.

Having established a set of optimized reaction conditions (2 mL EtOH, 5 mg Pd/C, 5 bar H₂, 100 °C, 1 h) we applied it to the extracted squalene.

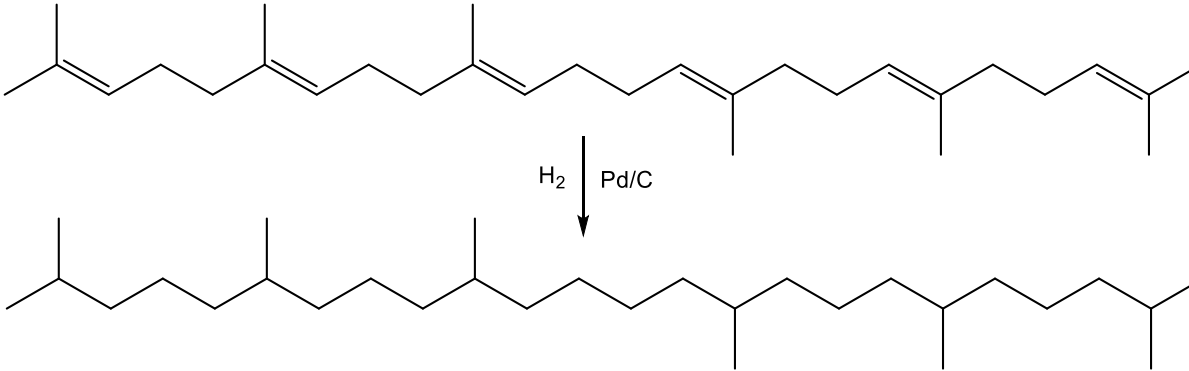
Table 23: optimization of the reaction conditions for the extracted squalene.

Entry	T (°C)	Time (h)	H ₂ (bar)	Conversion (%)	Selectivity (%)
1	120	2	5	100	31.8
2	100	1	5	100	25.0
3	150	4	10	100	49.8

Reaction conditions for 500 μL of squalene in 2 mL EtOH, 5 mg Pt/C 5 wt.%.

Unfortunately, results were not as good (**Table 23**). Even applying harsh conditions selectivity only reached 49.8 % (**Table 23, entry 3**) due to an incomplete hydrogenation of the double bonds. This can be due to two possible reasons: the FAME impurities strongly poisoned the catalyst or were hydrogenated as well. An improvement in the separation step is needed to achieve a complete selectivity for the hydrogenation of squalene. The green metrics for the hydrogenation of squalene are listed in **Table 24**.

Table 24: scheme of the reaction and green metrics. The two best results are considered for the two substrates, with the excess of H_2 being the only real waste produced. EMY is not presented since all reagents are considered benign.



	AE	EF	EMY
Stoichiometric	1.00	-	-
Actual, commercial squalene	1.00	0.46	-
Actual, extracted squalene	1.00	1.82	-

3.1.5 Conclusion

A protocol for the valorisation of vegetal ODD was investigated. A complete characterization of the components of the substrate far performed revealing a predominance of FFA and a low ($\approx 2\%$) content of squalene. The esterification of FFA to FAMES was completed in mild conditions using heterogeneous, recoverable acidic silica. The isolation of the FAMES was performed with liquid chromatography obtaining a fraction of pure FAME and a fraction containing $\approx 90\%$ squalene. The use of chromatography is fine for laboratory scale, however it is not ideal for a scale-up nor for the PI of the process, given its high operative costs which include a large use of solvents, so further trials with vacuum distillation may be desirable. Finally, we successfully optimized the hydrogenation of commercial squalene to squalane (**Table 25**) but were unable to translate them to the extracted squalene. Apart from that, we proved that a valorisation of ODD, a food waste, is possible through a green protocol.

Table 25: comparison between our experiments and the results in recent literature.

		Catalyst	Cat/sub (mol %)	Time (h)	T ($^{\circ}\text{C}$)	H_2 (bar)	Yield (%)
Squalene	Literature ²⁰⁵	SiliaCat Pd(0)	0.2	24	70	3	99.0
	Literature	Pd/C 2.5 %	0.2	16	180	3	100
	This work	Pd/C 5 %	0.5	1	100	5	98.4

3.2.0 MW-assisted reductive amination of aldehydes and ketones

3.2.1 Introduction and state of the art

Reductive amination is a common and elegant reaction for the synthesis of amines from aldehydes or ketones. It involves a fast condensation between the carbonyl group of the substrate with the amino group of the reagent, forming an imine, followed by the reduction of the imine to amine (**Fig. 42**). Different side-reactions are possible, also depending from substrate and conditions, with the most common being the reduction of the carbonyl to alcohol and the overalkylation between the substrate and the formed amine^{206,207}. The reaction is very flexible, since a huge variety of substrates and reducing agents are available.

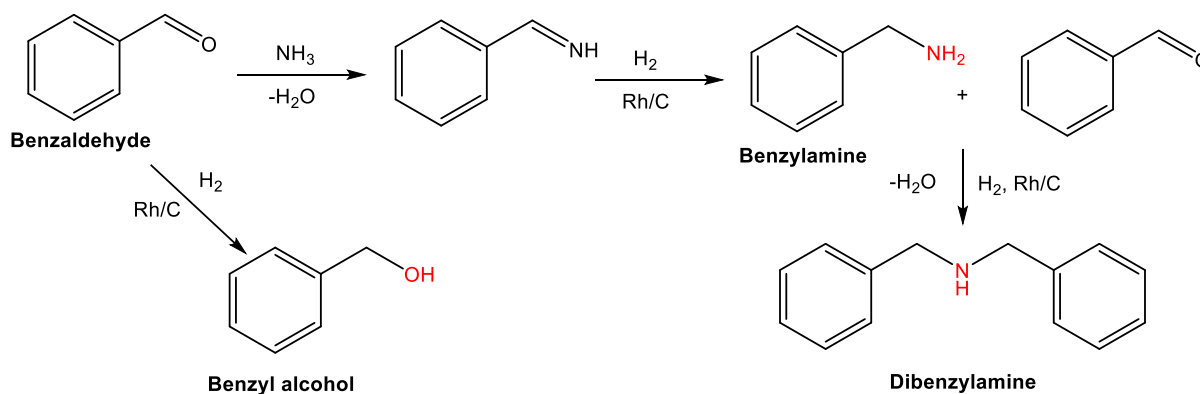


Figure 42: reaction scheme and possible products of benzaldehyde reductive amination with ammonia.

Aldehydes and ketones are abundant, diverse and cheap substrates, while amines are often fine chemicals needed for the synthesis of polymers and pharmaceuticals^{208–210}. Since a nucleophilic addition to the carbonyl is needed for the first reaction step, substituted amines tend to have higher reaction rates: aromatic amines such as aniline or long-chained aliphatic amines such as octylamine are ideal reagents. However, the use of ammonia is often preferred for different reasons: it is a cheap reagent, and the obtained primary amines can be further manipulated and substituted as needed, giving more freedom of operation to get the wanted products^{210,211}. As ammonia is the preferred reagent, H_2 is the desired reducing agent. It is the most environmentally friendly and leads to high atom-economy, plus it is easily removed from the reaction at the end of the process^{212–214}. Molecular hydrogen, however, does not react on its own and needs metallic catalysts to be activated. Cobalt and rhodium are two active metals for the reaction. One of the first examples of Co-based catalysis for the reductive amination of aldehydes and ketones is the work by Huang *et al.* where a Co/NC was prepared via pyrolysis and successfully applied for the conversion of different substrates²¹⁵, even though the reaction conditions were somewhat harsh: 110 °C, 12 h, 10 bar H_2 . Beller *et al.* synthesized Co nanoparticles encapsulated by carbon shells²¹⁶. This catalyst allowed the conversion of a large number of aldehyde and ketones using amines, nitro compounds or even ammonia. Also existing commercial drug molecules were successfully synthesized over the catalyst. Reaction conditions varied broadly from substrate to another, but yields were generally high, above 70 %. Rh was successfully employed for reductive amination reaction over different supports and in mild conditions^{217,218}. A particularly interesting example is the reductive amination of furfural to furfurylamine by Chatterjee and co-workers²¹⁹. The authors used a commercial Rh/ Al_2O_3 , molecular hydrogen and aqueous ammonia for the reaction, achieving a high

selectivity (>90 %) in relatively mild conditions (80 °C, 2h, 20 bar H₂) with an environmentally friendly approach. Indeed, the use of reductive amination for the conversion of bio-derived substrates is a relevant new approach for the synthesis of valuable compounds²²⁰. In this section, the reductive amination of different bio-derived amines and ketones is presented. The reactions are performed under H₂ using aqueous ammonia as reagent. Commercial and newly made Rh- and Co-based catalysts are used for the activation of hydrogen gas in the reduction step. To optimize the reaction conditions, the experiments are performed under MW, trying to improve the conditions found in literature, especially compared with the excellent work of Chatterjee *et al*²¹⁸.

3.2.2 Reductive amination of benzaldehyde

Benzaldehyde (BA) is a common reagent, both in laboratory and in industrial syntheses: its simple but reactive structure, thanks to its aromatic moiety, is ideal for controlled reactions on the carbonyl group. Though it is more commonly synthesized from scratch, it can be derived by natural feedstocks like almonds or almond oil, of which it also strongly resembles the fragrance²²¹. For these reasons (good reactivity, availability, natural-derived and easy to handle) we decided to use it as a substrate to screen the optimal reaction conditions. The structures of BA and benzylamine are shown in **Fig. 43**.

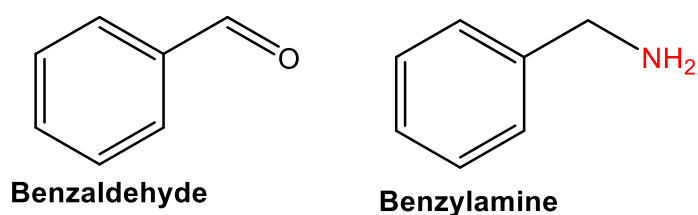


Figure 43: benzaldehyde and benzylamine chemical structure.

Starting from the cited work of literature, we started the screening with a commercial Rh/Al₂O₃ 5 wt.% catalysts. 100 μL of BA (0.98 mmol) and 10 mg of catalyst were dispersed in 5 mL of an aqueous ammonia solution (25 and 32 %) in a 15 mL glass vial. The reaction was run under MW radiation and magnetic stirring. In this first phase, the influence of different reaction parameters was assessed: time, temperature, concentration of ammonia and H₂ bars. After the reaction, the suspension was filtered on paper and the products were extracted in 5 mL CHCl₃ and diluted for GC-MS analysis. GC-FID analysis was also used for the quantification of the products and the yield calculation.

Table 26: reductive amination of benzaldehyde with aqueous ammonia.

Entry	Ammonia (%)	Time (h)	T (°C)	H ₂ (bar)	Conversion (%)	Selectivity (%)	Yield (%)
1	25	2	50	20	100	0.0	0.0
2	25	2	80	20	100	38.5	38.5
3	32	2	80	20	100	78.9	78.9
4	32	2	80	10	100	58.9	58.9
5	32	1	80	20	100	34.7	34.7

Reaction conditions: 100 μL of BA (0.98 mmol), 5 mL ammonia solution, 10 mg Rh/Al₂O₃ 5 wt.%.

Conversion was complete in all cases, however selectivity varied widely depending on the conditions (**Table 26**). The most common by-product was di-benzylamine, resulting from the

reductive amination between benzaldehyde and benzylamine instead than ammonia. When hydrogen pressure was lower also the unsaturated N-benzylidene benzylamine was observed in small quantity. From the data emerges how below 80 °C the reaction only leads to dibenzylamine (**Table 26, entry 1**) and that the concentration of ammonia had the greater influence over the selectivity (**Table 26, entry 3**). Also, time showed a significant influence (**Table 26, entry 5**): possibly at longer reaction times the equilibrium that exists in the reaction mixture shifts towards benzylamine. Hydrogen pressure was instead less significant. In general, higher temperature and ammonia concentration favour the reaction with ammonia, leading to the consumption of benzaldehyde with lower conversion to the secondary amine. After this first screening, Rh/Al₂O₃ was compared with a commercial Rh/C 5 wt.%. It was reported in literature that Al₂O₃ was the better support, however, in our experience that activated carbon is a strong MW absorber and can lead to improved results in such environment. Indeed, the results showed a superior activity of the latter (**Table 27**), allowing an overall reduction of reaction parameters maintaining an 88.0 % yield (**Table 27, entry 4**), higher than even the best result with Rh/Al₂O₃ (**Table 27, entry 1**). Green metrics for the reaction are listed in **Table 28**.

Table 27: comparison between commercial Rh/C 5 wt.% and Rh/Al₂O₃ 5 wt.%.

Entry	Catalyst	Ammonia (%)	Time (h)	H ₂ (bar)	Conversion (%)	Selectivity (%)	Yield (%)
1	Rh/Al ₂ O ₃	32	2	20	100	78.9	78.9
2	Rh/C	32	1	20	100	100	100
3	Rh/C	32	1	10	100	98.2	98.2
4	Rh/C	25	1	10	100	88.0	88.0

Reaction conditions: 100 µL of BA (0.98 mmol), 5 mL ammonia solution, 80 °C.

Table 28: reaction scheme and green metrics. The best yields for the two catalysts are considered. The EF considers H₂ as the only waste since the ammonia can be recycled. The EMY suffers from the excess of ammonia solution.

	AE	EF	EMY
Stoichiometric	0.85	0.17	6.31
Actual, Rh/Al₂O₃	0.85	8.34	0.07
Actual, Rh/C	0.85	4.06	0.07

We then tested the possibility of using a mixture of aqueous ammonia and alcohols as a solvent: BA has a low solubility in water (<0.1 mg/mL) but it is freely miscible with alcohols, so their use could improve the selectivity of the reaction. We arranged a set of experiments using mixtures of aqueous ammonia (32 %) with EtOH (96 %), *i*PrOH, 1,2-propandiol (1,2-PDO) and 1,3-propandiol (1,4-PDO) in different ratios: 4:1, 1:1 and 1:4. Also, equal dilutions with distilled water were tested as reference. The results, given by the selectivity towards benzylamine, are visualized in the following histogram (**Fig. 44**).

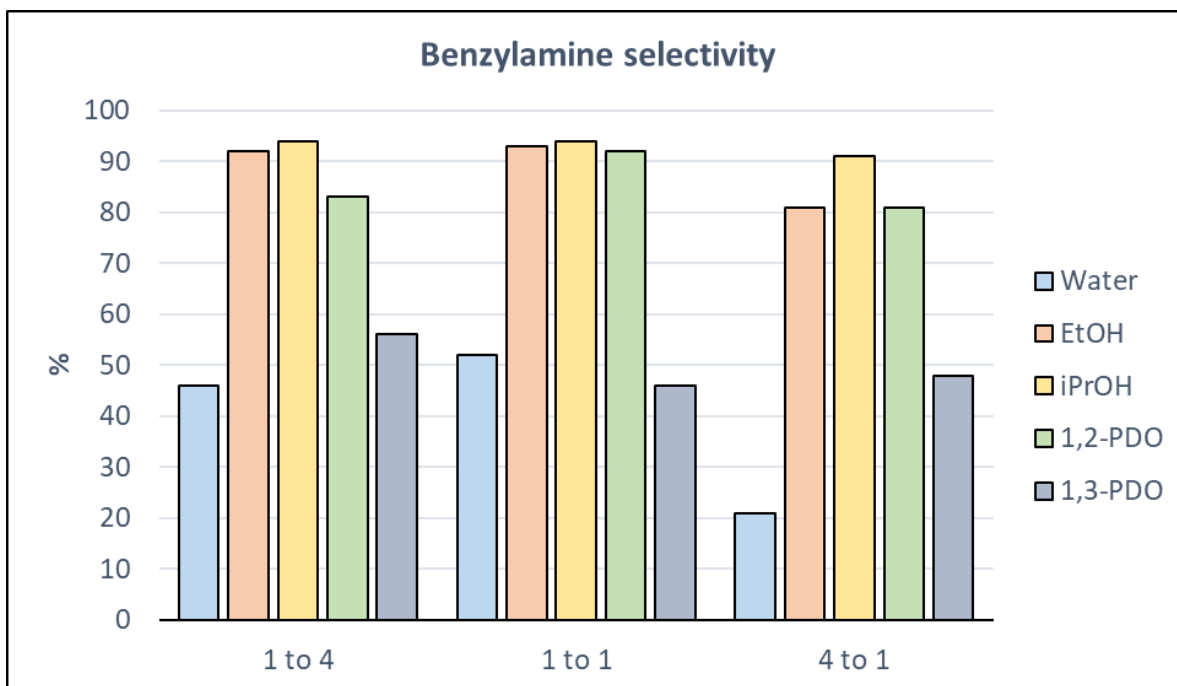


Figure 44: selectivity towards benzylamine in different solvents.

EtOH, *i*PrOH and 1,2-PDO gave the best, and very similar, results. It can be seen how up to 1:1 ratio the increased solubility improves the reaction before the dilution to 4:1 impedes it again. The use of alcohols gave consistently better result than the dilution in water. The use of alcohol allowed us to compare benzaldehyde with 4-methoxybenzaldehyde and 4-chlorobenzaldehyde (two less water-soluble derivatives) as substrates to investigate the role of the substituents. Results are listed in **Table 29**.

Table 29: substituent effect over benzylamine yield.

Entry	Substrate	Conversion (%)	Selectivity (%)	Yield (%)
1	Benzaldehyde	100	92.0	92.0
2	4-Methoxybenzaldehyde	100	68.3	68.3
3	4-Chlorobenzaldehyde	100	100	100

Reaction conditions: 100 μ L of substrate, 5 mL ammonia-EtOH 4:1 solution, 10 bar H₂, 2 h, 10 mg Rh/C 5 wt.%.

The data suggest that an electro-withdrawing substituent might suppress the over-alkylation, increasing the yield in benzylamine (**Table 29, entry 3**). This is also useful considering that the chlorine can also be easily cleaved after the conversion.

Finally, we tested some homemade catalysts. The reactions were run in aqueous NH₃ 25 %: these were the conditions where the activity of the commercial Rh/C started to drop, so were ideal to spot differences. The results (**Fig. 45**) show how the use of the ultrasonic horn improves the catalytic activity and also that metal loading plays an important role. Rh/HHT US 5% was the only one to give some benzylamine content, even though much lower than the commercial catalyst, and even the di-benzylamine content was among the highest. A homemade Rh/C 5 wt.% was also made using conventional stirring only, but it did not result in any catalyst activity in such conditions, showing that US were successful in improving the quality of the catalysts, even if progress is still needed to reach the commercial standard.

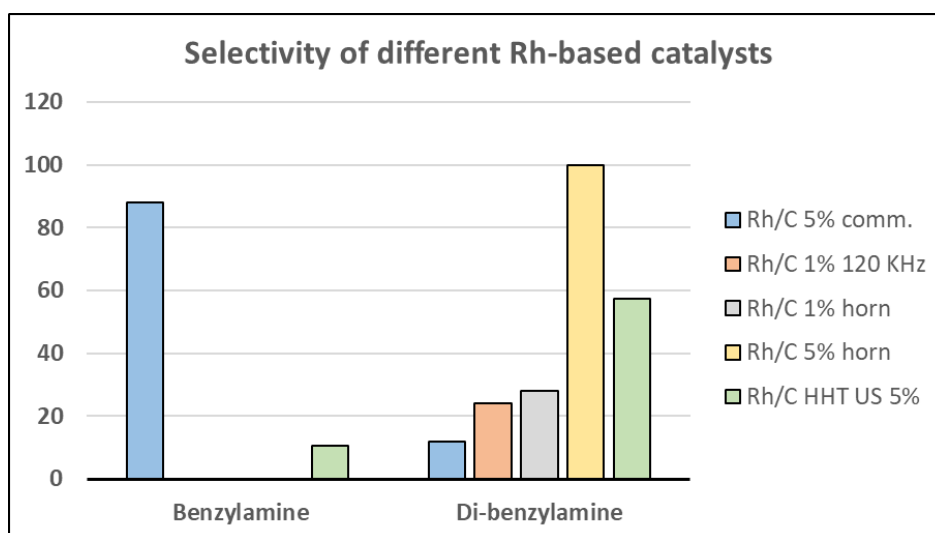


Figure 45: selectivity towards benzylamine and di-benzylamine for different catalysts.

Also, Co/C US 5% was used in the same conditions, however it showed a lesser activity respect to Rh/HHT: in aqueous NH₃ 25 % conversion was 93.5 % but with only a 2.1 % of benzylamine. Still, it was the only homemade catalyst supported on Norit® to convert BA to benzylamine.

3.232 Reductive amination of different aldehydes

Having optimized the reaction using BA, we tested other different substrates for the reaction (**Fig. 46**). Each aldehyde was treated in both NH₃ 32 %, NH₃ 25 % and NH₃-EtOH 1:1 in the same conditions for comparison: 80 °C, 2 h, 10 bar of H₂. Yields to the correspondent amines are displayed in the graph below (**Fig. 47**) since conversion was only complete; di-benzylamine and tri-benzylamine were found as by-products. As shown, benzaldehyde was the most reactive substrate in these conditions, followed by furfural. 3-phenylpropanal and hydroxymethyl furfural (HMF) only converted in specific solvents.

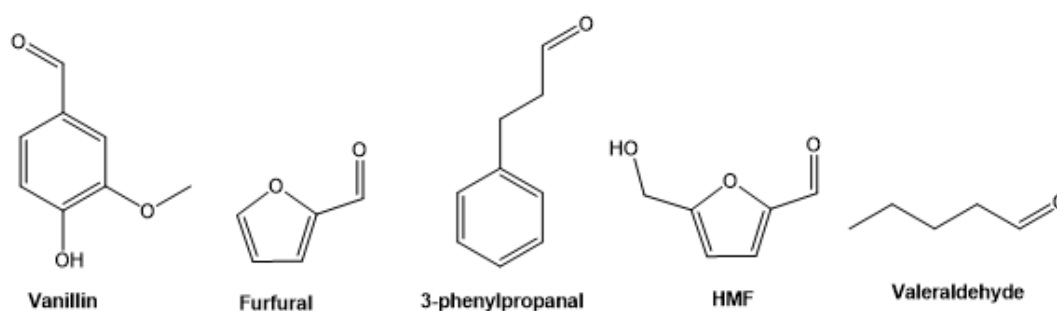


Figure 46: chemical structures of the aldehydes used as substrate.

Also, vanillin and valeraldehyde were tested, however the experiments were unsuccessful for opposite reasons: vanillin was only converted to its secondary amine with 48.6 yield using 32 % ammonia, while valeraldehyde was so reactive that only resulted in secondary and tertiary amines.

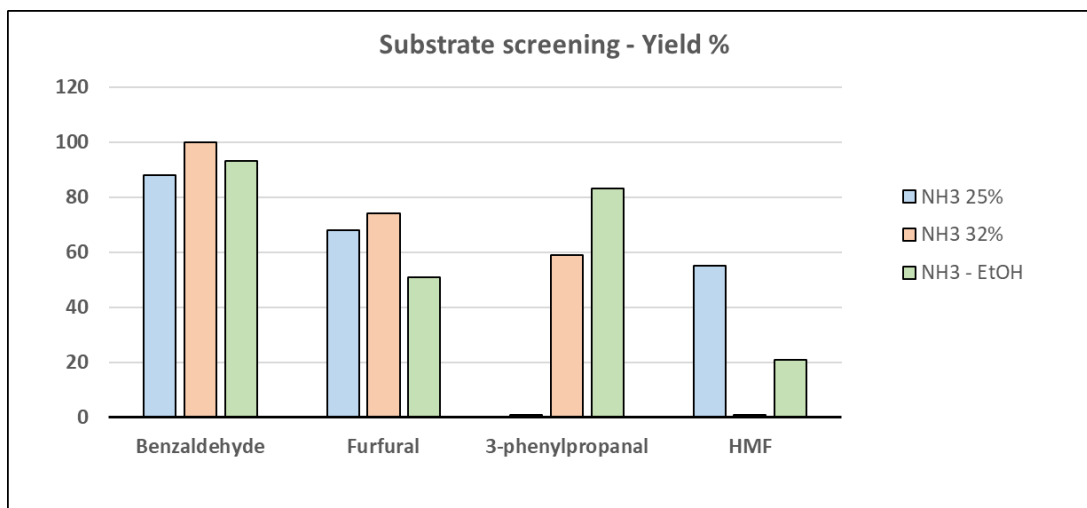


Figure 47: yield % of the reductive amination of different aldehydes.

Interestingly, when furfural was used as substrate it was possible to record some yield to the corresponding primary ammine even at 50 °C, even though 80 °C remained optimal (**Table 30**).

Table 30: selectivity towards furfurylamine at 50 °C.

Entry	Time (h)	H ₂ (bar)	Conversion (%)	Selectivity (%)
1	1	20	100	53.0
2	2	10	100	59.0

Reaction conditions: 100 µL of furfural (1.20 mmol), 5 mL ammonia 32 %, 10 mg Rh/C 5 wt.%.

3.2.3 Reductive amination of ketones

Firstly, we tested the feasibility of the reaction over acetophenone, a common laboratory reagent which, similarly to benzaldehyde, shows good reactivity and a simple structure, has a variety of uses in cosmetic and pharmacology and can be derived from natural sources. Acetophenone was converted to phenylethylamine starting from the same conditions used over benzaldehyde. The structures of acetophenone and phenylethylamine are shown in **Fig. 48**.

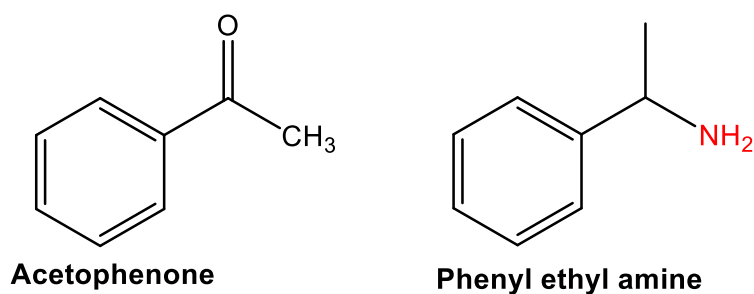


Figure 48: chemical structure of acetophenone and phenylethylamine.

Table 31: solvent and conditions screening for the reductive amination of acetophenone.

Entry	Solvent	Time (h)	H ₂ (bar)	Conversion (%)	Selectivity (%)	Yield (%)
1	NH ₃ 32%	2	10	100	5.5	5.5
2	NH ₃ 25%	2	10	100	10.9	10.9
3	NH ₃ 12%	2	10	100	7.6	7.6
4	NH ₃ -EtOH 1:1 ^a	2	10	100	0.0	0.0
5	NH ₃ 32%	2	5	100	34.2	34.2
6	NH ₃ 25%	2	5	100	43.3	43.3
7	NH ₃ 25%	2	3	65.9	53.2	35.1
8	NH ₃ 25%	3	3	98.1	35.2	34.5

Reaction conditions: 100 μ L of acetophenone (0.84 mmol), 5 mL ammonia solution, 80 $^{\circ}$ C, 10 mg Rh/C 5 wt.%. ^a NH₃ 32 %.

Interestingly, conversion was always high confirming the good reactivity of the substrate, however, a number of by-products (**Fig. 49**) resulted in low selectivity for phenyl ethyl amine, mostly due to two side reactions: the hydrogenation of the benzene ring and the reduction of the carbonyl group to alcohol (**Table 31**). Indeed, when hydrogen pressure and ammonia concentration were both high (**Table 31, entries 1 to 3**) around 40-45 % content of cyclohexyl ethyl amine was found, indicating that amination happened successfully but the product was further reduced by the Rh catalyst. Reducing the H₂ bars improved the selectivity towards the target amine, however below 5 bar conversion was incomplete. Using 3 h instead of 2 allowed an almost complete conversion of acetophenone, but it did not really improve the selectivity towards phenyl ethyl amine, instead 1-phenylethanol was the primary product (as was the case for all experiments except entries **5** and **6** in **Table 31**). The reduction of the keto-group is particularly tedious since it leaves no way for the amination to happen, and only further reduction of the benzene ring can occur. The green metrics for the reductive amination of acetophenone are listed in **Table 32**.

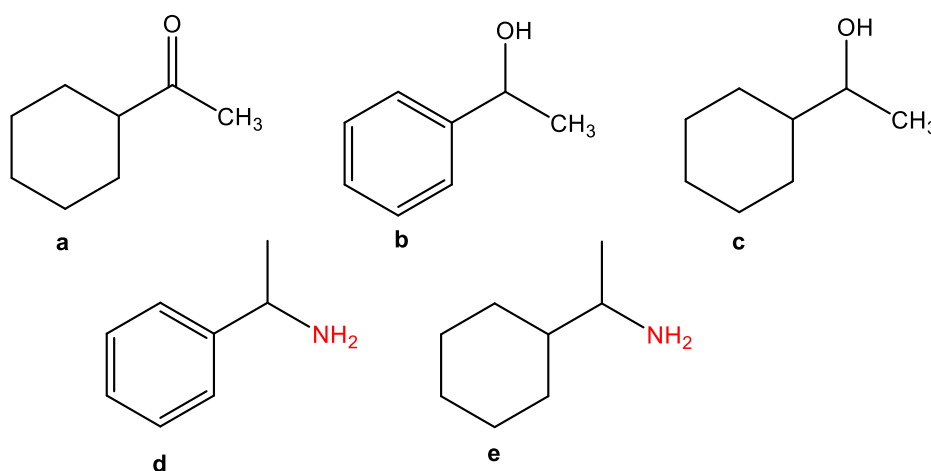
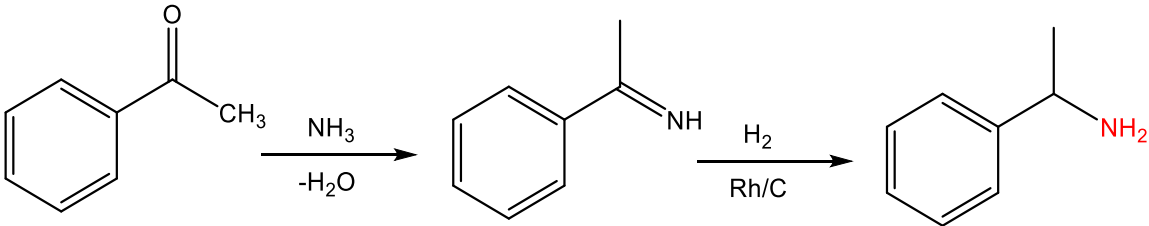
**Figure 49:** observed products of the reductive amination of acetophenone.

Table 32: reaction scheme and green metrics. The best yield is considered. For the EF only the H₂ is considered as a waste, while the EMY is decreased by the excess of ammonia solution and the incomplete yield.

	Acetophenone	Phenylethylamine	
Stoichiometric	AE 0.86	EF 0.18	EMY 5.88
Actual	0.86	5.03	0.03

Once again, we compared the results over acetophenone with 2-methoxyacetophenone and 4-chloroacetophenone (**Table 33**). The results show that both substituents decrease the conversion, however the methoxy group seems to impede the hydrogenation of the aromatic ring, thus allowing for a better selectivity for the amine products; the opposite happens for 4-chloroacetophenone.

Table 33: substituent effect over phenylethylamine yield.

Entry	Substrate	Conversion (%)	Selectivity (%)	Yield (%)
1	Acetophenone	100	43.3	43.3
2	2-Methoxyacetophenone	38.2	85.7	32.7
3 ^a	2-Methoxyacetophenone	98.9	58.5	57.9
4	4-Chloroacetophenone	53.7	9.3	5.0

Reaction conditions: 100 μ L of substrate, 5 mL ammonia 25 %, 80 °C, 2 h, 5 bar H₂. ^a 4 h.

Since mild reaction conditions seem to favour the simple reductive amination, we used the optimized ones for the reactions over our homemade catalysts (**Table 34**).

Table 34: acetophenone reductive amination over the non-commercial catalysts.

Entry	Catalyst	Time (h)	Conversion (%)	Selectivity (%)	Yield (%)
1	Rh/C 5% US	2	1.1	0.0	0.0
2	Co/C 5% US	2	0.0	0.0	0.0
3	Rh/HHT 5% US	2	56.4	43.8	24.7
4	Rh/HHT 5% US	3	54.0	49.2	26.6

Reaction conditions: 100 μ L of acetophenone (0.84 mmol), 5 mL ammonia 25 %, 80 °C, 5 bar H₂.

Unfortunately, our catalysts showed little if no activity for the reaction, with the exception of Rh/HHT 5% US. In the 2 h reaction it showed a good selectivity for the simple reductive amination (**Table 34, entry 3**), with the main product being once again the alcohol from the reduction of the carbonyl group. The conversion was incomplete, however, lowering the yield to 24.7 %. Increasing the reaction time to 3 h did not improve the conversion, and even though a slight improvement in selectivity was observed there is no real difference between the 2 h

experiment (**Table 34, entry 4**). The reduction of acetophenone to 1-phenylethanol is always an important side-reaction due to the aqueous environment.

After the screening over acetophenone we decided to use 4-(4-hydroxyphenyl)-2-butanone, known as raspberry ketone (RK), as a substrate. Once again, RK is a natural occurring molecule that has applications in food, cosmetic and pharmaceuticals. The structures of RK and raspberry amine are shown in **Fig. 50**.

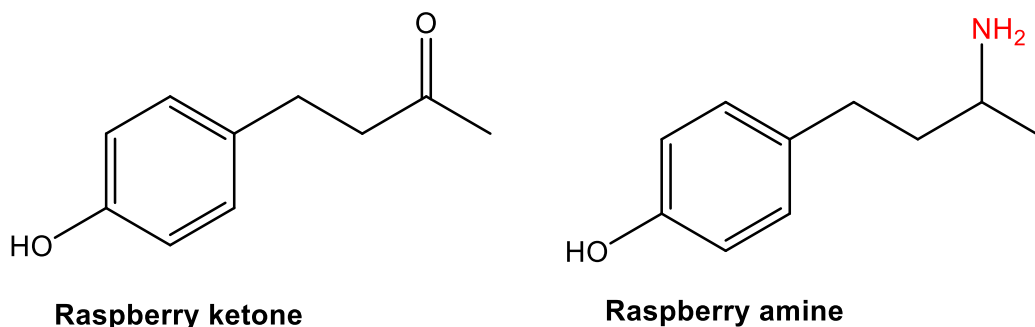


Figure 50: chemical structure of raspberry ketone and raspberry amine.

We firstly screened its reactivity over commercial Rh/C 5 wt.% using different ammonia solution (**Table 35**), as previously done with BA. RK showed good conversion to raspberry amine when EtOH was used (**Table 35, entry 3**); in all reactions the conversion was complete, however the hydrogenation of the aromatic ring occurred as a side reaction, lowering the selectivity. When the reactions were repeated at lower hydrogen pressure (5 bar) the selectivity improved greatly (**Table 35, entries 4 to 6**) allowing a 72.7 % yield with ammonia 25 %. The primary side-product was still the aliphatic ketone.

Table 35: solvent and conditions screening for the reductive amination of raspberry ketone.

Entry	Solvent	H ₂ (bar)	Conversion (%)	Selectivity (%)	Yield (%)
1	NH ₃ 32%	10	100	21.2	21.2
2	NH ₃ 25%	10	100	23.1	23.1
3	NH ₃ -EtOH 1:1 ^a	10	100	36.0	36.0
4	NH ₃ 32%	5	100	69.7	69.7
5	NH ₃ 25%	5	100	72.7	72.7
6	NH ₃ -EtOH 1:1 ^a	5	100	49.3	49.3

Reaction conditions: 100 mg of RK (0.60 mmol), 5 mL ammonia solution, 80 °C, 2 h, 10 mg Rh/C 5 wt.%. ^a NH₃ 32 %.

The reactions were repeated with our homemade catalysts with 25 % ammonia (**Table 36**). The results were peculiar, since both Rh/C US 5% and Co/C US 5% showed no conversion whatsoever while Rh/HHT US 5% not only reached complete conversion but also allowed a high selectivity of 63.0 % (**Table 36, entry 2**), competing with the hydrogenation of the benzene ring. Once again, the support seems to play a crucial role in the activity of the catalyst and opens possible further applications for ketone conversions on tailor-made catalysts.

Table 36: reductive amination of raspberry ketone over our non-commercial catalysts.

Entry	Catalyst	Conversion (%)	Selectivity (%)	Yield (%)
1	Rh/C US 5%	0.0	0.0	0.0
2	Rh/HHT US 5%	100	63.0	63.0
3	Co/C US 5%	0.0	0.0	0.0

Reaction conditions: 100 mg of RK (0.60 mmol), 5 mL ammonia 25 %, 80 °C, 5 bar H₂, 2 h.

Since we proved possible the conversion of RK we decided to test its reductive amination with octopamine, forming ractopamine (**Fig. 51**), a veterinary pharmaceutical used to enhance the feedstock growth. Since this was a synthesis of industrial interest, we compared different commercial catalysts for the reaction.

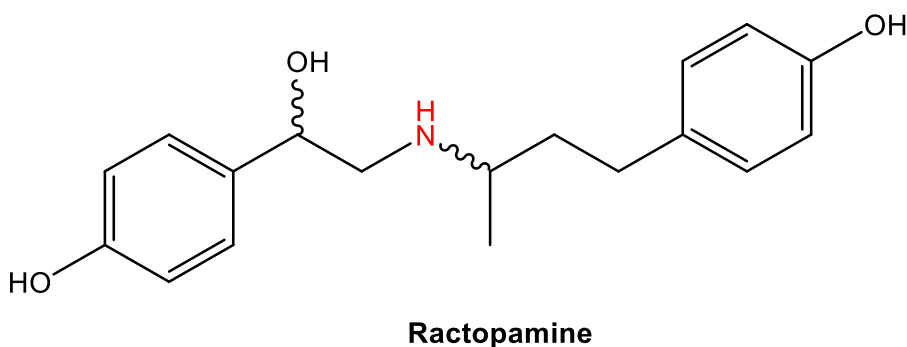
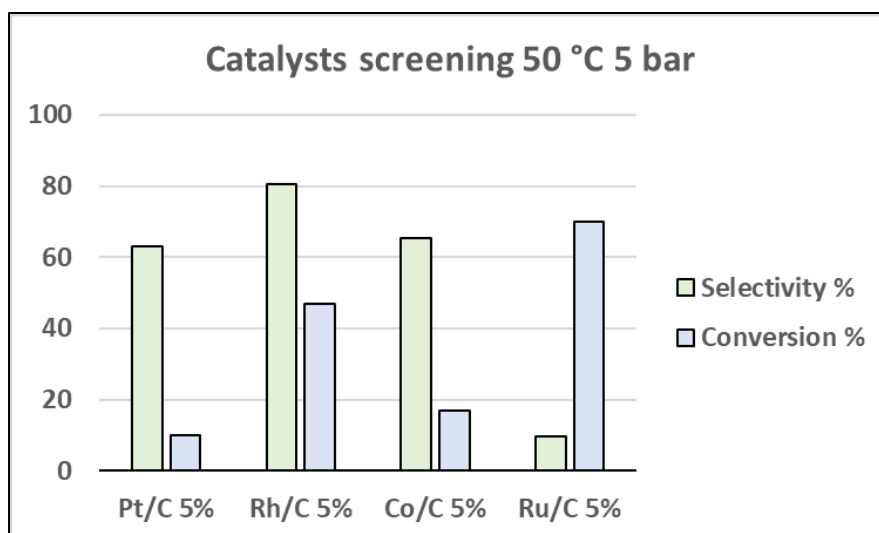


Figure 51: chemical structure of ractopamine.

110 mg of octopamine hydrochloride (0.60 mmol) and 100 mg of RK (0.60 mmol) were dissolved in 5 mL MeOH, 5 mg of catalyst were added. After the reaction, the catalyst was filtered and 100 μ L of the filtrate were collected and dried in a GC-MS vial. The dried sample was diluted in 1 mL of pyridine and derivatized with the addition of 50 μ L of N,O-Bis(trimethylsilyl)trifluoroacetamide (BSTFA) for GC-MS analysis. We tested the performances of commercial Pd/C, Rh/C, Ru/C plus our homemade Co/C all 5 wt.% to see the influence of the metal. Also, temperature and H₂ pressure were varied to optimize the reaction. The results for the different experimental conditions are shown in **Fig. 52**.



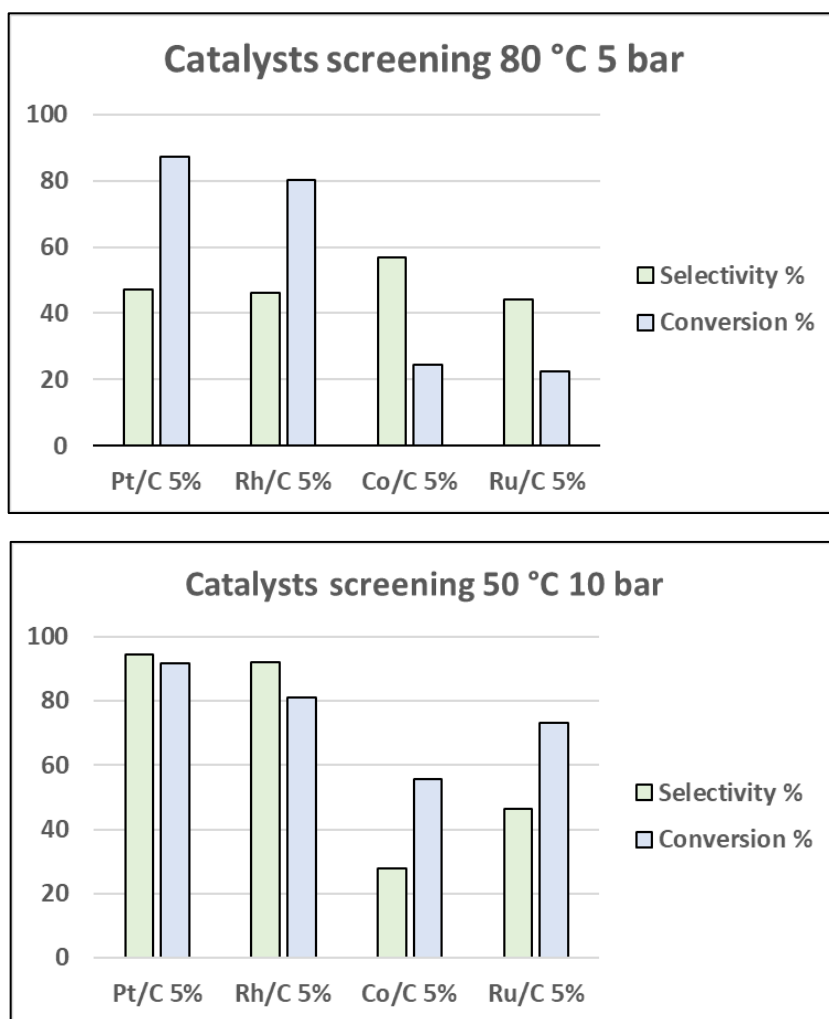


Figure 52: screening of reaction conditions for the synthesis of ractopamine over different catalysts.

As expected, increasing the temperature from 50 to 80 °C increased the conversion but lowered the selectivity. Increasing the H₂ pressure had a dramatically positive effect on both parameters. With mild conditions Rh/C is the best performing, however when H₂ pressure or temperature are increased its performance is equalled by Pt/C.

When we compared the homemade catalysts with the optimized conditions (50 °C, 10 bar H₂, 3 h), we noticed that the catalytic activity was less diverse than in the reductive amination of BA, even though Rh remains the best performing metal and in particular Rh/HHT US 5% (**Fig. 53**).

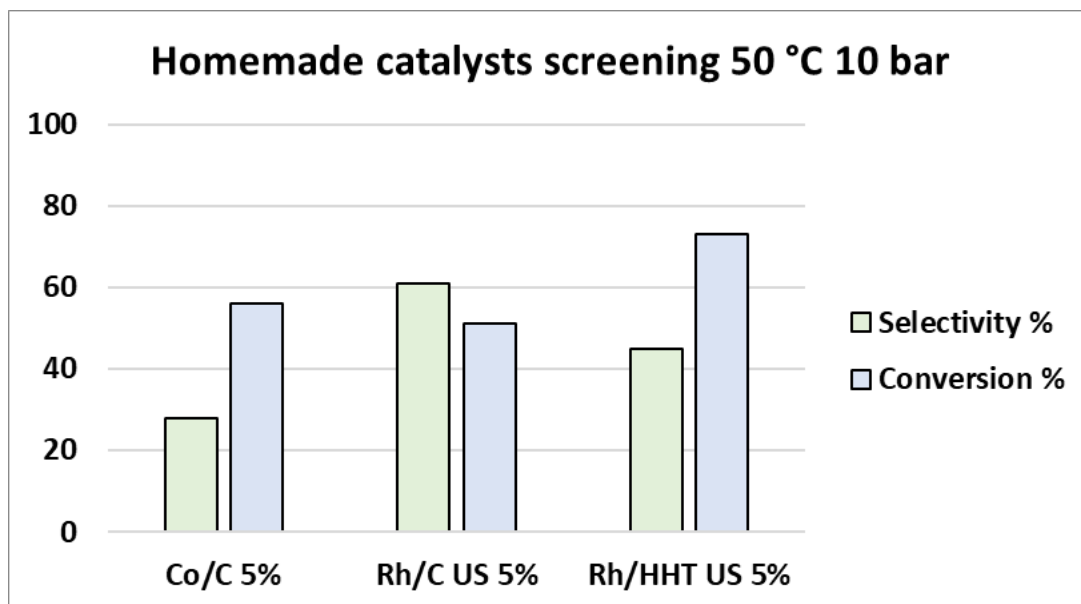


Figure 53: conversion of raspberry ketone and selectivity towards ractopamine over our non-commercial catalysts.

Up to now the general yield to ractopamine was considered, however we should also consider that ractopamine exists in four different isomers: RR, RS, SR, SS. Indeed, GC-MS analysis seem to show that different catalysts lead to different products with the same m/z (**Fig. 54**), suggesting some kind of stereoselectivity linked to the metal in use. Further investigations are needed: chiral HPLC analysis and NMR analysis of the purified products will be necessary to understand exactly what catalyst leads to what product; this is important because only the RR isomer has relevant biological activity.

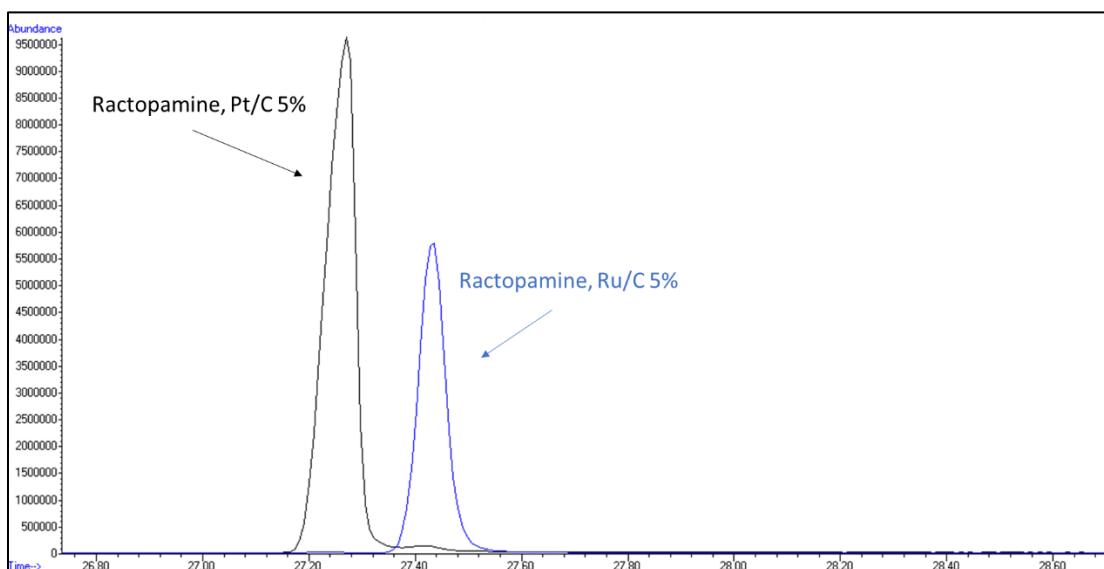


Figure 54: Pt/C 5 % and Ru/C 5 % show two different peak for ractopamine, after the same reaction conditions.

3.2.4 Conclusion

MW-assisted reductive amination was successfully applied over a range of substrates, both bioderived amines and ketones. Both commercial and newly synthesized Rh and Co-based heterogeneous catalyst were used for the reaction. The screening of the conditions over benzylamine showed that it was possible to reduce both the working time (avoiding the pre-equilibration time) and the H₂ bar respect to the recent literature. Acetophenone conversion was achieved in even milder conditions (only 3 bars of H₂) however the selectivity towards phenylethylamine was difficult to control, since the hydrogenation of the benzene ring had a significant influence in the distribution of products. This, however, only shows the reactivity of Rh-based catalysts and can be used to synthesized aliphatic amines. It seems somehow that in our conditions overalkylation is the main side-reaction starting with aldehydes, while the hydrogenation of the aromatic ring is more relevant with ketones. To the best of our knowledge, only few examples exist in literature for the reductive amination of acetophenone over a heterogeneous catalyst. A comparison with literature is presented in **Table 36**.

Table 37: comparison between our experiments and the results from recent literature.

		Catalyst	Cat/sub (g/g)	Time (h)	T (°C)	H ₂ (bar)	Yield (%)
Benzaldehyde	Literature ²¹⁹	Rh/Al ₂ O ₃ 5 %	0.01	3	80	20	77.1
	This work	Rh/C 5 %	0.1	2	80	10	98.1
Furfural	Literature ²¹⁹	Rh/Al ₂ O ₃ 5 %	0.01	3	80	20	91.5
	This work	Rh/C 5 %	0.1	2	80	10	75.0
Acetophenone	Literature ²²²	Ru/C 5 %	0.67	5	50	80	44.0
	This work	Rh/C 5 %	0.1	2	80	5	43.3

The newly synthesized catalyst showed a reduced activity for the reductive amination of the screening compounds respect to the commercial Rh/C, with the best result consistently obtained with the Rh/HHT US % catalyst: carbon nanofibers are clearly a promising support for the deposition of active metal nanoparticles. The homemade catalysts did, however, give good results in the synthesis of ractopamine (a pharmaceutical for veterinary use), comparable with the commercial Rh and Pt catalysts in the right conditions.

In general, it was proven that MW-assisted reductive amination is a feasible reaction to perform over heterogeneous catalyst and a wide group of substrates, with benign reagents. The green metrics are favourable, except for the EMY: in laboratory scale an excess of 5 mL of ammonia solution is easy to handle, however the concentration of reagent should be increased before moving to a bigger scale. Also, further characterization of the homemade catalysts is needed to define a structure-to-activity correlation and to improve their preparation.

3.3.0 MW-assisted hydroformylation of olefines

3.3.1 Introduction and state of the art

Hydroformylation is a common reaction that uses olefins as substrate and syngas (a mixture of CO and H₂) as reagent to produce aldehydes and alcohols. Hydroformylation has been extensively studied and used as an industrial synthesis for aldehydes, especially C₄ or shorter^{223,224}. Of course, catalysts are needed for a good conversion, and the first applications of metal catalysts regarded organometallic complexes which showed Rh and Co to be the most active²²⁵. Hydroformylation shows high conversion, selectivity, and atom economy, with the only drawback being the formation of aldehyde isomers as products: the branched (br) and linear (ln) form and controlling the selectivity towards one or the other is somewhat complicated. Another advantage of this reaction is that it consumes syngas, an abundant and cheap substrate that is far less “noble” than pure gasses. Syngas is mainly a by-product of oil refineries, however it can also be obtained from gasification of biomasses and municipal wastes^{226,227}. It is mostly used to produce ammonia, H₂ and methanol (**Fig. 55**), however, like in the case of hydroformylation, it can be used as a reagent for chemical conversions.

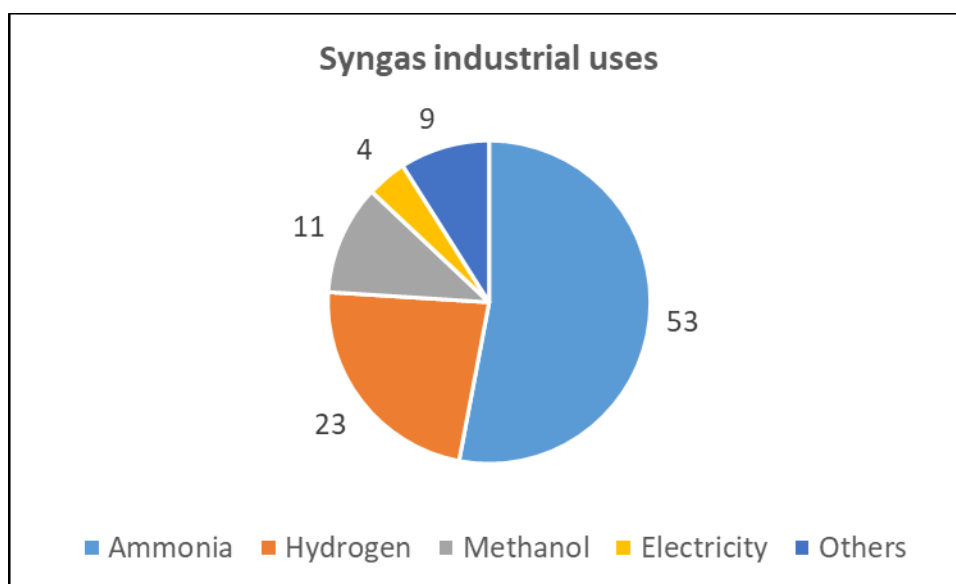


Figure 55: industrial consumption of syngas for different processes.

In this section the study of hydroformylation of olefins over heterogeneous catalysts and MW irradiation is presented. The objective was to improve the results from the literature and move towards greener conditions and protocols. Also, since the reductive amination of aldehydes was studied with the same catalysts, a one-pot synthesis of amines from olefines is presented. To mimic the use of syngas, 50:50 mixture of pure H₂ and CO were used in the experiments.

3.3.2 Hydroformylation experiments

In a recent article by Shi and co-workers a heterogeneous Rh catalyst supported over sulphated carbon nitride (Rh/S-g-C₃N₄) was prepared²²⁸. This catalyst showed remarkable activity for the hydroformylation of styrene to benzene acetaldehyde, reaching practically complete yield in aldehydes, with a branched to linear ratio of 53:47. The reaction was run in a stainless-steel autoclave using toluene as solvent, in 3 h and at 100 °C using 60 bars of syngas. Results could also be reproduced over 1-hexene, 1-octene and cyclohexene. Literature reports

the hydroformylation of styrene to benzene acetaldehyde over a commercial Rh/C 5 wt.% catalyst. This excellent work of literature was the starting point of our investigation, with the objective of optimizing the reaction conditions, test the applicability of MW and testing both commercial and homemade catalysts. The structures of styrene and benzene acetaldehyde are shown in **Fig. 56**.

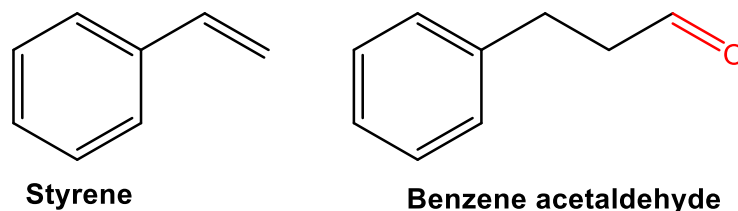


Figure 56: chemical structure of styrene and 3-phenyl propanal.

For the reaction condition screening, we started at 100 °C and 40 bars of syngas for 4 h; also, different solvents were tested to replace toluene which is toxic and environmentally problematic. In a typical reaction, 500 μ L of styrene (4.3 mmol) are dissolved in 9.5 mL of solvent and 10 mg of commercial Rh/C 5 wt.% are added. After the reaction the catalyst is filtered on paper, the filtrate is diluted to 2 mg/mL in an appropriate solvent for the GC-MS analysis. The green metrics for the reaction are listed in **Table 39**.

Table 38: screening of solvent and conditions for the hydroformylation of styrene.

Entry	Solvent	T (°C)	Conversion (%)	Selectivity (%)	Yield (%)
1	Toluene	100	55.5	100	55.5
2	CHCl ₃	100	22.9	100	22.9
3	EtOAc	100	92.0	88.1	81.0
4	EtOH	100	69.4	69.3	48.1
5	<i>i</i> PrOH	100	13.4	14.4	1.9
6	GVL	100	0.0	0.0	0.0
7	H ₂ O	100	0.0	0.0	0.0
8	EtOAc	120	100	97.6	97.6
9 ^a	EtOAc	120	66.6	100	66.6
10 ^b	EtOAc	120	78.4	95.9	75.2

Reaction conditions: 500 μ L of styrene (4.32 mmol), 9.5 mL of solvent, 40 bar syngas, 4 h, 10 mg Rh/C 5 wt.%.

Table 39: reaction scheme and green metrics. Hydroformylation is a green reaction, in the laboratory scale however it suffers from the excess of syngas which is not recovered. The EMY only accounts styrene (a carcinogenic) as non-benign reagent.

	AE	EF	EMY
Stoichiometric	1.00	-	1.29
Actual	1.00	53.3	1.15

Interestingly, in our conditions, toluene was not the best performing solvent (**Table 38, entry 1**) but it was outperformed both by EtOH (**Table 38, entry 4**) and EtOAc (**Table 38, entry 3**). The yield does not seem tightly related to the polarity of the solvent since both highly polar solvent like water and non-polar solvents like GVL and CHCl₃ gave poor results, it might be the case that an intermediate polarity is the optimal as is the case for EtOAc. Raising the temperature to just 120 °C allowed a complete conversion of styrene and almost a complete selectivity, with ethyl benzene being the prevalent by-product in all experiments. If the reaction time is halved also conversion drops, however the use of acetic acid in catalytic amount (50 µL) allowed a good conversion even in 2 h (**Table 38, entry 10**).

Despite the presence of ethyl benzene as the only by-product, selectivity was usually high in general, however we should also discriminate the selectivity between the linear and the branched aldehyde, which is somehow influenced by the choice of solvent but less so by temperature. The different branched to linear aldehydes ratios are listed in **Table 40**.

Table 40: branched to linear aldehyde ratios.

Entry	Solvent	T (°C)	Branched/linear
1	Toluene	100	1.5
2	CHCl ₃	100	2.8
3	EtOAc	100	1.3
4	EtOH	100	1.3
5	<i>i</i> PrOH	100	0.8
6	EtOAc	120	1.0

In all cases, except with *i*PrOH (**Table 40, entry 6**) a slight excess of the branched aldehyde is found post-reaction. Unfortunately, the results did not translate as well over the homemade Rh catalysts, especially because of the low conversion of styrene, so we only relied on commercial Rh/C for further tests. Interestingly, the two catalysts showed identical activity in these conditions (**Table 41**).

Table 41: hydroformylation of styrene over our non-commercial catalysts.

Entry	Catalyst	Conversion (%)	Selectivity (%)	Yield (%)
1	Rh/C 5% US	20.0	90.0	18.0
2	Rh/HHT 5% US	20.0	89.3	17.9

Reaction conditions: 500 µL of styrene (4.32 mmol), 9.5 mL EtOAc, 120 °C, 40 bar syngas, 4 h.

Having established a greener procedure for hydroformylation over Rh/C we decided to use different olefines ad substrates: 1-hexene, *trans*-stilbene, 1,7-octadiene and 1,1-diphenyl ethylene (1,1-DPE). Their structures are depicted in **Fig. 57**.

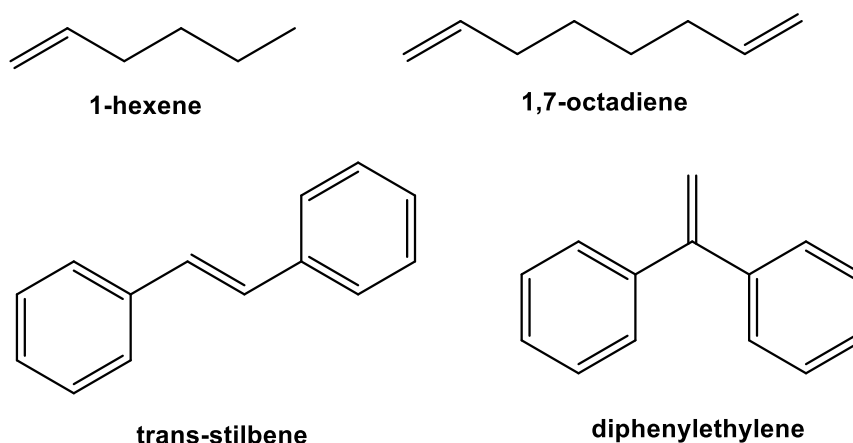


Figure 57: chemical structure of the different alkenes used as substrate.

Since the differentiation of the products becomes more difficult with the complexity of the starting material, both because of the formation of branched and linear products and the isomerization of olefins at high temperature that shifts the position of the double bonds, the raw yield and selectivity to aldehydes is presented as a result (**Table 42**). In hope to reduce the isomerization occurrence experiments with the addition of 50 μL of acetic acid (**Table 42 entries 5 to 8**).

Table 42: hydroformylation experiments over different alkenes, with and without acetic acid.

Entry	Substrate	Conversion (%)	Selectivity (%)	Yield (%)
1	1-hexene	100	88.2	88.2
2	1,7-octadiene	51.7	46.8	24.2
3	<i>trans</i> -stilbene	0.0	0.0	0.0
4	1,1-DPE	0.0	0.0	0.0
5	1-hexene ^a	100	100	100
6	1,7-octadiene ^a	64.3	71.2	45.8
7	<i>trans</i> -stilbene ^a	0.0	0.0	0.0
8	1,1-DPE ^a	0.0	0.0	0.0

Reaction conditions: 500 μL of substrate, 9.5 mL EtOAc, 120 $^{\circ}\text{C}$, 40 bar syngas, 4 h, 10 mg Rh/C 5 wt.%. ^a 50 μL of acetic acid.

The addition of acetic acid did non influence the distribution of aldehydes significantly; however, it did however improve the conversion and the selectivity towards the formation of aldehydes, except for *trans*-stilbene which showed no conversion at all, possibly because of the strong hindrance around its double bond. Common by-products for the 1,7-octadiene were cyclization products. This improvement may be attributed to the protonation of CO which could increase it electrophilicity for the addition to the double bond.

The addition of acetic acid also allowed us to improve the conversion of styrene over our homemade Rh/HHT 5 w.t.% using the same reaction conditions of the first test (120 $^{\circ}\text{C}$, 4h, 40 bar of syngas). We varied the concentration of acetic acid to spot the ideal quantity, however results show that acetic acid is already active in low concentrations (**Fig. 58**). Also, since it can drastically improve the conversion of styrene while being in a molar deficit suggests that it is involved in a catalytic cycle.

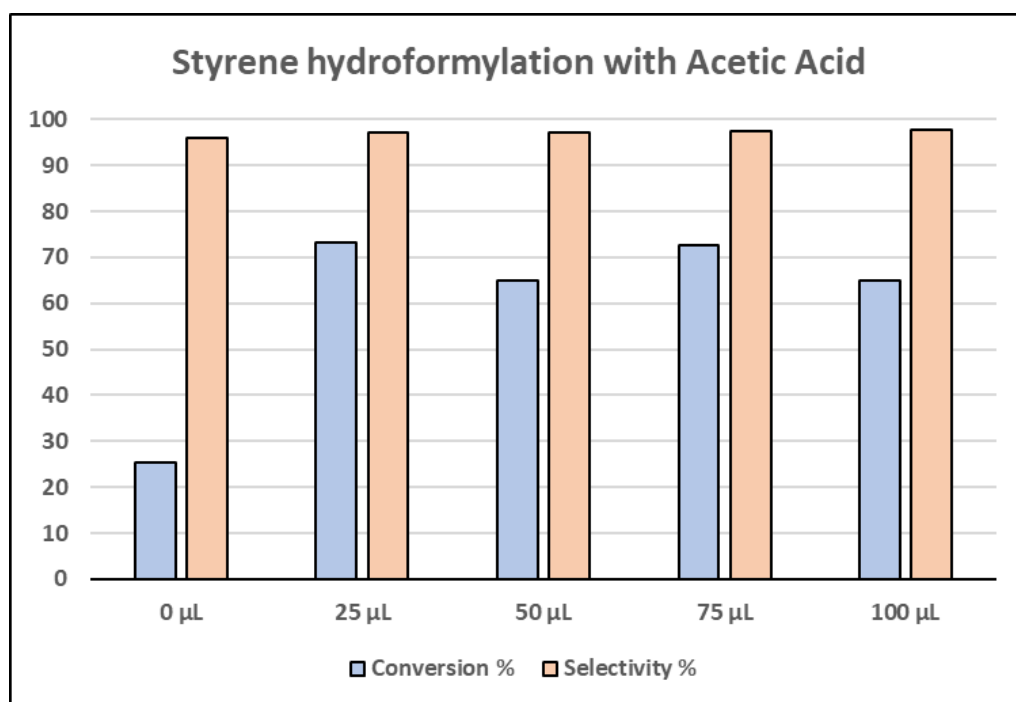


Figure 58: conversion and selectivity of styrene hydroformylation with acetic acid over our Rh/HHT 5 wt.% catalyst.

3.3.3 One-pot hydroformylation and reductive amination of olefines

Having established a reliable protocol for hydroformylation we decided to try to unite the two reactions on the same catalyst: hydroformylation of olefines to aldehydes first, and reductive amination of aldehydes to amines as second step. This would be an efficient and appealing process, dramatically increasing the efficiency of the amine synthesis (**Fig. 59**).

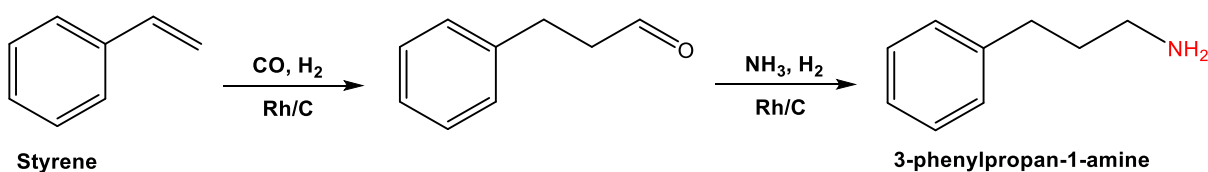


Figure 59: reaction scheme of the one-pot conversion of styrene to 3-phenylpropan-1-amine.

At first, the reaction conditions were optimized using styrene. The most intuitive way to perform a one-pot synthesis was simply to put the amine together with the substrate from the beginning and use the H₂ of the syngas for the amination also. For the amination we used both the 32 wt.% ammonia solution and octylamine and *p*-anisidine in pure form, since aqueous ammonia is not ideal to react with organic mixtures and may not lead to good conversions. When the ammonia is used, 5 mL of solvent are mixed with 4.5 mL of ammonia solution. When the organic amines are used, they are simply dissolved in the solvent before the reaction; they are added in 1:1 molar ratio to the substrate. Results are listed in **Table 43**.

Table 43: one-pot synthesis of amines with different reagents.

Entry	Solvent	Amine	Conversion (%)	Aldehydes (%)	Amines (%)	Yield (%)
1	EtOAc	ammonia	0.0	0.0	0.0	0.0
2	EtOH	ammonia	1.0	100	0.0	0.0
3	EtOAc	octylamine	87.4	0.0	44.6	39.0
4	EtOAc	p-anisidine	100	0.0	24.4	24.4

Reaction conditions: 500 μ L of styrene (4.32 mmol), 9.5 mL EtOAc, 120 $^{\circ}$ C, 40 bar syngas, 4 h.

From the first trials it was clear that a one-step process was not ideal with ammonia: not only it did not result in any amination, but it impeded hydroformylation also. Results were a little better for the organic amines, which form a homogeneous system and facilitate the mass transfer. To improve the results, we decided to split the conversion in two steps: hydroformylation was performed first for 2 hours, then the amines would be added, and the amination would take place for other 2 h under 20 bars of H₂. Results are listed in **Table 44**.

Table 44: two-step one-pot synthesis of amines from styrene.

Entry	Solvent	Amine	Conversion (%)	Aldehydes (%)	Amines (%)	Yield (%)
1	EtOAc	ammonia	83.8	8.1	68.3	57.2
2 ^a	EtOAc	ammonia	90.1	2.3	61.9	55.8
3 ^a	EtOH	ammonia	81.0	4.0	54.9	44.5
4	EtOAc	octylamine	97.1	0.0	68.7	66.7
5	EtOAc	p-anisidine	88.8	0.0	47.2	41.9

Hydroformylation conditions: 500 μ L of styrene (4.3 mmol), 4.5 mL EtOAc, 120 $^{\circ}$ C, 40 bar syngas, 2 h. ^a 150 $^{\circ}$ C. Reductive amination conditions: 4.0 mL ammonia 32 %, 20 bar H₂, 80 $^{\circ}$ C, 2 h.

The improvement with the two-step approach is dramatic with ammonia (**Table 44, entry 1**), however in EtOAc only the over-alkylated amine is observed, while with EtOH the primary amine is obtained: this difference persists even though the concentration of ammonia is virtually equal. Some experiments were performed at 150 $^{\circ}$ C to compensate for the halved reaction time (**Table 44, entries 2 and 3**), however this did not appear to lead to significant benefits, so 120 $^{\circ}$ C is still advised. In EtOH, aqueous ammonia performs surprisingly similar to the organic amines, leading to a good selectivity towards the primary amine. If the general yield to amines is considered, ammonia still gives good results, however the best performing is octylamine, which is not surprising since its aliphatic chain leads to a better reactivity and solubility in the organic solvent (**Table 44, entry 4**). When octylamine is used, however, about 20 % content of the tertiary amine is found in the products: this is still a reductive amination product, albeit a less desirable one. Still, this demonstrates the robustness of the approach and the good activity of the catalyst under MW radiation.

To conclude the investigation, we decided to run some one-pot synthesis on 1-hexene as substrate, since it showed excellent reactivity towards the hydroformylation (**Table 45**). Once again, since a wide variety of products can be observed (derived by the shift of the double bond leading to different branched products) the crude selectivity in amines is reported.

Table 45: two-step one-pot synthesis of amines from 1-hexene.

Entry	Catalyst	Amine	Conversion (%)	Amines (%)	Yield (%)
1	Rh/C 5 w.t.%	ammonia ^a	100	100	100
2	Rh/C 5 w.t.%	octylamine	100	100	100
3	Rh/C 5 w.t.%	p-anisidine	100	81.1	81.1
4	Rh/HHT 5 w.t.%	ammonia ^{a,b}	100	100	100
5	Rh/HHT 5 w.t.%	octylamine ^b	100	56.0	56.0
6	Rh/HHT 5 w.t.%	p-anisidine ^b	100	90.1	90.1

Hydroformylation conditions: 500 μ L of 1-hexene (4.0 mmol), 9.5 mL EtOAc, 120 $^{\circ}$ C, 40 bar syngas, 4 h. Reductive amination conditions: 20 bar H₂, 80 $^{\circ}$ C, 2 h. ^a 4.0 mL ammonia 32 %. ^b 50 μ L of acetic acid.

1-hexene was fully converted in all experiments, with excellent yields towards the relative amines. However, only the secondary amines were observed, showing that the primary aliphatic amine is very reactive while possibly the secondary amine is hindered enough to stop further alkylation.

3.3.4 Conclusion

The synergy between MW irradiation and the heterogeneous Rh/C catalyst for the hydroformylation of olefines was demonstrated. We drastically reduced the amount of syngas (which is the primary waste of the synthesis) respect to literature achieving a 97.6 % yield from styrene in 4 h, and of 75.2 % in only 2 h with the addition of acetic acid in catalytic amounts. It was even possible to substitute toluene with ethyl acetate as solvent, further reducing the EMY of the reaction. The solvent can be evaporated and recycled, thus it does not weight on the EF. A comparison with literature is presented in **Table 46**.

Table 46: comparison between our experiments and the results in recent literature.

		Catalyst	Solvent	Cat/sub (g/g)	Time (h)	T ($^{\circ}$ C)	Syngas (bar)	Yield (%)
Styrene	Literature ²²⁸	Rh/S-g-C ₃ N ₄	Toluene	0.001	3	100	60	99.9
	Literature ²²⁹	Rh(I)/MnMOF	Toluene	0.002	18	80	80	100
	Literature ²³⁰	Rh black	Toluene	0.2	4	100	60	77.0
	This work	Rh/C 5 %	EtOAc	0.02	4	120	40	97.6

Our catalytic system showed a preference for terminal alkenes such as 1-hexene and 1,7-octadiene, while substituted alkenes showed no conversion. With 1-hexene a complete yield to aldehydes was possible with the addition of acetic acid in catalytic amounts. After these good results we moved on to a one-pot synthesis of aliphatic amines from olefins. A one-step approach did not achieve satisfactory yields, seems the presence of amines seemed to impede the hydroformylation step. When the two reactions were separated in two steps (one with syngas at 120 $^{\circ}$ C and one with H₂ at 80 $^{\circ}$ C, for a total of 4 h) results improved greatly both using aqueous ammonia and organic amines for the amination. In 4 h styrene achieved almost full conversion with an average yield in amines of 53.2 %, while 1-hexene was always fully converted with an average amine yield of 97.3 %. To the best of our knowledge, this is the first time that this one-pot synthesis of amines is reported over a heterogeneous Rh catalyst, and it has huge potential for further scale-up and application.

3.4.0 One-pot MW-assisted synthesis of isosorbide from glucose

3.4.1 Introduction and state of the art

Isosorbide is a bio-derived chemical building block that has drawn much attention in recent years thanks to its stability, non-toxicity, and the possibility to functionalize its two hydroxyl groups to obtain tailor-made products. Isosorbide can be obtained from glucose via hydrogenation to sorbitol and two dehydrations (intra-molecular condensations) to form the double-ring structure. Three possible isomers can form: isosorbide, isomannide and isoidide (**Fig. 60**). These three molecules can be directly obtained starting from the appropriate substrate (sorbitol, mannitol or iditol) or can be isomerized in reaction conditions²³¹. Of the three, isosorbide is the most interesting: its structure has one hydroxyl in *endo* and one in *exo* configuration, this gives it greater reactivity compared to isomannide and even if isoidide would be even more reactive it is primarily synthesized from idose, which is not found in nature, otherwise is produced only in small quantities from epimerization. The *endo* group is the most reactive of the two²³², thanks to its enhanced nucleophilicity because of the intra-molecular bond that forms, however the *exo* group might react preferably with sterically encumbering substrates: this tunability grants isosorbide much flexibility as a substrate for chemical modifications. Indeed, many examples exist of its application for the synthesis of high-boiling green solvents, bio-polymers and bio-fuels or fuel additives^{233,234}. One interesting example is the synthesis of poly(isosorbide)terephthalate (PIT): a polymer with excellent physical properties and candidate for the substitution of the oil-derived PET²³⁵. Another important application is the synthesis of isosorbide dinitrate: an active principle for the prevention of chest pain in humans^{236,237}. Dimethyl isosorbide is a promising high-boiling green solvent for organic chemistry reactions²⁷ that can be directly synthesized from sorbitol in dimethyl carbonate, another green solvent²³⁸.

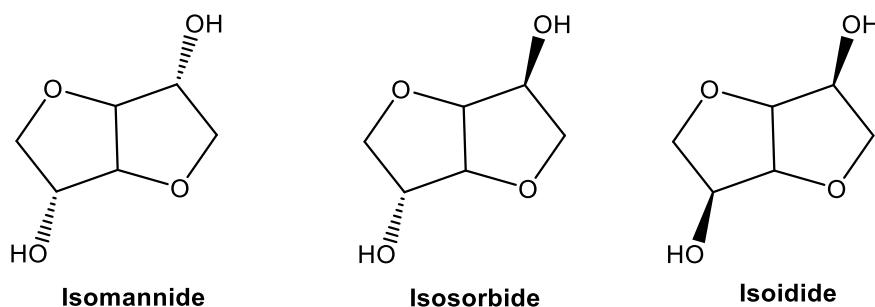


Figure 60: chemical structure of isosorbide and its isomers isomannide and isoidide.

It is clear that isosorbide is a potent building-block for sustainable productive processes and that the research interests over this molecule are well justified. Despite the number of experiments and studies on its synthesis, however, it can still be a tricky reaction especially when a direct conversion of glucose or cellulose is wanted. Glucose reduction to sorbitol can be catalysed by transition metals and can be performed in water using molecular hydrogen or alcohols as hydrogen donors for the proper reduction^{239–242}. Many works report the use of Ru-based heterogeneous catalysts for the reaction, given its excellent properties for hydrogenation reactions^{243,244}. Sorbitol dehydration to isosorbide has 1,4-sorbitan as intermediate as the C1 hydroxyl is protonated and cyclization occurs on the C4 carbon. However different sorbitans can form (**Fig. 61**), leading to formation of humins instead of

isosorbide: this is one of the main drawbacks of the reaction and can lead to low selectivity. 3,6-sorbitan also leads to isosorbide but is usually formed in negligible quantities^{245,246}.

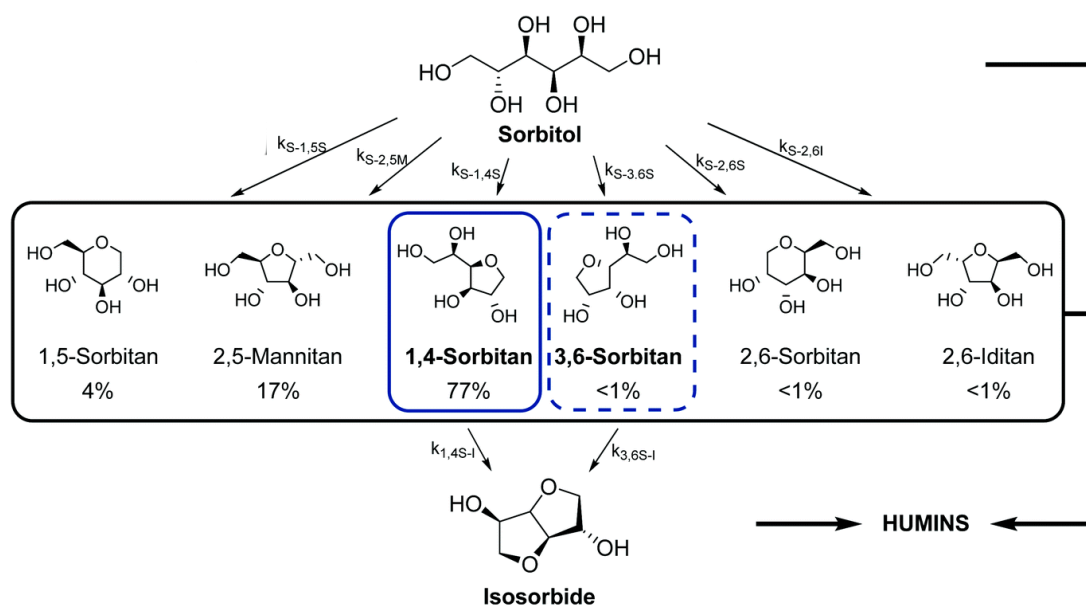


Figure 61: possible pathways for the dehydration of sorbitol²⁴⁵.

This reaction step can be acid-catalysed using mineral acids or, more interestingly, heterogeneous acids such as zeolites or acid resins^{247–249}. If the catalyst is active enough, the reaction can also happen in water, as demonstrated by Otomo *et al.* in their work²⁵⁰. They obtained an excellent yield (80 %) in isosorbide over β zeolites working at 200 °C for 18 h; it was found that high Si:Al ratios improved the activity of the catalyst: they proposed that Al-rich zeolites coordinated more water, thus slowing the mass transfer and impeding the dehydration. Temperature also played a crucial role: at temperature lower than 200 °C conversion was slow, while above it side-reactions begin to occur more prominently. Similar results were also found in the study by Kobayashi and co-workers: once again a zeolite screening resulted in β zeolites giving the best yields in isosorbide, with the Si:Al ratio playing an important role²⁵¹. The best result was a 76 % yield working at 126 °C for 2 h; notably, the reaction was performed in neat conditions using a temperature above sorbitol melting point (95 °C).

One-pot syntheses of isosorbide from glucose or even cellulose are reported in literature and are the most attractive examples for the scalability of the reaction. Many of these examples rely on mineral acids for the dehydration step²⁵² while one of the first examples of heterogeneous acid catalyst employed the acidic resin Amberlyst 70 while the reduction was performed with a commercial Ru/C catalyst: the best result was a 56 % yield, however reaction conditions were pretty harsh: 16 h, 50 bar H₂ and 180 °C²⁵³. A much more recent and interesting approach was taken by Brandi and co-workers: they managed to set up a flow process for the one-pot conversion of an aqueous glucose feed to isosorbide in a two-step approach. Firstly, glucose was hydrogenated to sorbitol over a Ni-based catalyst supported over N-doped carbon and H₂ (25 mL/min at 40 bars) at 150 °C followed by the dehydration step over a β zeolite at 220 °C, allowing a final yield of 56 % in isosorbide²⁵⁴. To the best of our knowledge, nobody reported the interaction between such heterogeneous catalysts and MW radiation for the conversion of glucose to isosorbide. In this section, the study and

optimization of the conversion of glucose to isosorbide are presented, aiming for a one-pot synthesis enhanced by MW. Trials for the direct conversion of cellulose are also presented.

3.4.2 Glucose hydrogenation to sorbitol

At first, we started investigating the possibility to use *i*PrOH for the reduction of glucose by hydrogen-transfer (**Fig. 62**). As for the use of H₂, the hydrogen transfer is often catalysed by noble metals, so we compared at first three Ru-based catalysts synthesized by the research group of professor Cavani at the University of Bologna: Ru/C, Ru/TiO₂ and Ru/Al₂O₃ all 1 wt.%. For the reaction, 100 mg of glucose (0.56 mmol) were dissolved in 3 mL of *i*PrOH and 10 mL H₂O and 50 mg of catalyst were added. The reaction was run at 180 °C for 4 h. After the reaction, the catalyst was filtered, and the filtrate was evaporated under vacuum. 2 mg of sample were then collected and dissolved in 1 mL of pyridine and derivatised with BSTFA for GC-MS analysis. In these conditions, only Ru/C 1 % resulted in only a 3.5 % yield in sorbitol while the other catalysts only produced xylitol, erythritol and, oddly, short-chained acids such as acetic and lactic acid. When Ru/C 3 wt% was used, however, the yield drastically increased to 86.0 %.

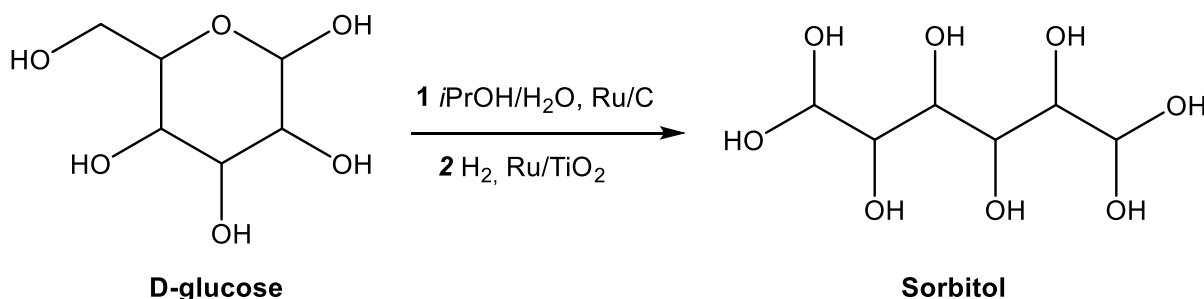


Figure 62: reaction scheme of the hydrogenation of glucose to sorbitol with *i*PrOH or H₂.

Since no H₂ pressure was needed for these tests, we then decided to run further optimization tests in an Anton Paar Monowave 300 reactor (**Table 47**): differently from Synthwave, inside the Monowave is a standing wave that has always the maximum intensity over the sample. Monomodal reactors such as Monowave enhance the efficiency of MW ensuring maximum energy transfer to the reaction vessel. Indeed, it was possible to maintain a high yield with much lower temperature and reaction time. However, the selectivity drastically dropped when water was not added (**Table 47, entries 3 and 4**).

Table 47: catalytic hydrogen transfer in *i*PrOH for the hydrogenation of glucose to sorbitol.

Entry	<i>i</i> PrOH (mL)	H ₂ O (mL)	Time (h)	T (°C)	Conversion (%)	Selectivity (%)	Yield (%)
1	3	10	2	150	100	83.2	83.2
2	3	10	1	120	95.6	86.5	86.5
3	3	-	1	120	84.7	0.0	0.0
4	5	-	1	120	100	5.5	5.5

Reaction conditions: 100 mg of glucose (0.56 mmol), 50 mg Ru/C 3 wt.%.

On one hand, the monomodal setup drastically improved the activity of Ru/C 3%, on the other it was still not possible to remove water from the solvent: this would have been a problem for the subsequent dehydration, so we once again performed hydrogenation tests under H₂ pressure in the Synthwave. We also decided to remove the solvent at once, running the

reaction at 155 °C, just above glucose melting point. We compared the catalysts again and this time it was Ru/TiO₂ to give the best performance: it was possible to have complete conversion and high selectivity in just 1 h under 20 bar H₂. Ru/TiO₂ 3% was then the catalyst of choice for the hydrogenation, to be performed under H₂ pressure.

3.4.3 Sorbitol dehydration

Once sorbitol is formed, it still needs two dehydration steps to convert to isosorbide (**Fig. 63**). However, different dehydration products are possible, among which only 1,4-sorbitan leads to sorbitol, while the others lead to complex condensation products called humins. We decided to test some solid dehydrating agents instead than mineral acids as often reported in literature. We tested three commercial zeolites and Na₂SO₄ for the dehydration of sorbitol. The two zeolites were, as described in a previous paragraph, a H β with SiO₂/Al₂O₃ of 360 and two HY with ratios of 30 and 5.1.

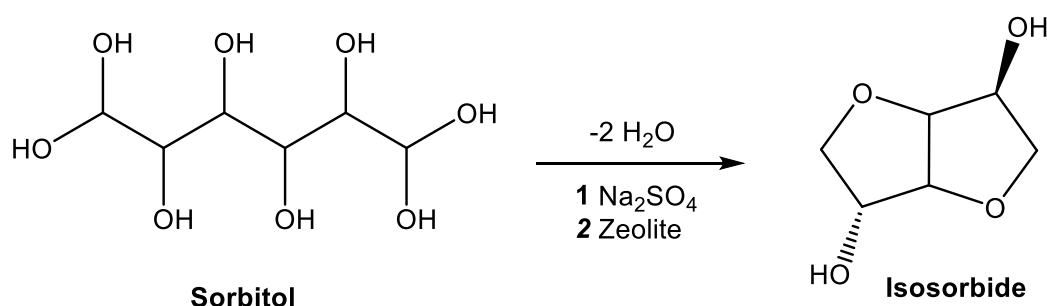


Figure 63: reaction scheme of the dehydration of sorbitol to isosorbide over Na₂SO₄ or zeolites.

Sorbitol has a melting point of only 95 °C, so we firstly screened the materials at 120 °C using a weight ratio of 1:1 to the substrate, for 2 h. Results are presented in **Table 48**.

Table 48: yield % in isosorbide over different dehydrating materials.

Entry	Dehydrating agent	Conversion (%)	Selectivity (%)	Yield (%)
1	Na ₂ SO ₄	50.7	60.2	30.5
2	Zeolite H β	40.0	87.5	35.0
3	Zeolite HY 5.1	100	0.0	0.0
4	Zeolite HY 30	29.5	65.9	19.4

Reaction conditions: 100 mg of sorbitol (0.55 mmol), 100 mg of dehydrating agent, 120 °C, 2 h.

Surprisingly, despite its low acidity, Zeolite H β was the best performing (**Table 48, entry 2**) and, when temperature was risen to 190 °C in subsequent tests the selectivity towards isosorbide grew to 98.0 %. As for zeolite HY 5.1, it was too strong a dehydrating agent, resulting only in short-chained acids and humins. Na₂SO₄ gave good results, however the recovery of the products was challenging, requiring washings with MeOH and filtrations to get close to a complete recovery, so it was ultimately discarded.

3.4.4 One-pot reaction

The two reaction steps were optimized in two very different temperatures so, since it is desirable to perform a synthesis at the lowest temperature possible, two possibilities were considered: running the conversion in one step at an intermediate temperature or divide it in two steps each at its appropriate temperature (**Fig. 64**).

For the one-pot one-step process a temperature of 175 °C was used and substrate, catalyst and H β zeolite are present from the start under 20 bar H₂ for 2 h. With this, the conversion of glucose was of 77.3 % but sorbitol was still present in the products leading to a yield of only 4.9 % of isosorbide. For the one-pot two-steps process the hydrogenation of glucose was run at 155 °C for 1 h, after which the H β zeolite is added, and the dehydration is run at 190 °C for 1 h under 20 bars of N₂. This improved the conversion to 100 % but again with sorbitol residues and an isosorbide yield of 16.0 %. The result was again improved when 200 mg of zeolite were used instead of 100 mg, this enabled a total conversion of sorbitol and an isosorbide yield of 54.9 %. The green metrics for the one-pot reaction are listed in **Table 49**.

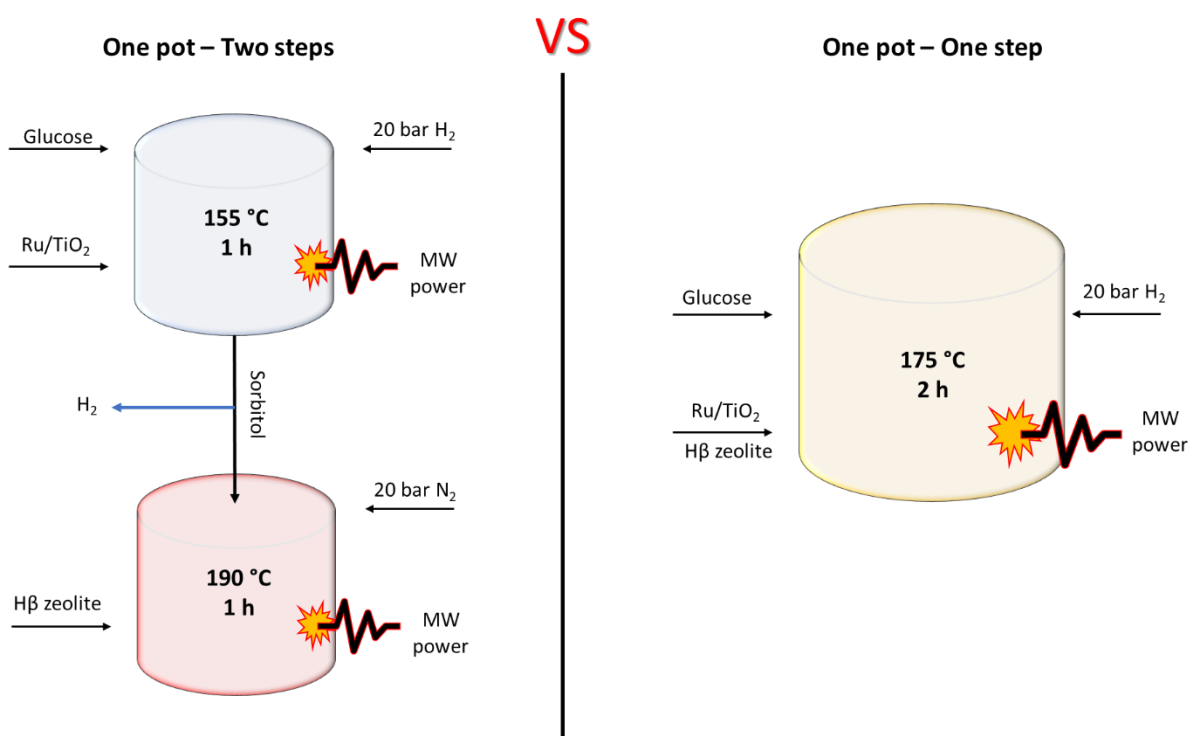


Figure 64: visual representation of the one-pot conversion of glucose to isosorbide in one step or two steps.

3.4.5 Conclusion

We successfully investigated and developed a green approach for the synthesis of isosorbide starting from glucose. The reduction of glucose to sorbitol was achieved both with the H-transfer mechanism using *i*PrOH as a reactive solvent and with gaseous H₂. We also avoid the use of solvents, working above the melting point of the reagents; this had a great impact on the EMY of the synthesis and simplified the recovery of the products. Also, the use of mineral acids has been avoided in favour of H β zeolite as heterogeneous acid catalyst.

The screening of different Ru-based catalysts showed that Ru/TiO₂ 3 wt.% had the greatest activity, thanks to the positive interaction between the metal nanoparticles and the support. These screening allowed the development of a one-pot synthesis, both in one and two steps. The one-step approach run at 175 °C for 2 h led to the complete conversion of glucose and an isosorbide yield of 54.9 %. MW had a huge role in allowing a complete process in such a short reaction time. The green metrics of the process are good, since the reaction is stoichiometric and avoids toxic additives, however the EF still suffers from two criticalities: the high pressure of H₂ needed and the difficulty in the recovery of the mixed zeolite and catalyst after reaction. The deposition of Ru nanoparticles over an acidic support, perhaps zeolites itself, may solve the latter. As for now, a comparison with literature is presented in **Table 51**.

Table 51: one-pot results compared with those in recent literature.

		Catalyst	Acid catalyst	Cat/sub (g/g)	Time (h)	T (°C)	H₂ (bar)	Yield (%)
One-pot	Literature ²⁵⁴	Ni/NDC	H β zeolite	0.53	50 ^a	230	40	83.0
	Literature ²⁵⁵	Ru/C	H ₂ SO ₄	0.19	2	220	40	60.0
	This work	Ru/TiO ₂	H β zeolite	0.20	2	175	20	54.9

^a flow system.

Preliminary experiments starting directly from cellulose were attempted using formic acid both as H-donor and to hydrolyse the substrate and using molten salts both as solvents for cellulose and as dehydrating agents. Though promising, this approach only achieved low conversions, since cellulose is difficult to attack without strong acids to dissolve it. The best yield to isosorbide so far was only of 1.7 % using FA and Na₂SO₄. In most cases the formation of LA occurred as side-reaction. More research is needed, but these tests demonstrated that it is possible to obtain isosorbide directly from cellulose avoiding the use of mineral acids or other toxic reagents.

References

191. Rohmer M, Seemann M, Horbach S, et al. *J Am Chem Soc*, 1996, **118**, 2564–2566.
192. Pham DM, Boussouira B, Moyal D, et al. *Int J Cosmet Sci*, 2015, **37**, 357–365.
193. Lozano-Grande MA, Gorinstein S, Espitia-Rangel E, et al. *Int J Agron*, 2018, **2018**, 1–13.
194. Popa O, Băbeanu NE, Popa I, et al. *Biomed Res Int*, 2015, **2015**, 1–16.
195. Rosales-Garcia T, Jimenez-Martinez C, Davila-Ortiz G. *Int J Environ Agric Biotechnol*, 2017, **2**,

1662–1670.

196. Krulj J, Brlek T, Pezo L, et al. *J Sci Food Agric*, 2016, **96**, 3552–3558.
197. Czaplicki S, Ogrodowska D, Zadernowski R, et al. *Polish J Food Nutr Sci*, 2012, **62**, 235–239.
198. Gunawan S, Kasim NS, Ju Y-H. *Sep Purif Technol*, 2008, **60**, 128–135.
199. Chang CJ, Chang Y-F, Lee H-Z, et al. *Ind Eng Chem Res*, 2000, **39**, 4521–4525.
200. Ibrahim N 'Izzah, Mohamed IN. *Life*, 2021, **11**, 1–19.
201. Farvin KHHS, Anandan R, Kumar SHS, et al. *J Med Food*, 2006, **9**, 531–536.
202. Reddy LH, Dubernet C, Mouelhi SL, et al. *J Control Release*, 2007, **124**, 20–27.
203. Reddy L, Couvreur P. *Curr Pharm Des*, 2008, **14**, 1124–1137.
204. Wang JJ, Sung KC, Yeh CH, et al. *Int J Pharm*, 2008, **353**, 95–104.
205. Pandarus V, Ciriminna R, Béland F, et al. *ACS Omega*, 2017, **2**, 3989–3996.
206. Liu J, Song Y, Ma L. *Chem – An Asian J*, 2021, **16**, 2371–2391.
207. Irrgang T, Kempe R. *Chem Rev*, 2020, **120**, 9583–9674.
208. Vardanyan R, Hruby V *Synthesis of Essential Drugs*, 1st ed. Cambridge: Academic Press.
208. Lawrence SA, *Amines: synthesis, properties, and applications*. Cambridge: Cambridge University Press, 2004.
210. Kim H, Chang S. *Acc Chem Res*, 2017, **50**, 482–486.
211. Kim J, Kim HJ, Chang S. *European J Org Chem*, 2013, 3201–3213.
212. Sukhorukov AY. *Front Chem*, 2020, **8**, 215.
213. Bähn S, Imm S, Neubert L, et al. *ChemCatChem*, 2011, **3**, 1853–1864.
214. Mäki-Arvela P, Simakova IL, Murzin DY. *Catal Rev - Sci Eng*. Epub ahead of print 2021. DOI: 10.1080/01614940.2021.1942689.
215. Mao F, Sui D, Qi Z, et al. *RSC Adv*, 2016, **6**, 94068–94073.
216. Jagadeesh R V., Murugesan K, Alshammari AS, et al. *Science*, 2017, **358**, 326–332.
217. Huang L, Wang Z, Geng L, et al. *RSC Adv*, 2015, **5**, 56936–56941.
218. Sajiki H, Ikawa T, Hirota K. *Org Lett*, 2004, **6**, 4977–4980.
219. Chatterjee M, Ishizaka T, Kawanami H. *Green Chem*, 2016, **18**, 487–496.
220. He J, Chen L, Liu S, et al. *Green Chem*, 2020, **22**, 6714–6747.
221. Paula Dionísio A, Molina G, Souza de Carvalho D, et al. In: *Natural Food Additives, Ingredients and Flavourings*. Woodhead Publishing, 2012, pp. 231–259.
222. Ikenaga T, Matsushita K, Shinozawa J, et al. *Tetrahedron*, 2005, **61**, 2105–2109.
223. Sheldon RA. Springer, Dordrecht, pp. 86–103.
224. Bohnen HW, Cornils B. *Adv Catal*, 2002, **47**, 1–64.
225. Srivastava VK, Bhatt SD, Shukla RS, et al. *React Kinet Catal Lett*, 2005, **85**, 3–9.
226. Centi G, Perathoner S. *Catal Today*, 2020, **342**, 4–12.

227. El-Nagar RA, Ghanem AA. *Sustain Altern Syngas Fuel*. Epub ahead of print 27 November 2019. DOI: 10.5772/INTECHOPEN.89379.
228. Shi Y, Lu Y, Ren T, et al. *Catalysts*, 2020, **10**, 1–13.
229. Tang P, Paganelli S, Carraro F, et al. *ACS Appl Mater Interfaces*, 2020, **12**, 54798–54805.
230. Liu S, Dai X, Wang H, et al. *Chinese J Chem*, 2020, **38**, 139–143.
231. Nôtre J Le, Van Haveren J, Van Es DS. *ChemSusChem*, 2013, **6**, 693–700.
232. Lemieux RU, McInnes AG. *Can J Chem*, 1960, **38**, 136–140.
233. Fenouillot F, Rousseau A, Colomines G, et al. *Prog Polym Sci*, 2010, **35**, 578–622.
234. Rose M, Palkovits R. *ChemSusChem*, 2012, **5**, 167–176.
235. Storbeck R, Ballauff M. *Polymer (Guildf)*, 1993, **34**, 5003–5006.
236. Brewster LM. *ESC Hear Fail*, 2019, **6**, 487–498.
237. ECHA *Substance information: 2-methyl-2H-isothiazol-3-one*, <https://echa.europa.eu/it/substance-information/-/substanceinfo/100.001.583>.
238. Aricò F, Aldoshin AS, Tundo P. *ChemSusChem*, 2017, **10**, 53–57.
239. Zhang X, Durndell LJ, Isaacs MA, et al. *ACS Catal*, 2016, **6**, 7409–7417.
240. Gong B, Yan L, Chen M, et al. *Chinese J Org Chem*, 2017, **37**, 3170–3176.
241. Jin X, Yin B, Xia Q, et al. *ChemSusChem*, 2018, 71–92.
242. García B, Moreno J, Morales G, et al. *Appl Sci*, **10**. Epub ahead of print 1 March 2020. DOI: 10.3390/app10051843.
243. Mishra DK, Dabbawala AA, Park JJ, et al. *Catal Today*, 2014, **232**, 99–107.
244. Guo X, Wang X, Guan J, et al. *Chinese J Catal*, 2014, **35**, 733–740.
245. Dabbawala AA, Mishra DK, Huber GW, et al. *Applied Catal A, Gen*, 2015, **492**, 252–261.
246. Dussenne C, Delaunay T, Wiatz V, Wyart H, Suisse I, Sauthier M, *Green Chem.*, 2017, **19**, 5332–5444.
247. Barbaro P, Liguori F, Moreno-Marrodan C. *Green Chem*, **18**. Epub ahead of print 2016. DOI: 10.1039/c6gc00128a.
248. Jeong S, Jeon KJ, Park YK, et al. *Catalysts*, **10**. Epub ahead of print 2020. DOI: 10.3390/catal10020148.
249. Morales G, Iglesias J, Melero JA, et al. *Top Catal*, 2017, **60**, 1027–1039.
250. Otomo R, Yokoi T, Tatsumi T. *Appl Catal A Gen*, 2015, **505**, 28–35.
251. Kobayashi H, Yokoyama H, Feng B, et al. *Green Chem*, **17**. Epub ahead of print 2015. DOI: 10.1039/c5gc00319a.
252. Bonnin I, Mereau R, Tassaing T, et al. *Beilstein J Org Chem* 16143, 2020, **16**, 1713–1721.
253. Yamaguchi A, Sato O, Mimura N, et al. *Catal Commun*, 2015, **67**, 59–63.
254. Brandi F, Khalil I, Antonietti M, et al. *ACS Sustain Chem Eng*, 2021, **9**, 927–935.
255. Keskiaväli J, Rautiainen S, Heikkilä M, et al. *Green Chem*, 2017, **19**, 4563–4570.

4.0 Scaled processes

As discussed in the general introduction, minimizing the working volume of a process does not mean reducing the output of product but instead making the process more efficient overall. So, a scale-up done properly can still meet the terms of PI and bring forth the principles of green chemistry. In this chapter, some processes that were optimized and scaled-up to the gram size are presented. It will also be discussed how this meets with green chemistry and PI.

4.1 MW-assisted hydrogenation of LA to GVL in a flow reactor

Levulinic acid is a ketoacid obtained from glucose or fructose via hydrolysis^{256–258}. It is a flexible platform chemical that can be converted to a variety of compounds of interest such as succinic acid (for the synthesis of biopolymers) or levulinic esters (high-boiling green solvents). It can also be hydrogenated to γ -valerolactone (GVL) and 1,4-pentanediol (1,4-PDO)¹⁷⁰. GVL has numerous applications as green solvent for organic chemistry²⁵⁹ and biomass conversion²⁶⁰. The reaction scheme is presented in **Fig. 65**.

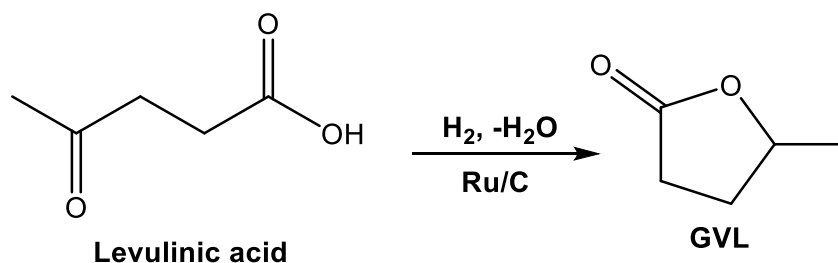


Figure 11: reaction scheme of the hydrogenation of LA to GVL.

GVL is a colourless liquid with a boiling point of 205 °C, its distinctive aroma makes it an ingredient for perfumes and food additives²⁶¹. It can be classified as a polar aprotic solvent and its remarkable stability allows its use in different reactions, however it can still be converted to other useful chemicals such as valeric acid which is a green fuel additive^{262,263}. As a solvent, GVL can be used to solubilize cellulose and lignin to convert them to high added-value products such as furfural or HMF^{264,265}, or to run proper organic reactions such as peptide synthesis²⁶⁶. The hydrogenation of LA to GVL is extensively reported in literature, often using supported Ru catalysts and hydrogen pressure^{267–271}. However, few examples exist on the application of MW for this process: in the following pages the optimization (from previous work) of the MW-assisted batch hydrogenation of LA to GVL is presented together with the follow-up translation to a flow reactor. The passage from batch to flow not only allowed the intensification of the process, but also a scale up of the synthesis was performed.

During my master's degree work of thesis, our research group developed a fast and green hydrogenation process from LA to GVL, both with molecular hydrogen and *i*PrOH as a H-donor. The two processes were optimized separately in two different systems: the hydrogenation with H₂ was performed in the MW autoclave Synthwave, while Anton Paar Monowave 300 was used for the H-transfer reactions. Also, two catalysts synthesised by Professor Cavani's research group at the University of Bologna were used for the study: Ru/C for the hydrogenation and Ru/TiO₂ for the hydrogen transfer.

The optimized conditions for both processes are reported in **Table 52** and **Table 53**.

Table 52: optimized batch conditions for LA hydrogenation with catalytic hydrogen transfer.

Entry	Catalyst	Loading (wt.%)	Time (h)	Conversion (%)	Selectivity (%)
1	Ru/C	3	1	100	94.4
2	Ru/C	3	0.5	100	100
3	Ru/TiO ₂	1	1	94.0	100
4	Ru/TiO ₂	3	1	100	100

Reaction conditions: 25 μ L of LA (0.25 mmol), 5 mL *i*PrOH, 150 $^{\circ}$ C.

Table 53: optimized batch conditions for LA hydrogenation with H₂.

Entry	Catalyst	Loading (wt.%)	Time (min)	H ₂ (bar)	Conversion (%)	Selectivity (%)
1	Ru/C	3	2	7	100	100
2	Ru/C	3	1	7	89.6	100
3	Ru/TiO ₂	3	2	7	10.3	100
4	Ru/TiO ₂	3	2	10	100	100

Reaction conditions: 25 μ L of LA (0.25 mmol), 150 $^{\circ}$ C.

These fast conversions were only possible thanks to MW radiation and allowed us to investigate the possibility to transfer the reaction from batch to flow, while also achieving a scale-up of it. Indeed, for the flow tests a flow MW reactor (Milestone FlowSynth) was used, with modification to work with a three-phase system. The batch experiments were in neat LA (without solvent), however this would not have been possible for larger scale, so aqueous solutions were prepared. The liquid and the H₂ gas could be pumped simultaneously thanks to a three-way connection followed by a non-return valve. A scheme is provided in **Fig. 66**.

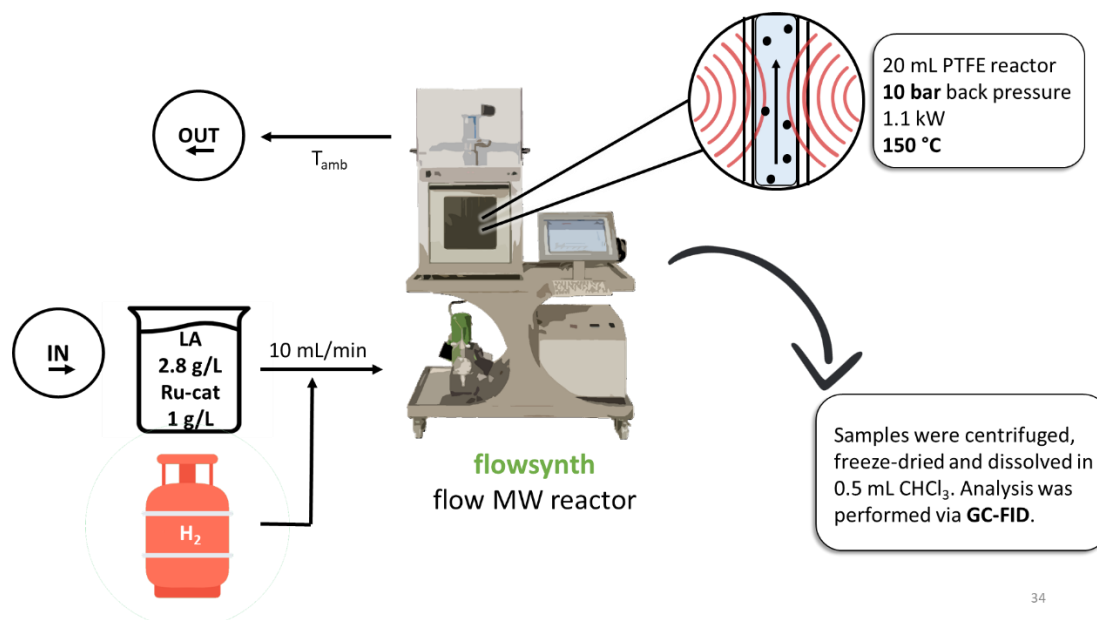


Figure 66: scheme of the process of the MW-assisted flow hydrogenation of LA to GVL.

The heterogeneous catalysts and the LA solution were stirred together before being pumped into the reactor to allow good homogeneity and to diminish the stress on the solid catalyst due to MW radiation: each portion is irradiated for 2 min only and not for the entire process of 30 min. The reaction chamber had a volume of 20 mL, so a 10 mL/min flux was set in order to reproduce the optimized reaction time of the batch experiments. A back-pressure valve just before the output regulated the internal pressure to 10 bar avoiding the boiling of water and again to mimic the previous experiments with H₂ gas. A sample of 2 mL was taken every 2 min (equal to the residence time in the reactor) once the operating conditions were reached, for a total of 30 min. A 15 min heating ramp was used, during which the output was discarded. Both Ru/C 3 wt.% and Ru/TiO₂ 3 wt.% were tested for two consecutive runs: after the first, the catalyst was centrifuged, recovered and reused in the same conditions.

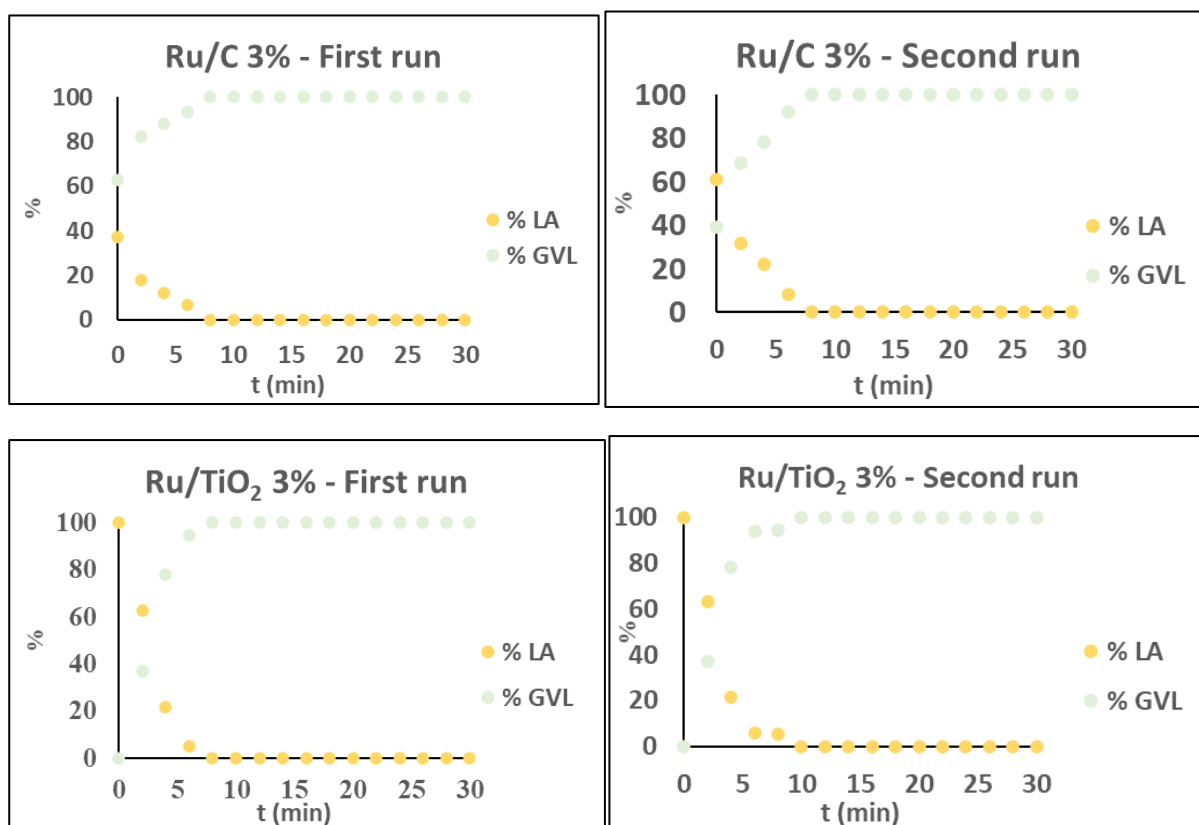


Figure 67: GVL content over time for the two catalytic runs over Ru/C 3 wt.% and Ru/TiO₂ 3 wt.%.

As shown in **Fig. 67**, both catalysts performed well and could reach complete selectivity in the time of the experiment, with Ru/C being more active already at the start of the sampling. It can be observed that the delay to reach the 100 % selectivity is longer on the second run, possibly because now, other than the stabilization of temperature inside the reactor, also the re-activation of the catalyst is happening *in situ*. However, we could reproduce the results of the batch trials but in a much larger scale: treating not 25 μ L but 0.5 L of solution at a time.

4.1.1 Conclusion

We successfully run a green, MW-assisted flow synthesis of GVL starting from LA over two Ru-based heterogeneous catalysts. We started from an in-depth study with batch experiments that allowed an optimization of reaction conditions both with molecular H₂ and with *i*PrOH as H-transfer. The MW irradiation allowed a fast conversion of LA in just 2 min, which then allowed for the transition from batch to flow.

With the flow setup we could dramatically improve the productivity, processing 2.8 g of LA (instead of 30 mg) in a 20 mL reactor (instead of 1 L reactor in batch), perfectly in line with the PI requirements, maintaining a complete conversion and selectivity to GVL. The successful application of different reaction mechanism, catalysts and the transition from batch to flow show how promising this reaction is for the synthesis of a green platform chemical using MW as an enabling technology for PI.

4.2.0 Caffeine and chlorogenic acid isolation from green coffee extract

Caffeine is a well-known bioactive alkaloid found in plants, especially in coffee and tea plants^{272,273}. Pure caffeine has pharmaceutical applications but is mostly used as an ingredient for energy drinks^{274–276}. The extraction of caffeine is indeed performed for two reasons: to have a caffeine-free product (de-caffeinated coffee and tea) and to re-sell the extracted natural caffeine as a high added-value product. Traditionally, caffeine extraction was performed using non-polar organic solvents, such as chloroform or dichloromethane in which caffeine has a high solubility^{272,277}. Extraction with supercritical CO₂ (scCO₂) is the most common process nowadays for foods: caffeine can be solubilized in scCO₂ and co-solvents and this method has the advantage that at ambient pressure the solvents are immediately removed, avoiding the risk of contamination^{278–280}. The use of scCO₂ is a well-established technology, however it still has important operative costs, which reduce the profit margin especially when starting from a low-priced raw product such as an extract. More recently, some research works are pushing beyond the available technologies, looking to improve results and sustainability using new solvents or applying MW and US for the extraction of active compounds^{281–283}.

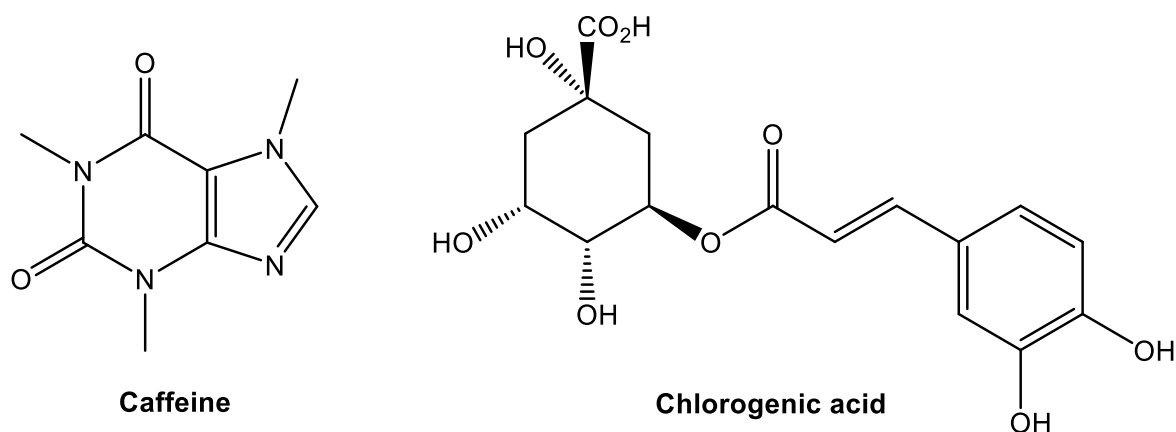


Figure 68: chemical structure of caffeine and chlorogenic acid.

Another valuable class of compounds found in vegetable extracts are chlorogenic acids. Chlorogenic acids (ChIA) are a class of polyphenols that shares the basic structure with chlorogenic acid which is the ester between caffeic and quinic acid. ChIA have antioxidant properties, especially when hydrolysed to caffeic acid which is a strong antioxidant, as well as anti-inflammatory, anti-microbial and possibly antitumoral^{284–286}. ChIA can be extracted from plants or be naturally consumed with vegetable foods²⁸⁷. Given their many possible applications for pharmaceuticals and nutraceuticals, they make for a valuable target for extraction and purification. The structures of caffeine and ChIA are shown in **Fig. 68**.

Our goal was to test new possible methodologies for the extraction of natural caffeine and ChIA without the use of toxic reagents or solvents. We decided to test CD complexation and the adsorption onto ion-exchange resins as green and scalable alternatives. Indeed, caffeine and ChIA complexation with β CD is extensively reported in literature^{288–291}. We started from a crude caffeine with a certified composition of 50 wt. % caffeine and 20-30 wt.% ChIA (**Table 54**).

Table 54: list of components in the crude caffeine.

Component	Content (wt.%)
Caffeine	50.0
Chlorogenic acids	20.0-30.0
Lipids	0.3
Oligosaccharides	1.5
Polysaccharides	14-15
Proteins	5.0
Other	11.0-13.0

4.2.1 Caffeine isolation via CD complexation

Caffeine and ChIA are present together in the starting material and are its major components. They can form complexes with each other, increasing their solubility in water at room temperature: it was indeed possible to dissolve 20 g of crude caffeine (10 g of caffeine) in 50 mL of water, whereas caffeine solubility at room temperature would be of 1.1 g in the same volume. Both molecules, however, can be complexed by β CD so we aimed for caffeine complexation and precipitation at low temperature. The formed solid could then be filtered and pure caffeine recovered via EtOH (50 %) washings. With caffeine removed, ChIA would concentrate in the mother liquors up to 60 wt.%. β CD are preferred over others because of their low price and because their solubility (and the solubility of their complexes) is lower at room temperature, so they are easy to recover.

In a typical experiment, 20 g of crude caffeine are dissolved in 50 mL of hot (80 °C) water under magnetic stirring. To the homogeneous mixture is then added an equimolar amount (70 g) of β CD to caffeine, both room temperature and 70 °C were tried for the complexation step. For the room temperature experiments, longer complexation time were necessary so we tested both a 3 h stirring and an overnight (15 h) stirring so see how it would impact the recovery. For the recovery of the complex, it was precipitated at 3 °C, once again leaving the sample to rest for 3 h or overnight. A general scheme is presented in **Fig. 69**.

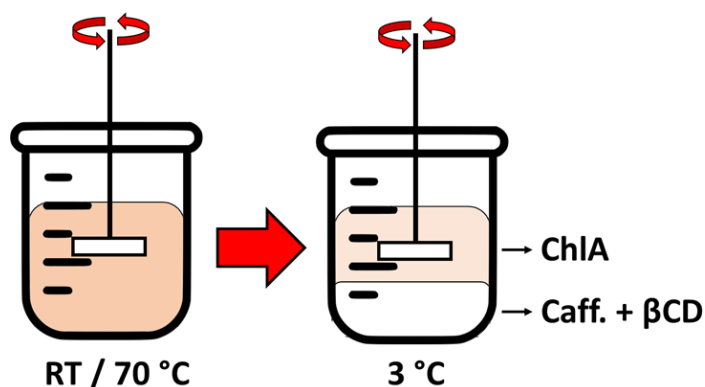


Figure 69: scheme of the process for caffeine complexation: β CD are added to the suspension and stirred, when the temperature is decreased the complex precipitates.

Once finished the complexation and precipitation step, the mixture is collected and filtered through a por.3 glass filter: in order to maintain a low temperature, not to redissolve the precipitated complex, every piece of glassware was priorly stored in an ice bath. Vacuum filtration was performed and the filtrate (caffeine mother liquor) was collected for UV-Vis analysis. The solid residue was then washed again with 3x15 mL of cold (3 °C) water and the washings collected as well for analysis. The obtained solid was then freeze-dried and a portion of it was dissolved in water (20 mg/L) for UV-Vis analysis.

Table 55: time and temperature screening for the caffeine complexation and removal.

Entry	Complexation		Precipitation		Precipitate (g)	Caffeine Content (wt.%)	Yield (%)
	T (°C)	Time (h)	T (°C)	Time (h)			
1	r.t.	3	3	3	64.5	7.7	48.5
2	r.t.	15	3	3	64.6	7.6	40.4
3	70	0.5	3	3	62.1	4.3	26.5
4	r.t.	3	3	15	63.3	8.0	50.1
5	r.t.	15	3	15	63.2	7.1	45.0

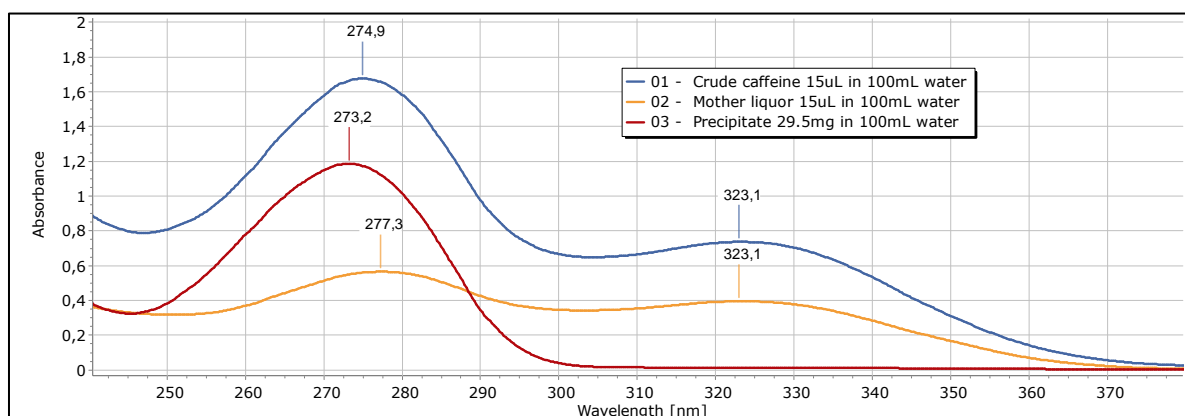


Figure 70: UV-Vis of the samples from the 3 h stirring and cold precipitation protocol.

For this one-step protocol, the best result is 3 h r.t. stirring followed by 15 h of rest at 3 °C (**Table 55, entry 4**), however the difference in caffeine removal is so small compared with the 3 h resting experiment (**Table 55, entry 1**) that these second are considered as the optimal conditions. As seen from the UV-Vis analysis (**Fig. 70**) the caffeine peak (273 nm) has a sharp fall after the treatment, but it is still present. Also, the relative concentration of ChIA red-shifts the caffeine peak to higher nm; in the solid caffeine is practically pure and its peak falls on the theoretical position. However, the observed concentration also tells that the weight % of caffeine in the precipitate is only of 0.08 % which is not convenient for easy manipulation. Also unfortunately, caffeine removals all fall around 40-50 %, which is not acceptable as a final result. The only outlier is the 70 °C experiment which has the lowest solid recovery and caffeine removal as well, so high temperature processes were discarded.

Since caffeine is still present in the first mother liquor, attempts were made to add a second 26 g portion of β CD to it and repeat the process to increase caffeine removal, however the higher relative content of ChIA impeded CD complexation and even contaminated the

complexes, so only traces of caffeine were present in the second solid without a significant improvement. It is important to underline that since the complex between caffeine and ChIA is very soluble, it is impossible to completely remove caffeine as long as ChIA are present.

With these results a scale-up of the process was not possible, since β CD were not efficient enough and a huge quantity was needed to treat even a small amount of crude caffeine. We then proceeded with the ion-exchange resins process instead.

4.2.2 Ion-exchange resin treatment of crude caffeine

Ion-exchange resins are functionalized polymers able to exchange small ions with a liquid solution; their most common application is the softening of waters exchanging Ca^{2+} with Na^+ to prevent carbonates precipitation. Many different resins exist in the market, different both

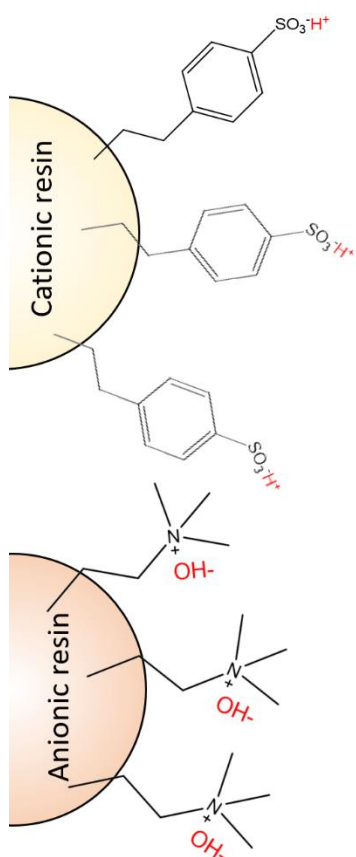
for their polymer structure and for their functionalization; commonly they are classified as weak or strong. Weak resins have carboxylic (weak acid) or tertiary amino (weak base) residues, while strong resins have sulfonic (strong acid) or ammonium salts (strong base) residues (**Fig. 71**).

Our target, this time, was the adsorption of ChIA on a strong anionic (basic) resin: in solution, the ChIA would separate from their counterions and bond to the resin, while a OH^- is released in exchange. Once ChIA are removed, caffeine is expected to precipitate from the liquid.

In a first experiment, 10 g of crude caffeine are dissolved in 30 mL of water. To that, 5 g of dry anionic resin were added. The suspension was magnetically stirred for 5 h, then put in the fridge at 3 °C overnight to allow a complete precipitation of caffeine.

The mixture was once again transferred to a glass filter. After the filtration the mother liquor is collected, and the solid is washed 3x10 mL of cold water. After that, to recover the caffeine, the solid is washed again but with 3x10 mL of boiling water: this purified caffeine is collected and freeze dried to obtain the dry solid. Finally, the washed resin is collected for the recovery of ChIA. A general scheme is presented in **Fig. 72**.

Figure 71: possible composition of a strong cationic and a strong anionic resin.



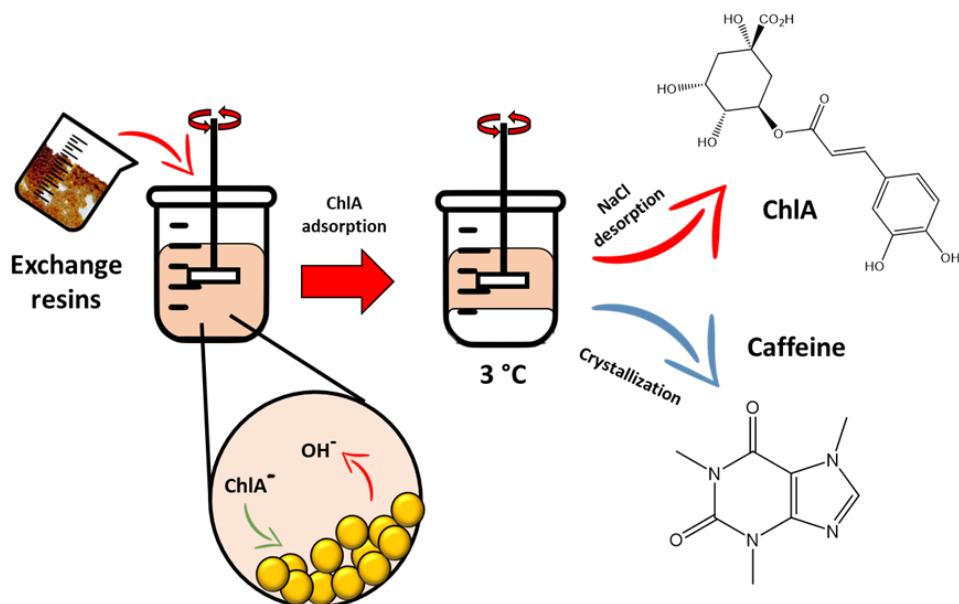


Figure 72: scheme of the process of ChIA adsorption onto ion-exchange resins. As ChIA are adsorbed by the anionic resin caffeine precipitates.

This first experiment resulted in a 70.2 % of caffeine recovery, directly as a dry solid. The rest of the caffeine stayed in the mother liquor because UV-Vis analysis revealed that ChIA had not been completely removed. As long as ChIA remain in solution they will solubilize caffeine, reducing the yield. We then set-up another experiment where the anionic resin was added portion-wise instead than all together. Finally, for 10 g of crude caffeine, 7.5 g of anionic resin were necessary to completely remove ChIA from the solution. This resulted in a staggering 95.0 % removal of caffeine (**Fig. 73**). The isolated caffeine was dried and analysed both via UV-Vis and ¹H-NMR resulting in a purity of 98 % (**Fig. 74**).

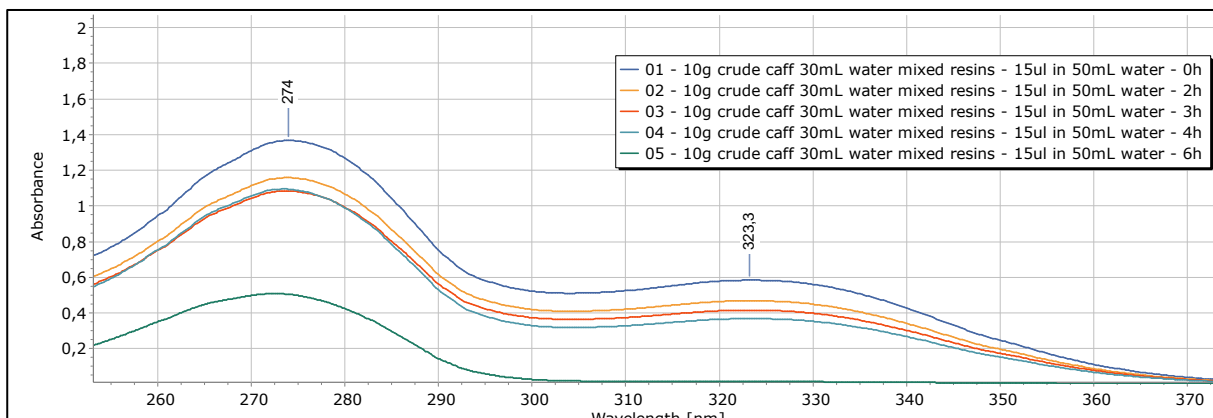


Figure 73: caffeine (274 nm) and ChIA (323 nm) content of the liquid over time.

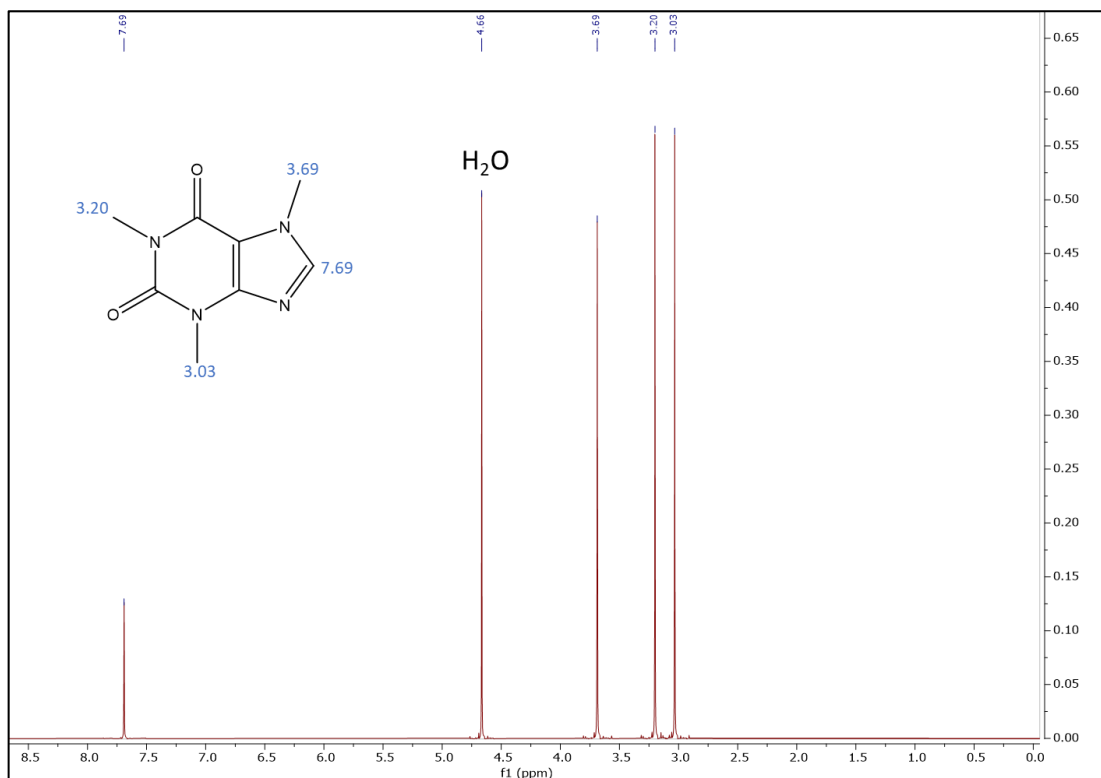


Figure 74: ^1H NMR in D_2O of the crystallized caffeine and peak identification.

These good results allowed us to plan a scale-up to 200 g of substrate. The 200 g of crude caffeine were dissolved in 400 mL water; the suspension was stirred by a mechanical head-stirrer with a Teflon propeller and the resin was added portion-wise. Samples were collected periodically for UV-Vis analysis to check the adsorption of ChIA (**Fig. 75**): if all ChIA were removed the process stopped, otherwise we continued with the addition of resins and periodic analysis. Finally, the process lasted 5 h and 160 g of dry anionic resin were used.

After the adsorption process, the solids were washed as previously described. The boiling water containing the caffeine was allowed to cool to room temperature, then it was kept in fridge overnight to allow the crystallization; the crystals were filtered and washed and the solid dried. 79 g of caffeine were isolated directly from the first crystallization and another 12 g were isolated from the washings and the supernatant, adding up to a 91 % removal from the crude.

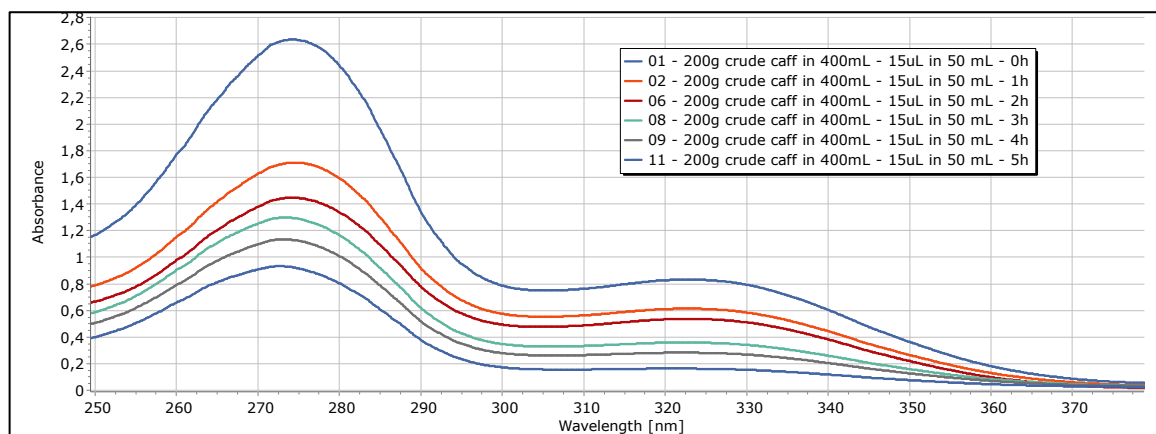


Figure 75: caffeine (273 nm) and ChIA (323 nm) content in the liquid over time.

4.2.3 Chlorogenic acids recovery

Having successfully removed caffeine from the crude material without the use of toxic solvents or costly equipment, we still needed to address the recovery of chlorogenic acids from the anionic resins. ChIA are polyphenols with various nutraceutical applications. We decided to test different desorption processes starting from a “model” material: ChIA adsorption was performed again from a ChIA-rich (50 wt.%) green coffee extract in the same conditions as with the crude caffeine. The objective was only to have enough material rich in ChIA to test different desorption conditions. All desorption experiments involved 15 g of resin suspended in 30 mL of solution under magnetic stirring in an 80 mL glass Beker. The resins were left to exchange for 1 h.

The tested possibilities were:

- **Desorption in brine:** a simple 20 wt.% NaCl solution was prepared, exchanging the adsorbed ChIA with the Cl⁻ ions. This would be the simplest and cheapest method. The only detail to mind is that, since resin was used in excess respect to the mmol of ChIA, OH⁻ ions were also exchanged leading to a rapid increase in pH as the exchange progressed. To avoid the decomposition of ChIA, concentrated HCl was added dropwise to maintain pH below 7. Finally, when no more pH increasing was measured, HCl additions were used to reach pH 2 ensuring protonation of ChIA in solution.
- **Desorption with NaOH 5 M:** a solution of NaOH 5 M was added in 250 µL portions until the theoretical amount (20 mmol) to regenerate the 15 g of resin was reached. After every portion a 5 min pause was used to allow the resin to exchange with the solution. The pH was not controlled, and a deep-green coloration was immediately seen.
- **HCl additions:** 2 mL of concentrated HCl were added to exchange the ChIA with the chloride ions, directly obtaining the protonated product. Since acidic conditions can lead to ChIA hydrolysis, a 50 % EtOH solution was used as a solvent to slow the degradation. This process was also tested both at r.t. and 65 °C.
- **CD complexation:** using the HCl addition to desorb the ChIA, we tested the possibility to immediately complex them with a stoichiometric amount of βCD (15.0 g) or RAMEB (17.0 g). This with the double objective of impeding the degradation of ChIA and shift the equilibrium towards their desorption. RAMEB were added at r.t., however 65 °C were needed with βCD to solubilize them in the liquid. Since CD are poorly soluble in alcohols, 80 mL of distilled water were used instead of EtOH 50 %.

After the desorption the mixtures were filtered, a portion of the filtrate diluted 1:2000 in distilled water and analysed at UV-Vis to check for the content of ChIA. The rest of the filtrate was dried and weighted. The yield is calculated from the expected ChIA content of 4.7 g for 15 g of resin. Results are presented in **Table 56**.

Table 56: ChIA desorption and recovery with different methodologies.

Entry	Desorption Method	Dried filtrate (g)	ChIA content (%)	Yield (%)
1	Brine	14.4	25.2	77.2
2	NaOH 5 M	10.8	9.7	22.3
3	HCl r.t.	0.9	18.2	3.5
4	HCl 65 °C	0.8	0.2	0.0
5	HCl RAMEB	16.0	8.7	29.6
6	HCl β CD	15.3	9.0	29.3

Surprisingly, the use of NaOH was less harmful to ChIA respect to warm HCl, however degradation was still observed. The best result, by far, was with simple NaCl, which is an optimal result. The use of CD hugely improved the yield respect to HCl alone, however the results were not good enough to justify their use, also because further separation steps would be needed to recover ChIA from the complex.

To check if a complete yield was possible, the 15 g of resin treated with brine were treated again with a clean brine solution and then with 30 mL of NaOH 5 M. However, these two portions did not result in a significant amount of ChIA: the second brine solution was practically clean, while the NaOH decomposed the residual ChIA.

We then applied the one-step brine desorption methodology to the resins coming from the 200 g processes, both in one and two steps. Resins were suspended in 360 mL of NaCl 20 %, using concentrated HCl to control the pH. The resins were then filtered, the filtrate dried under vacuum. Since this first filtrate still contains mostly inorganic salts, it was resuspended in 300 mL of EtOH (96 %) and filtered: the deep-red filtrate contained the ChIA, while the sodium salts remained on the filter as a pale-yellow solid. The second filtrate was dried again under vacuum, obtaining the final solid product. The ChIA contents were calculated via UV-Vis analysis; also, portions of the solids were put to the muffle and heated to 600 °C to calculate the inorganic content (**Table 57**).

Table 57: comparison of the ChIA recovery in one or two steps.

Entry	Process	Dried filtrate (g)	ChIA content (%)	Inorganics (%)	Yield (%)
1	One-step	40.0	55.1	1.0	44.2
2	Two-steps	66.0	39.4	59.6	52.0

Interestingly, the two products differed much for the inorganics content, which was much higher in the two-step process. However, the simplest explanation might be an incomplete protonation of ChIA after the desorption. Yields were similar, both around 50 %, with a small advantage again for the two-steps process. Finally, the best results for the upscaled process reached a 91 % removal of caffeine and a 52 % ChIA recovery from the resin.

4.2.4 Conclusion

The development of a green procedure for caffeine and chlorogenic acids purification from a crude substrate is reported. The first attempt to recover caffeine via complexation inside β CD was only partially successful: the high concentration of ChIA prevented a complete recovery of caffeine (\approx 50 %) and also the huge excess of CD needed for the complexation made the methodology highly impractical. However, the use of ion exchange resins proved very effective: the strong anionic resins bonded the ChIA, allowing caffeine to precipitate from the liquid. The precipitated caffeine was removed with hot (80 °C) water and crystallized, while the ChIA were desorbed with brine and separated from the salts in EtOH. This process allowed the treatment of 200 g of sample (a tenfold increase from preliminary experiments) with a 91 % removal of caffeine. The recovery of ChIA proved more problematic, remaining at 52 %.

Starting from a low value material we were able to isolate two highly valuable target compounds with good yield using only benign solvents and recyclable resins for the adsorption process. This process was also easily scaled maintaining the results from the preliminary trials, showing the possibility for larger scale application. The use of toxic organic solvents was avoided and only cheap and readily available materials and reagents were used to treat the substrate (water, NaCl, EtOH).

References

256. Signoretto M, Taghavi S, Ghedini E, et al. *Molecules*, **24**. Epub ahead of print 30 July 2019. DOI: 10.3390/molecules24152760.
257. Kang S, Fu J, Zhang G. *Renew Sustain Energy Rev*, 2018, **94**, 340–362.
258. Pyo SH, Glaser SJ, Rehnberg N, et al. *ACS Omega*, 2020, **5**, 14275–14282.
259. Kerkel F, Markiewicz M, Stolte S, et al. *Green Chem*, 2021, **23**, 2962–2976.
260. Tabasso S, Grillo G, Carnaroglio D, et al. *Molecules*, 2016, **21**, 1–9.
261. Horváth IT, Mehdi H, Fábos V, et al. *Green Chem*, 2008, **10**, 238–24.
262. Dong LL, He L, Tao GH, et al. *RSC Adv*, 2013, **3**, 4806–4813.
263. Lange JP, Price R, Ayoub PM, et al. *Angew Chemie - Int Ed*, 2010, **49**, 4479–4483.
264. Xue Z, Zhao X, Sun RC, et al. *ACS Sustain Chem Eng*, 2016, **4**, 3864–3870.
265. Alonso DM, Gallo JMR, Mellmer MA, et al. *Catal Sci Technol*, 2013, **3**, 927–931.
266. Kumar A, Sharma A, de la Torre BG, et al. *Molecules*, **24**. Epub ahead of print 5 November 2019. DOI: 10.3390/molecules24214004.
267. Yan ZP, Lin L, Liu S. *Energy and Fuels*, 2009, **23**, 3853–3858.
268. Cao S, Monnier JR, Williams CT, et al. *J Catal*, 2015, **326**, 69–81.
269. Adeleye AT, Louis H, Akakuru OU, et al. *AIMS Energy 2019 2165*, 2019, **7**, 165–185.
270. Ruppert AM, Grams J, J??drzejczyk M, et al. *ChemSusChem*, 2015, **8**, 1538–1547.
271. Luo W, Sankar M, Beale AM, et al. *Nat Commun*, 2015, **6**, 1–10.

272. Hu X, Wan X, Bal R, et al. *Sep Sci Technol*, 2003, **38**, 3609–3624.
273. Machado KN, Freitas AA de, Cunha LH, et al. *Food Chem*, 2018, **239**, 180–188.
274. Patil PN. *Int J Pharm Sci Rev Res*, 2012, **16**, 76–83.
275. Welsh EJ, Bara A, Barley E, et al. *Cochrane Database Syst Rev*. Epub ahead of print 20 January 2010. DOI: 10.1002/14651858.cd001112.pub2.
276. Ahluwalia N, Herrick K. *Adv Nutr*, 2015, **6**, 102.
277. Hulbert GJ, Biswal RN, Mehr CB, et al. *Food Sci Technol Int*, 1998, **4**, 53–58.
278. Reddy V, Saharay M. *J Phys Chem B*, 2019, **123**, 9685–9691.
279. Kopcak U, Mohamed RS. *J Supercrit Fluids*, 2005, **34**, 209–214.
280. De Azevedo ABA, Mazzafera P, Mohamed RS, et al. *Brazilian J Chem Eng*, 2008, **25**, 543–552.
281. Bermejo DV, Mendiola JA, Ibáñez E, et al. *Food Bioprod Process*, 2015, **96**, 106–112.
282. Koturevic B, Adnadjevic B, Jovanovic J. *Green Process Synth*, 2017, **6**, 555–563.
283. Carciochi RA, Dieu V, Vauchel P, et al. *Food Bioprod Process*, 2021, **127**, 266–275.
284. Naveed M, Hejazi V, Abbas M, et al. *Biomed Pharmacother*, 2018, **97**, 67–74.
285. Santana-Gálvez J, Cisneros-Zevallos L, Jacobo-Velázquez DA. *Mol* 2017, Vol 22, Page 358, 2017, **22**, 358.
286. Sato Y, Itagaki S, Kurokawa T, et al. *Int J Pharm*, 2011, **403**, 136–138.
287. Lu H, Tian Z, Cui Y, et al. *Compr Rev Food Sci Food Saf*, 2020, **19**, 3130–3158.
288. Szmeja S, Gubica T, Ostrowski A, et al. *Int J Mol Sci*, 2021, **22**, 4191.
289. Shao P, Zhang J, Fang Z, et al. *Food Hydrocoll*, 2014, **41**, 132–139.
290. Chao J, Wang H, Zhao W, et al. *Int J Biol Macromol*, 2012, **50**, 277–282.
291. Alvarez-Parrilla E, De La Rosa LA, Torres-Rivas F, et al. *J Incl Phenom*, 2005, **53**, 121–129.

5.0 General conclusion

In this work of thesis, the topics of green chemistry and process intensification were studied and presented with different approaches. The synthesis of new heterogeneous materials was first described: the objective was to test new preparation methods with green materials to obtain samples for catalysis, adsorption and antimicrobial application. The use of green solvents and bioderived reagents was coupled with heterogeneous catalysis and the use of enabling technologies for the synthesis of different high added-value compounds.

The solventless synthesis of 200 g of β CD-based cross-linked polymer and of 20 g of RAMEB-based polymer under ball-mill resulted in active materials for the adsorption of pollutants from wastewaters which is a topic of huge importance in pharmaceutical and chemical industries. The insoluble polymers were successfully tested for the adsorption of dyes and bioactive compounds of different structures both in batch and in flow also resulting in improved performances compared to a commercial β CD-based equivalent. Also, the polymers were used as support for the deposition of Rh and Au nanoparticles with three different impregnation procedures: mechanical stirring, US and ball-mill. The obtained catalysts were tested in model hydrogenation and oxidation reaction with great results, even better than the commercial equivalents. These experiments showed the flexibility of such materials, obtained from cheap and benign materials.

The US-assisted metal nanoparticles deposition was also tested over citrus pectin for the deposition of Au and Ag nanoparticles. The effect of US and reducing agents was investigated, showing that US significantly helped in improving the dispersion and reducing the size distribution altogether. The pectin was also doped with the broad spectrum antibiotic oxytetracycline and the antimicrobial capacity of such materials was tested with the zone of inhibition experiments over gram-positive and gram-negative bacteria; results showed that the pectin prepared with US had superior activity and the presence of metal nanoparticles enhanced the activity of the drug, possibly acting as antibiotic carriers.

A series of Rh-based heterogeneous catalysts was also prepared under US. The use of carbon nanowires drastically improved the activity of the catalyst respect to simple activated carbon in all the subsequent experiments, sometimes also achieving results comparable with the commercial Rh/C equivalent. A Co/C catalyst was also prepared as a possible alternative to Rh (which is very expensive) and in some reductive amination experiments it achieved competitive results. However, improved preparations need to be developed since up to now the commercial Rh/C was still the best performing catalyst.

The synergy between MW irradiation and the heterogeneous catalysts allowed us to improve the results of different syntheses compared to literature. The reductive amination of aldehydes and even ketones over Rh and Co-based catalysts was performed with good yields, especially with ketones it was possible to work with mild conditions: a result that is rarely reported in literature. The hydroformylation of olefines to aldehydes was also performed with complete yields with Rh/C. This also allowed us to setup a one-pot conversion of olefines to amines in only 4 h once again with 100 % yield. Finally, the MW-assisted one-pot synthesis of isosorbide from glucose is reported with 54.9 % yield: the procedure used no solvent and even substituted mineral acids (common in literature) with a heterogeneous H β zeolite.

To conclude, two examples of scaled-up processes are reported. The first is the hydrogenation of LA to GVL in a flow MW reactor. The synthesis was first optimized in batch and then translated to the flow equipment: this allowed us to convert 1.4 g of LA in 30 min instead of the 28 mg in each batch, without increasing the size of the reactor. The synthesis was performed over two Ru-based catalysts (Ru/C and Ru/TiO₂) which were also successfully reused for a second catalytic test maintaining complete selectivity towards GVL. Also, the extraction and purification of caffeine and chlorogenic acids from a crude natural substrate is reported. The use of recyclable ion-exchange resins allowed the complete adsorption of chlorogenic acids and the subsequent precipitation of caffeine. After crystallization caffeine was recovered with >90 % purity and 91 % yield. Chlorogenic acids were desorbed with brine and separated from the salts with EtOH washings allowing a 52.0 % recover. The procedure avoided the use of toxic organic solvents and expensive equipment and it allowed a scale up from 10 g to 200 g of treated crude per batch.

6.0 Materials and methods

6.1 Synthesis and characterization of cyclodextrin insoluble polymers

For the synthesis of β CDPIS dried food-grade β CD were used, while dried RAMEB purchased from Sigma-Aldrich were used for Me β CDPIS. A high-energy planetary ball mill Retsch PM100. The ball-mill is equipped with stainless steel balls using a 50 mL stainless steel jar and can work up to 33.3 g (650 rpm). In our case a 450 rpm speed was used, inverting the rotation every 15 min. Epichlorohydrin purchased from Sigma-Aldrich was used for the cross-linking.

The FESEM images were recorded with a Tescan S9000G FESEM 3010 microscope (30 kV) equipped with a high brightness Schottky emitter and fitted with energy dispersive X-ray spectroscopy (EDS) analysis by a Ultim Max Silicon Drift Detector (SDD, Oxford). The powdered samples were deposited on a stub coated with a conducting adhesive and inserted in the chamber by a fully motorized procedure.

The adsorption isotherms were obtained maintaining the samples in motion over a Heidolph Synthesis 1 equipped with an oscillating plate (up to 1000 rpm) and twelve sample positions for 50 mL glass vials distributed over four zones: every zone can be heated independently up to 180 °C. For our work the heating was disabled, and the rotation was set to 450 rpm.

The UV-Vis analysis was performed with a Cary 60 UV-Vis spectrophotometer (Agilent Technologies) recording the whole spectra between 200-800 nm with an acquisition rate of 600 nm/min using a 3 mL quartz cuvette.

The reagents used for the adsorption tests, the nanoparticles preparation and the catalytic tests were all purchased by Sigma-Aldrich. The BM catalysts were prepared with the Retsch PM100, the US catalysts were prepared with a titanium ultrasonic horn connected to a Hainertech (Shouzhou) ultrasound generator working at 21.0 kHz and 50 W.

6.2 Synthesis and characterization of doped pectin

Pectin Citrus was purchased from Alfa Aesar. AuCl_3 (anhydrous), AgNO_3 and NaBH_4 (98 %) were all purchased from Sigma-Aldrich; L-ascorbic acid (sodium salt, 99 %) was purchased from Alfa Aesar. For the antibiotic coupling oxytetracycline hydrochloride, EDC (98 %) and N-hydroxysuccinimide (98 %) were all purchased from Alfa Aesar.

The US pectin were prepared using an ultrasonic plate connected to a MG 200 TFD MF 40-80-120 ultrasound generator (Weber Ultrasonics). The generator can work up to 200 W of power and with frequencies of 40, 80 or 120 kHz. A steel serpentine immersed in the bath was used to maintain ambient temperature during the sonication.

The UV-Vis quantification of oxytetracycline was performed with a Cary 60 UV-Vis spectrophotometer (Agilent Technologies) recording the whole spectra between 200-800 nm with an acquisition rate of 600 nm/min using a 3 mL quartz cuvette. The DR-UV-Vis spectra of the Au@pectin samples were recorded with a Cary 5000 UV-Vis-NIR spectrophotometer.

6.3 Synthesis of Rh and Co-based catalysts

RhCl₃ and Co(II) acetate were purchased from Sigma-Aldrich. For the catalysts supported on activated carbon Norit CA1 from wood (Sigma-Aldrich) was used. Carbon nanowires (HHT) were given us from the Chemistry Department of the University of Milan. The US samples were prepared with a titanium ultrasonic horn connected to a Hainertech (Shouzhou) ultrasound generator working at 21.0 kHz and 50 W.

6.4 MW-assisted syntheses and relative analysis

For the MW-assisted experiments two reactors were used. For most of the experiments a SynthWAVE reactor (Milestone srl.) was used. The reactor is a multimode MW equipped with multiple gas inlets, able to operate up to 300 °C and 199 bars. Integrated sensors continuously monitor the internal pressure and temperature allowing the software to adjust, in real-time, the applied MW power to follow a predefined temperature profile. The MW cavity has a 1 L volume, however we worked with 50 mL or 15 mL glass vials put in multi-position holders, immersed in 200 mL of brine solution. For some tests a monomode MW reactor Monowave 300 (AntonPaar) was used to maximize the MW density over the sample. 30 mL glass vials were used, stirred at 450 rpm. The reactor can work up to 300 °C and 30 bar of internal pressure. The temperature is monitored continuously by an IR sensor in contact with the vial while the internal pressure is measured from the rubber cap.

For the flow hydrogenation of LA a flow MW reactor (Flowynth, Milestone srl.) was used. The multimode system is equipped with a vertical PTFE-TFM flow-through reactor (VR: 20 mL), which can work up to a maximum of 200 °C temperature and 30 bar, able to operate in open or closed loop mode. A three-way connection fitted with a nonreturn valve allows to pump simultaneously solutions and gaseous feeds, even under pressure.

When needed, derivatization of protic compounds was performed adding 50 µL of BSTFA to 1 mL of sample at a concentration between 2-4 mg/mL. The sample was then left to react at 60 °C for 1 h in an oil bath to ensure complete derivatization.

The GC-MS analysis were performed with a 6850 Network GC System with a 5973 Network Mass Selective Detector and 7683B Automatic Sampler. GC-FID analysis were performed with a 7820A Network GC System. Both were equipped with a Mega snc. capillary column (OV1701; length 25 m; i.d. 0.25 mm; film thickness 0.30 µm).

6.5 Caffeine and chlorogenic acids isolation

Shelf-dry food grade βCD were used for the complexation of caffeine. For the adsorption of chlorogenic acids a strong anionic resin was used: Ambersep 900 (quaternary ammonium, 64 wt.% moisture, 0.8 meq/mL) purchased from Sigma-Aldrich.

The pH was monitored with a pH 211 (Hanna instruments) pH-meter equipped with a glass-bulb sensor directly in contact with the liquid. UV-Vis analysis were performed with a Cary 60 UV-Vis spectrophotometer (Agilent Technologies) recording the whole spectra between 200-800 nm with an acquisition rate of 600 nm/min using a 3 mL quartz cuvette.

7.0 Acknowledgments

These three years of Ph.D. research enriched me far beyond the skills I acquired working under a fume hood; it feels stereotypical to say, but I have really grown as a person, and professionally. I wish thereby to thank the Huvepharma's managers Ing. Nicola De Risi and Dr. Cosimo Faggiano for backing up my project, providing the resources to fulfil it and welcoming me in company facilities. A deep acknowledgement also goes to my tutor, Prof. Giancarlo Cravotto, for having me in his team and guiding my research towards fruitful results. I wish to thank also Dr. Luisa Boffa, Dr. Emanuela Calcio Gaudino, Dr. Laszlo Jicsinszky, Prof. Maela Manzoli and Prof. Silvia Tabasso for all the ideas we shared and the help they gave me. I wish to thank all my amazing colleagues from the Organic Chemistry group of the Department of Drug Science and Technology and in particular Marco Belluati, Giorgio Grillo, Francesco Mariatti and Federico Verdini among others, with whom I worked closely all these years: if I know what it means to work in a team and enjoy it, it is all thanks to you folks.

Finally, this goes to my family and all my loved ones for their wholehearted support: I hope to make you proud of your dedication to this humble human being.